AN ABSTRACT OF THE DISSERTATION OF

Cheng Li for the degree of Doctor of Philosophy in Biological & Ecological Engineering presented on March 16, 2017.

Title: Electrical Conductivity in Mixed-species Biofilms for Enhancing Energy Generation in Anaerobic Microbial Systems.

Abstract approved: _____

Hong Liu

Further enhancement of energy generation is desired for practical application of anaerobic microbial systems such as microbial fuel cells (MFC) and anaerobic digesters (AD). A possible approach is to enhance the ability of microbial communities to transfer electron extracellularly in the form of electrical current. Critical to perform direct extracellular electron transfer (DEET) is the establishment of electrical connections between electron donors and acceptors in microbial communities. These connections can be facilitated through conductivity of microbial assemblages (e.g. biofilms and granules). Current understanding towards the microbially constructed conductivity is limited and two distinct theories of conductive mechanisms have emerged: an incoherent redox conduction model and a coherent metallic-like conduction model. While single species biofilms of *Geobacter sulfurreducens* have been thoroughly studies in terms of conductivity, conductive behaviors, and conductive mechanisms, these conductive features of mixed-species communities remain unexplored.

The present dissertation aims to evaluate the electrical conductivity of mixed-species exoelectrogenic and methanogenic biofilms and develop strategies to enhance the

energy generation in anaerobic microbial systems. Conductive behaviors of these mixed-species biofilms were investigated during the initial growth period, over various nonconductive distances, and at different metabolic modes such as deprivation of substrate. Conductive mechanisms were elucidated by examining the conductance of these mixed-species biofilms over a range of redox potentials and at different intensities of magnetic field. Correlations between biofilm conductivity, microbial community, strength of magnetic field, and power/current generation were also investigated in mixed-species MFCs.

Results demonstrated that both mixed-species exoelectrogenic biofilms and methanogenic biofilms exhibited conductivities (2651 and 71.8 μS/cm, respectively) across non-conductive gaps. Electrochemical gating analysis indicated that electron transfer in exoelectrogenic and methanogenic biofilms occurs through incoherent redox conduction. For exoelectrogenic biofilms, increase of biofilms conductance correlates with the increase of power output of MFCs during the startup period. Deprivation of substrate decreased the biofilm conductivity by an order of magnitude. Exoelectrogenic biofilms are capable of extending their conductive structures on the millimeter scale. The redox conductivity of exoelectrogenic biofilms was also confirmed by the dependence of conductance on magnetic field, in which biofilm conductance increased along with the increase of magnetic field intensity. This conductive behavior resembles the negative magnetoresistance in certain conductive polymers that has ever been observed in biofilms before. The strong correlation observed between biofilm conductivity and *Geobacter* spp. in the metabolically diverse anaerobic communities suggests that the efficiency of direct extracellular electron transfer may provide pressure for microbial communities to select

for species that can produce electrical conduits. Application of static low intensity magnetic field to MFC can increase the conductivity of exoelectrogenic biofilms on anode of MFC and thereby enhance the power/current generation of MFC. These results propose feasible approaches by which energy generation and start-up times may be improved in engineered anaerobic microbial systems such as MFC and AD.

Electrical Conductivity in Mixed-Species Biofilms for Enhancing Energy Generation in Anaerobic Microbial Systems

by
Cheng Li

A DISSERTATION

submitted to

Oregon State University

in partial fulfillment of
the requirements for the
degree of

Doctor of Philosophy

Presented March 16, 2017
Commencement June 2017

Doctor of Philosophy dissertation of Cheng Li presented on March 16, 2017

APPROVED:

Major Professor, representing Biological & Ecological Engineering

---

Head of the Department of Biological & Ecological Engineering

---

Dean of the Graduate School

I understand that my dissertation will become part of the permanent collection of Oregon State University libraries. My signature below authorizes release of my dissertation to any reader upon request.

Cheng Li, Author

ACKNOWLEDGEMENTS

I would like to thank my advisor Dr. Hong Liu first and for most. Her patient and guidance throughout my Ph.D. program help me to find the joy of being a researcher and truly identify the limiting factors in my experiments. I would also like to thank my committee members Dr. Alex Chang, Dr. Frank Chaplen, Dr. Mark Dolan, Dr. Kaichang Li, who encouraged me and discussed with me during my study.

I would like to thank my major co-author Keaton Larson Lesnik, who has been serving as one of greatest peer mentors at all time. I would like to thank Dr. Yanzhen Fan, who encouraged me to think boarder and supported my ideas. I would also like to express my gratitude to all my lab mates Shoutao Xu, Ningshengjie Gao, and Luguang Wang for all their tolerance and support. It is truly a honor to work with all of you.

Last but not the least, I would like to express my gratitude to my mother Ying Wang and my father Junqin Li who passed away in 2011 for their trust in me. I would like to show my appreciation to Robin Ryan, my advisor when I served as the president of Chinese Association of Oregon State University, who has encouraged me to live out the leadership in my life, Wanda Crannell and all members in Minorities in Agriculture, Natural Resources, and Related Sciences OSU chapter who has taken me in and taught me about the importance of diversity, and brothers and sisters at Chinese Christian Church of Corvallis, who support me and love me as family.

CONTRIBUTION OF AUTHORS

Dr. Hong Liu provided oversight and revisions to all manuscripts.

Dr. Yanzhen Fan provided guidance with electrode design and integration into MFC.

Keaton Larson Lesnik conducted metagenomics experiments and provided constructive suggestion from the perspective of microbiology and contributed to the revisions of certain manuscripts.

TABLE OF CONTENTS

TABLE OF CONTENTS (Continued)

TABLE OF CONTENTS (Continued)

Page

TABLE OF CONTENTS (Continued)

LIST OF FIGURES

LIST OF FIGURES (Continued)

Figure | Page

LIST OF FIGURES (Continued)

Figure Page

LIST OF FIGURES (Continued)

Figure Page

LIST OF TABLES

Table Page

1 Introduction

1.1 Extracellular Electron Transfer in Microbial Communities

Microorganisms constantly acquire energy through reactions that are based on electron transfer reactions associated with the oxidation and reduction of chemical compounds in order to live and reproduce (Kato, 2015). All organisms conduct redox reactions intracellularly through the utilization of soluble or gaseous chemical compounds, but select microorganisms also possess the ability to acquire energy by transferring electrons extracellularly to or from redox active minerals and even other microbial cells. This ability to transfer electrons extracellularly provides a competitive advantage in environments where diffusion is limited and the availability of electron donors and acceptors is scarce. The transfer of electrons between microbial cells enables syntrophic partnerships that are essential for the functioning of microbial communities in various engineered and natural systems (McInerney et al., 2009; McInerney et al., 2008; Stams et al., 2006; Stams & Plugge, 2009).

1.1.1 Extracellular Electron Transfer (EET)

Extracellular electron transfer (EET) can be roughly categorized into two mechanisms: indirect EET and direct EET. Indirect EET is carried out by the diffusional transportation of small molecules. These small molecules include intermediate products of metabolic processes (e.g. hydrogen and formate in methanogenesis and zero-valent

sulfur in anaerobic methane oxidation) and various types of electron shuttles (e.g. humic substance, phenazine, and anthrahydroquinone disulfonate (AQDS)) (Bryant et al., 1967; Rabaey et al., 2005; Sieber et al., 2014; Stams et al., 2006; Wagner, 2015). In direct EET, electrons are transferred in the form of electrical current between donors and acceptors (Lovley, 2011a; Lovley, 2011b). Compared to the indirect diffusion of small molecules, direct EET represents a more specific and efficient process. The conventional understanding of direct EET was that EET only occurs on the molecular scale, however, recent evidence suggests that it can be on the scale of micrometer (Lovley, 2016; Malvankar & Lovley, 2014; Phan et al., 2016; Snider et al., 2012; Yates et al., 2015). Stable electronic connections need to be established in order to transfer electrical current over the substantial distances (> 1 mm). Microorganisms may employ various types of specialized cell-produced proteins (Malvankar et al., 2011; Pirbadian & El-Naggar, 2012; Xu et al., 2016; Yates et al., 2016a) and/or recruit conductive materials (Chen et al., 2014a; Chen et al., 2014b; Kato et al., 2012a; Kato et al., 2012b; Liu et al., 2012; Nakamura et al., 2010) from the environment to establish these electronic connections and construct conductive assemblages (e.g. biofilms, granules, consortia, and multicellular filaments).

1.1.2 Engineering and Environmental Significance of Microbial Conductivity

The further characterization and elucidation of electron conduction mechanisms in microbial assemblages represents a significant challenge that has the potential to influence many fields. Microbial fuel cells (MFC) and anaerobic digesters (AD) are

engineered anaerobic microbial systems that use microorganisms in the form of microbial assemblages to convert the chemical energy stored in organic substance to respectively electricity and methane. It has the potential to be used for wastewater treatment and bioenergy production (Logan, 2009; McCarty et al., 2011). Electrical connections are important for the functioning of MFC (Li et al., 2016b; Malvankar et al., 2012a; Malvankar & Lovley, 2014; Malvankar et al., 2012c; Malvankar et al., 2011) and AD (Kato et al., 2012a; Liu et al., 2012; Morita et al., 2011; Rotaru et al., 2014a; Rotaru et al., 2014b). A major challenge in developing these systems for practical applications has been the limited understanding of electron transfer within the microbial communities and improving direct EET is a key to their enhancement. Direct EET is also critical to various biogeochemical cycles and may contribute significantly to many other important cellular processes such as biofilm formation, cell-to-cell recognition, and infection (Ericsson et al., 2015; Humphries et al., 2017; Lovley, 2016; Tschirhart et al., 2017).

1.2 Fundamentals of Electrical Conductivity in Microbial Assemblages

The discovery of new types of electronic connections between cells is ongoing (Lovley, 2016). Likewise, the conduction mechanisms at the heart of these connections is still being investigated. Two distinct mechanistic theories involving microbial conductivity have emerged: an incoherent redox conduction model and a coherent metallic-like conduction model. The redox conduction model in microbial assemblages describes a multi-step electron superexchange process while the metallic-like model is based on the understanding of pili filaments produced by *Geobacter* spp. (Malvankar et

al., 2012b; Malvankar et al., 2015; Malvankar et al., 2011; Tan et al., 2016; Vargas et al., 2013).

1.2.1 Redox Conductivity

1.2.1.1 Electron Transfer through a Network of Electroactive Sites

The current conceptual model of redox conduction in conductive redox polymers features a network of closely associated (< 20 Å) molecular electron traps referred as electroactive sites or redox sites in which electrons are transferred via a multi-step electron superexchange process (Figure 1.1.A.) (Dalton et al., 1990; Inzelt, 2012; Oyama et al., 1986; Phan et al., 2016). In abiotic redox polymers, these electroactive sites possess redox centers that are mostly organic or organometallic monomers (Inzelt, 2012). In conductive microbial assemblages, microorganisms produce and/or recruit a series of extracellular redox molecules to serve as electroactive sites, which may include outer membrane cytochromes (Pirbadian et al., 2014; Pirbadian & El-Naggar, 2012; Pokkuluri et al., 2004; Snider et al., 2012; Strycharz-Glaven et al., 2011; Yates et al., 2016a), Fe-S proteins (Yates et al., 2016a), and adsorbed flavins (Okamoto et al., 2014; Xu et al., 2016).

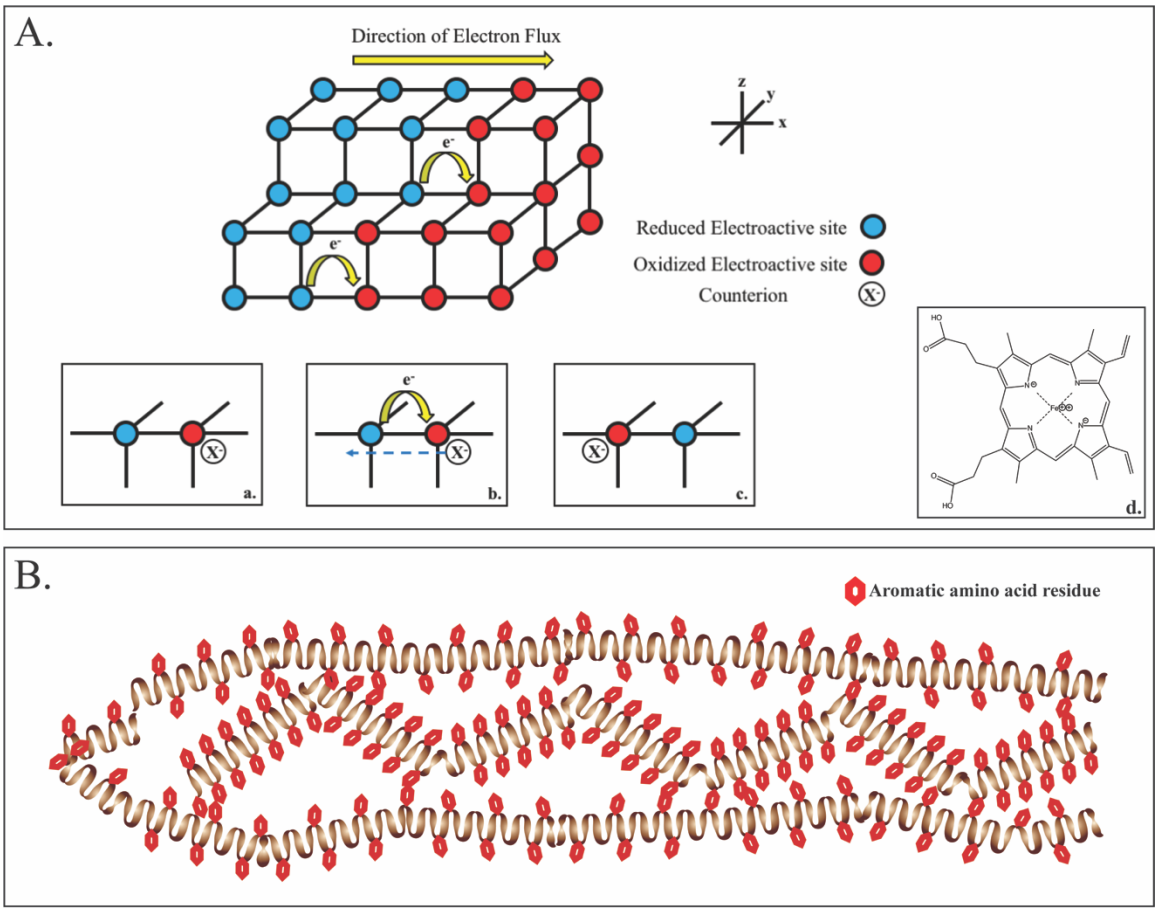

Figure 1.1. A.) Schematic of superexchange through an idealized three dimensional lattice of reduced and oxidized electroactive sites within a redox conductive microbial assemblages. Insets depict a single electron superexchange event: a. before exchange, b. electron exchange accompanying the diffusion of a counterion, c. after exchange, and d. redox center of cytochromes (Figures are adapted by Dalton et al., 1990. and Pokkuluri et al., 2004). B.) Predicted structure of a *G. sulfurreducens* pilus filament based on nuclear magnetic resonance spectroscopy. Aromatic amino acid residues responding for the π-π stacking are highlight in red. (Figure is adapted by Malvankar et al., 2015.).

During electron transfer in redox polymers, electrons are conducted in a bucket-brigade manner between adjacent electroactive sites via an electron self-exchange reaction called superexchange or electron hopping. This superexchange is a typical bimolecular reaction that requires the involvement of both reduced (occupied) and oxidized (hole) electroactive sites. The opportunity for electrons to exchange is maximized when the population of oxidized and reduced electroactive sites are equal (Dalton et al., 1990; Malvankar et al., 2012b; Strycharz-Glaven et al., 2011). Within the redox polymers this can be measured as electrical conductivity. Electron exchange and conductivity is limited when electroactive sites are completely reduced or oxidized within the conduction network (Li et al., 2016b; Malvankar et al., 2011; Snider et al., 2012). Since the oxidation states between reduced and oxidized electroactive sites typically differ by one electron, the presence of compensating small, mobile counterions are essential in maintaining electroneutrality of the whole redox polymer during superexchange (inserts of Figure 1.1.A.) (Dalton et al., 1990). Therefore, the hydration state of redox polymers (mixed conductors contain both ionic and electronic conductions) affects ion mobility and must be considered when measuring redox conduction (Dalton et al., 1990; Phan et al., 2016).

1.2.1.2 Driving Forces of Redox Conduction Events

Superexchange of an electron from a reduced site to an oxidized site is realized by the application of driving forces to overcome the energy barrier between the two

oxidation states (Malvankar et al., 2011; Yates et al., 2015). These driving forces may include a concentration gradient of reduced/oxidized electroactive sites or a gradient of electric field. These can be induced by the natural buildup of reduced/oxidized species during substrate utilization or the experimental application of a small voltage bias (Dalton et al., 1990; Phan et al., 2016; Strycharz-Glaven et al., 2011; Strycharz-Glaven & Tender, 2012). Both types of driving forces can exist and affect electron superexchange through microbial assemblages simultaneously.

When substrates are being utilized by microorganisms, electrons need to be transferred to extracellular electron acceptors, to maintain thermodynamic favorability of the reaction (Sieber et al., 2012). Assimilated electrons from the oxidation of substrates are transferred from the intracellular level reactions to extracellular electroactive sites through various portal proteins, thus creating a group of reduced electroactive sites (occupied) (Dalton et al., 1990; Pirbadian et al., 2014; Pirbadian & El-Naggar, 2012; Strycharz-Glaven et al., 2011). Alternatively, electron uptake by the extracellular electron acceptor creates a group of oxidized electroactive sites and a concentration gradient is established.

The application of a small voltage bias will result in the electrolysis of electroactive sites near the electrode surface until the ratio of reduced to oxidized electroactive sites achieves steady state (Dalton et al., 1990; Phan et al., 2016). Electron mobility within the conduction network follows Fick's law of diffusion (Dalton et al., 1990; Strycharz-Glaven et al., 2011). When counterion mobility of microbial samples are insufficient the introduction of a small bias voltage will result in the formation of an

electric field gradient and drive the electron transfer along the direction of increasing positive charge within the gradient (Dalton et al., 1990; Phan et al., 2016; Strycharz-Glaven et al., 2011).

1.2.2 Metallic-like Conductivity

The model of coherent metallic-like conduction suggests that the conductivity of certain microbial assemblages is similar to the conductive mechanisms of synthetic organic metallic polymers such as polyaniline and poly-acetylene in which charges are delocalized and spread throughout the polymers (Malvankar et al., 2011). Metallic-like conductivity is not tied to the oxidation states of localized electroactive sites like redox conductivity. This type of conductivity has been observed in pure culture biofilms of *G. sulfurreducens* (Malvankar et al., 2011). Research suggests that this conductivity is conferred by the type IV pili filaments of *G. sulfurreducens* and evolved in a relatively recent evolutionary event and currently only expressed in a small group of bacteria (Holmes et al., 2016; Liu et al., 2013; Lovley, 2016; Malvankar et al., 2012b; Malvankar et al., 2015). The electrical connections conferred by pili filaments of *Geobacter* spp. resemble those of semi-conductive organic metals (Chen et al., 2014a; Chen et al., 2014b; Liu et al., 2015; Rotaru et al., 2014a; Rotaru et al., 2014b). Analysis using high resolution X-ray diffraction suggests that the tight stacking of aromatic amino acids along the longitudinal axis of pili filaments permits π-π overstacking leading to a delocalized electronic state (Figure 1.1.B.) (Malvankar et al., 2015). Direct visualization of charge propagation along individual pili filament by atom force microscopy (AFM) and

electrostatic force microscopy (EFM) further demonstrated the conductive nature of these pili filaments (Malvankar et al., 2014b). However, the conductivity of single species biofilms of *G. sulfurreducens* displayed positive correlation with temperature, more in line with redox conductor, when the hydration state was maintained (Phan et al., 2016; Yates et al., 2015).

1.3 Experimental Design for the Investigation of Conductive Mechanisms

The observation of conductive current through living materials is a relatively new discovery. Elucidation of conductive mechanisms underlying the observed conduction may have impacts on various disciplines. Measuring the conductivity and elucidating conductive mechanisms present many challenges. From the standpoint of experimental design these challenges include designing an appropriate electrode assembly, ensuring the proper development of biomass on the electrodes, preventing interfering currents, and distinguishing the conduction model (Phan et al., 2016; Snider et al., 2012; Yates et al., 2016b). The purpose of the following section is to discuss these challenges and strategies to overcome them.

1.3.1 Selecting Electrode Geometries/Configurations

In order to measure conduction current through microbial assemblages, microbial assemblages need to be developed or deposited onto electrodes. Although advanced microscopic techniques such as EFM or AFM can be employed to visualize the change of electrical charge density through conductive assemblages or verify the conductive

property of proposed assemblages, quantitative measurement of conduction current still requires the use of electrodes (Lovley & Malvankar, 2015; Malvankar et al., 2012b; Malvankar et al., 2014b). Therefore, it is important to choose the right electrode geometry to suit the needs of each individual study. Previous studies on abiotic conductive polymers suggest that ideal electrode design consists of two parallel electrode surfaces opposite to each other and straddled by a thin microbial assemblage (Figure 1.2.) (Anderson & Reilley, 1965; Dalton et al., 1990; McDuffie et al., 1966; Sanderson & Anderson, 1985; Snider et al., 2012; Strycharz-Glaven et al., 2011). Different configurations of this same electrode design have been developed to fit the needs of each individual studies. These configurations include a large split electrode (Li et al., 2016a; Li et al., 2016b; Liu et al., 2012; Malvankar et al., 2012a; Malvankar et al., 2012c; Malvankar et al., 2011; Morita et al., 2011; Summers et al., 2010), an interdigitated array (IDA) electrode (Phan et al., 2016; Snider et al., 2012; Strycharz-Glaven et al., 2011; Yates et al., 2016a; Yates et al., 2015; Yates et al., 2016b), and nano-electrodes (Adhikari et al., 2016; El-Naggar et al., 2010; Leung et al., 2013; Leung et al., 2011).

One of the most popular electrode configurations is a large, gold-coated surface (6.45 or 7 cm^2) that has been split in the middle thereby separating the conductive surface into two halves, and creating a thin nonconductive gap, ranging from 50 to 1000 μm (Li et al., 2016a; Li et al., 2016b; Liu et al., 2012; Malvankar et al., 2012a; Malvankar et al., 2012c; Malvankar et al., 2011; Morita et al., 2011; Summers et al., 2010). This two-probe configuration can also be further modified into a four-probe configuration that contains three nonconductive gaps dividing the main electrode surface into four separate

electrodes (Malvankar et al., 2012b; Malvankar et al., 2011). The use of the four probe configuration is used to avoid contact resistance created by stacking of reactor parts (Malvankar et al., 2011). The large conductive electrode surface areas and thin non-conductive gaps in these configurations ensures proper biofilm development across the nonconductive gaps and promotes the growth of microbial assemblages with relatively low growth rates (Li et al., 2016b).

The IDA electrode configuration contains two long and narrow parallel Au or Pt electrodes that are interdigitated as 65 pairs of microelectrode bands (2 mm long, 10 μm wide, and 90 nm thick) and separated from each other by 5 μm nonconductive gaps (Chidsey et al., 1986; Phan et al., 2016). This electrode configuration produces lower signal-to-noise ratios and has been widely used in the characterization of redox conduction in single species biofilms of *Geobacter sulfurreducens* and electroautotrophic cathodic biofilms (Phan et al., 2016; Snider et al., 2012; Strycharz-Glaven et al., 2011; Yates et al., 2016a; Yates et al., 2015; Yates et al., 2016b). However, the smaller electrode surface of IDA may also impose difficulties on establishing reliable association of microbial assemblages with electrodes (Malvankar et al., 2016).

Nano-electrodes are specifically designed to evaluate the conductivity of smaller scale microbial appendages and assemblages (Adhikari et al., 2016; El-Naggar et al., 2010; Leung et al., 2013; Leung et al., 2011). The configuration Adhikari et al 2016. used to measure the conductivity of individual *Geobacter* pilus filament contained 14 nanoelectrode bands measuring 10 μm long, 2 μm wide, and 30 nm thick (Adhikari et al., 2016). However, electrochemical measurement on this scale might be easily interfered by

residues from purification processes of biological samples. A strategy to avoid the interference should be accounted into experimental design when nano-electrodes are used to measure the conductivity of specific cell appendages or smaller scale microbial assemblages.

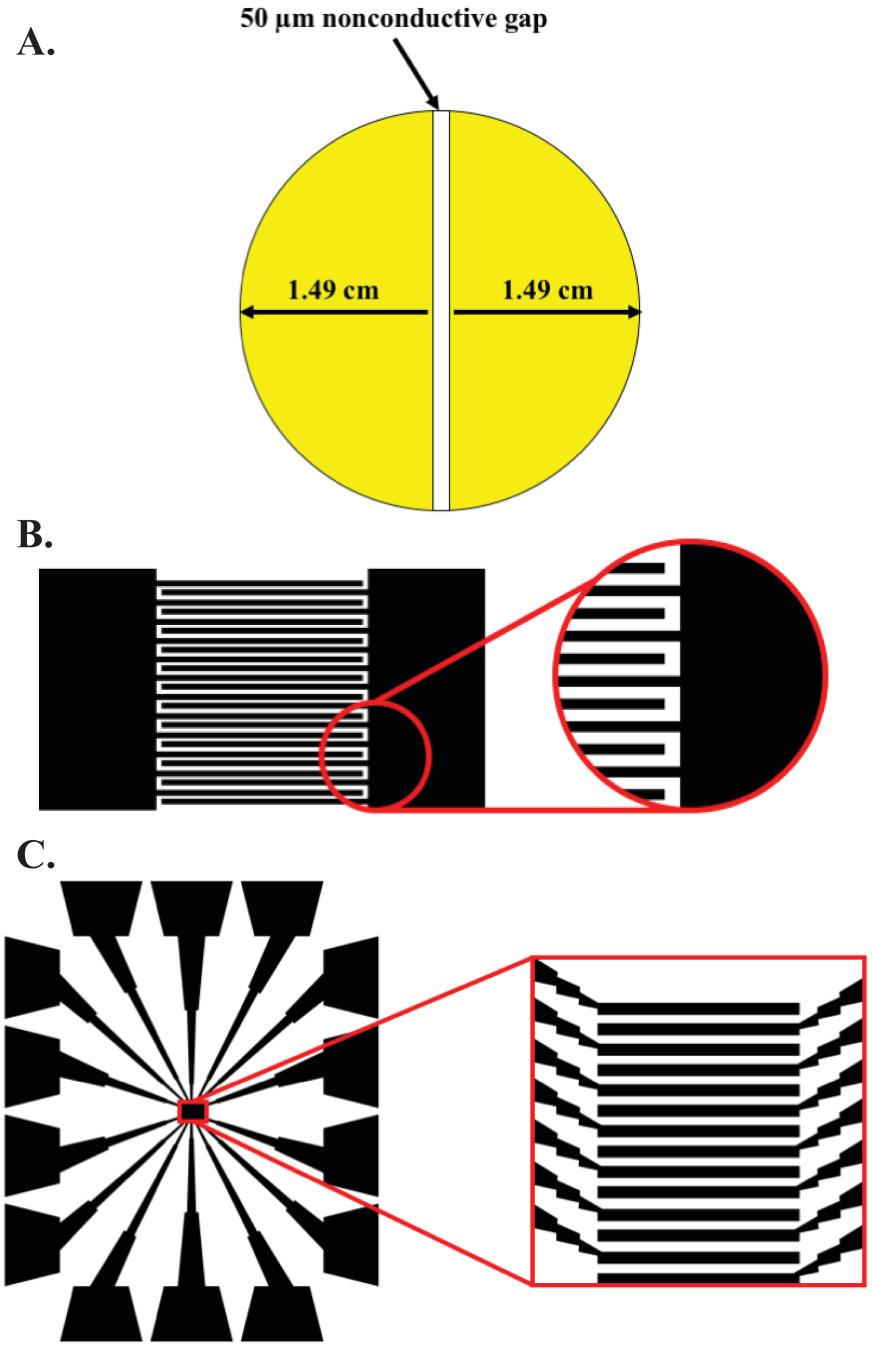

Figure 1.2. Electrode configuration of A. large split electrode, B. interdigitated array (IDA) electrode, large split electrode, and C. nano-electrodes. (Figures are adapted from Li et al., 2016a; Dalton et al., 1990; and Adhikari et al., 2016)

1.3.2 Avoiding Interfering Currents

Regardless of the conductive mechanism, conductive microbial assemblages are living materials that contain large numbers of electroactive sites. Encountering interfering currents caused by charging of pseudocapacitance (change in redox state of electroactive sites), catalytic substrate utilization, and/or diffusion of counterions is inevitable (Yates et al., 2016b). Therefore, experiments should be carefully designed to account for such interfering currents during measurements of conduction current. Failure to do so may lead to an overestimation of conductivity and affect interpretations. For example, conductivities of exoelectrogenic biofilms may vary significantly between measurements when using different electrode configurations. Reported conductivity values of *G. sulfurreducens* biofilms ranged from ~5 µS/cm using an IDA (Phan et al., 2016; Snider et al., 2012; Yates et al., 2015; Yates et al., 2016b) to ~5 mS/cm when a large split electrode was used (Malvankar et al., 2011). The large difference between individual measurements may affect the identification of limiting factors in respect to the optimization of current production in applied systems like microbial fuel cells (MFCs). In a MFC biofilm electron transfer model, when a conductivity value near the upper end of what has been observed (2.44 mS/cm) was used, the current density of the last step of electron transfer, which was suggested as the rate limiting step of direct EET in such biofilms, as determined to be 270 A/m^2, more than 300 times higher than the real MFC performance (0.82 A/m^2) (Lee et al., 2016). Thus, the authors concluded that the direct

EET enabled by the conductivity of biofilms is not the current limiting factor in anodic biofilm (Lee et al., 2016). However, if a lower end biofilm conductivity value (5 μS/cm) obtained from another study is used, the current density of last step of electron transfer would be nearly 500 times smaller and similar to observed MFC performance (calculated as 0.55 A/m^2). Interfering currents may cause these differences between observed conductivity values (Snider et al., 2012; Strycharz-Glaven et al., 2011; Yates et al., 2016b). Addressing these differences is an essential step towards understanding conductivity and direct EET in anodic biofilms of MFCs as well as other conductive microbial assemblages.

There are several precautions that may be taken to account for these interfering currents. These include decreasing the total assemblage-coated surface area (Snider et al., 2012; Strycharz-Glaven et al., 2011; Yates et al., 2016b), removal of substrate (Li et al., 2016b), subtracting the catalytic current, and utilization of steady state experiments (Dalton et al., 1990). Even when charging current associated with the double-layer capacitance of the electrode setup is properly controlled the change in redox state of electroactive sites will result in a charging current (Yates et al., 2016b). To limit the total amount of effective electroactive sites, the total volume of biomass developed on the electrodes and gap area should be controlled. Therefore, electrode configurations such as IDAs that contain smaller surface areas (0.039 cm^2) may reduce the contribution of charging current (Yates et al., 2016b). In other instances, the use of slope of the current and applied voltage curve to calculate the resistance of examined assemblages may also account for a large portion of the charging current and thereby should be used when

smaller surface electrodes is not available or inappropriate for designed experiments (Li et al., 2016b).

Catalytic current comes from the assimilation of substrate and may become a significant problem when measuring the conduction current in exoelectrogenic biofilms (Yates et al., 2016b). The interference of catalytic current can be eliminated by removal of substrate or subtracting the catalytic current from the measured current (Li et al., 2016b; Snider et al., 2012). Removal of the substrate may alter the redox potential of examined assemblages and therefore the period of substrate removal should be limited in order to avoid any potential damage to the biofilm or large scale metabolic shifts (Li et al., 2016b). Precise estimation of catalytic current may require the use of a bi-potentiostat (Snider et al., 2012).

During redox conduction, the change in net oxidation state of the microbial assemblage is accompanied by current related to the diffusion of counterions. To avoid capturing current related to counterion diffusion, steady state experiments in which no net oxidation state changes occur within the examined assemblages should be used and additional time should be allowed for such current to dissipate (Dalton et al., 1990). Transient experiments such as cyclic voltammetry and chronoamperometry are not recommended.

1.3.3 Distinguishing the Conduction Models

As discussed in previous sections, two distinct conductive mechanisms have been identified, both composed of varying components to sustain their conductivity (localized

electroactive sites versus pili filaments). Depending on the mechanism present differential responses in assemblage conductivity will be observed following changes of internal conditions such as redox potential, temperature, and hydration state (Malvankar et al., 2011; Phan et al., 2016; Snider et al., 2012; Strycharz-Glaven et al., 2011; Yates et al., 2015; Yates et al., 2016b). When the conductance is measured as a function of redox potential in electrochemical gating analysis (EGA), redox conductors display a peak-manner at a gate potential in which half the electroactive sites are oxidized and the other half are reduced (Dalton et al., 1990; Snider et al., 2012). In contrast, metallic-like conductors behave in a sigmodal-manner upon the changes of redox potential as charge carriers are trapped by the Coulomb potential of anions at lower gate voltages and transited to metallic state at higher gate voltages (Malvankar et al., 2011; Yuen et al., 2007).

Insight into the conductive mechanism can also be accomplished by examining the temperature dependency of assemblages conductivity (Malvankar et al., 2011; Morita et al., 2011). Increasing conductance upon decreases in temperature (negative correlation) is suggestive of metallic-like conductivity (Heeger, 2001), while redox conductivity displays positive correlation with temperature in biological range (Phan et al., 2016; Yates et al., 2015). It should be noted that extreme conditions should be avoided in order to preserve the biological features of the examined microbial assemblages (Phan et al., 2016). For example, the use of vacuum conditions may dehydrate the biological samples and interfere with the interpretation of conductive mechanisms (Morita et al., 2011; Phan et al., 2016). Water content should also be carefully considered as it is essential to the

formation of drive forces during redox conduction (Dalton et al., 1990; Phan et al., 2016; Yates et al., 2015).

1.4 Challenges and Objectives

Further understanding of microbially constructed conductive features is essentially important for the future enhancement of energy generation in engineered anaerobic microbial systems such as MFC and AD. The abovementioned hypothetical mechanisms were deducted based on experiments that conducted by using single species biofilms of *Geobacter sulfurreducens*. In spite of mixed-species communities are more widely used in engineered anaerobic microbial systems and more efficient on energy generation compared to single species cultures (Liu et al., 2012; Logan, 2009; Morita et al., 2011), the conductive features especially the conductive mechanism of many mixed-species community assemblages possessing the ability to perform direct EET remain unknown.

The objectives of this dissertation are to evaluate the electrical conductivity, examine important conductive behaviors, investigate the conductive mechanisms, and explore feasible approaches to increase the conductivity in mixed-species microbial assemblages with an ultimate goal of enhancing the performance of engineered anaerobic microbial systems for energy generation from renewable resources. These objectives are addressed in the following chapters of the present dissertation in the format of manuscript:

1) Chapter 2: To elucidate the conductive mechanism of mixed-species exoelectrogenic biofilms, to examine relationship between the power output of

MFC and development of biofilm conductance, and to investigate the conductive behaviors of mixed-species exoelectrogenic biofilms on unconnected surface of split electrode and after removal of substrate.

2) Chapter 3: To investigate the conduction distance of mixed-species exoelectrogenic biofilms and to evaluate the conductance development of mixed-species exoelectrogenic biofilms when growing across extended distance from 50 μm to 1 mm.
3) Chapter 4: To evaluate the conductivity and conductive mechanism of mixed-species methanogenic biofilms, to examine the current producing ability of methanogenic biofilms when serving as the anodic biofilms of MFC, and to investigate the relationship between biofilm conductivity and the community membership across microbial communities with different metabolic activities.
4) Chapter 5: To examine the potential impact of static low intensity magnetic field on power/current production of MFC, to evaluate application of static low intensity magnetic field as a feasible approach to increase conductivity of mixed-species exoelectrogenic biofilms, and to confirm the redox conduction model in mixed-species exoelectrogenic biofilms by assessing the magnetic field dependence of conductance.

In Chapter 6, conclusion from these studies were summarized and future works on boarder aspects were discussed. In Appendix, a published review article was also included to suggest the potential of applying the conclusions of this dissertation to other microbial technologies.

2 Redox Conductivity of Current-Producing Mixed-Species Biofilms

Cheng Li, Keaton Larson Lesnik, Yanzhen Fan, and Hong Liu

Plos One
San Francisco, California, US
May 9, 2016
http://dx.doi.org/10.1371/journal.pone.0155247

Abstract: While most biological materials are insulating in nature, efficient extracellular electron transfer is a critical property of biofilms associated with microbial electrochemical systems and several microorganisms are capable of establishing conductive aggregates and biofilms. Though construction of these conductive microbial networks is an intriguing and important phenomenon in both natural and engineered systems, few studies have been published related to conductive biofilms/aggregates and their conduction mechanisms, especially in mixed-species environments. In the present study, current-producing mixed-species biofilms exhibited high conductivity across non-conductive gaps. Biofilm growth observed on the inactive electrode contributed to overall power outputs, suggesting that an electrical connection was established throughout the biofilm assembly. Electrochemical gating analysis of the biofilms over a range of potentials (-600 – 200 mV, vs. Ag/AgCl) resulted in a peak-manner response with maximum conductance of 3437 ± 271 μS at a gate potential of -360 mV. Following removal of the electron donor (acetate), a 96.6% decrease in peak conductivity was observed. Differential responses observed in the absence of an electron donor and over varying potentials suggest a redox driven conductivity mechanism in mixed-species biofilms. These results demonstrated significant differences in biofilm development and conductivity compared to previous studies using pure cultures.

Keywords: Microbial Fuel Cell, Microbial Electrochemical Systems, Biofilm, Conductivity, Exoelectrogens

2.1 Introduction

The efficient extracellular transference of electrons is critical to the functioning of many biological processes in both natural and engineered environmental systems (Kato et al., 2012b; Reguera, 2011; Sieber et al., 2012). Much of our current understanding of extracellular electron transfer in these environments is largely based on the indirect transfer of small molecules such as hydrogen and formate, but recent evidence suggests that extracellular electron transfer through electrical current is prevalent (Kato et al., 2012a; Kato et al., 2012b; Malvankar et al., 2014a; Summers et al., 2010). In diffusion-limited environments, such as biofilms and sediments, direct extracellular electron transfer via electrical currents could offer significant advantages over small molecule exchange. It is likely that physical connections in the form of aggregates and biofilms are often established in order to support electrical interactions between microorganisms and extracellular electron acceptors including other microorganisms and electrodes (Kato et al., 2012a; Kato et al., 2012b; Lovley, 2011b; Summers et al., 2010). Biofilms and methanogenic aggregates associated with microbial fuel cells (MFCs) and anaerobic digesters have been found to exhibit electrical conductivity further reinforcing the hypothesis that interactions via electrical currents are a critical component of these environments (Malvankar et al., 2012a; Malvankar et al., 2011; Morita et al., 2011).

Biofilm and aggregates conductivity is often associated with the presence of specific microbial species that use direct extracellular electron transfer as a primary means of respiration (Malvankar et al., 2012a; Malvankar et al., 2011; Morita et al., 2011; Shrestha et al., 2014; Summers et al., 2010). This includes both *Geobacter*

sulfurreducens and *Shewanella oneidensis*, two species known to produce conductive extracellular appendages known as microbial nanowires. The conductive properties of many of these microbial nanowires have been characterized in detail using techniques such as atomic force microscopy (El-Naggar et al., 2010; Gorby et al., 2006; Malvankar et al., 2012b; Pirbadian et al., 2014). However, biofilms of *G. sulfurreducens* are the only pure cultures of which conductivity has been examined to date with conductivity up to 5000 μS cm^{-1} having been previously reported (Malvankar et al., 2011).

The conduction mechanism of nanowires and biofilms is currently not well-established and is still being explored. Though the conductivity of *S. oneidensis* nanowires appear to be dependent on the presence of redox cofactors like c-type cytochromes that are typically associated with extracellular electron transfer, the nanowires of *G. sulfurreducens* appear to have a conductivity that is independent of redox cofactors (El-Naggar et al., 2010; Malvankar et al., 2011; Pirbadian et al., 2014). Some experimental evidence suggests that the microbial nanowires of *G. sulfurreducens* possess delocalized electronic states representing a metallic-like conductivity that is conferred to whole biofilms (Malvankar et al., 2012b). However, other studies have refuted this theory and indicated that electron transfer in whole biofilms of *G. sulfurreducens* proceeds through a concentration gradient-driven electron transfer process involving localized redox cofactors referred as electron hopping (Bond et al., 2012; Snider et al., 2012; Vargas et al., 2013).

Conductive properties have also been recognized in various mixed consortia including methanotrophic aggregates in which electron transfer is hypothesized to

proceed through multi-heme cytochromes (Snider et al., 2012; Strycharz-Glaven et al., 2011). Conductivity is also a recognized property of mixed-species MFC biofilms enabling multilayer cell stacking and efficient cell-electrode contact conducive to high power outputs and coulombic efficiencies (Malvankar et al., 2012a). A conductivity of 250 μS cm^{-1}, around 5% of the pure culture biofilms of *G. sulfurreducens*, was observed in a *G. sulfurreducens*-dominated (52% *Geobacter* spp.) mixed-species MFC biofilms. However, additional characterization of mixed-species communities in terms of their extracellular electron transfer mechanisms has yet to be performed. Because several microbial species are capable of producing various conductive proteins/redox cofactors the combination of different species could affect the overall conductive characteristics of mixed-species biofilms (Kiely et al., 2011; McGlynn et al., 2015). Future enhancement of microbial electrochemical systems (MESs) could depend on the elucidation and optimization of the extracellular electron transfer processes within mixed-species biofilms (Kato Marcus et al., 2007; Malvankar et al., 2012c; Torres & Krajmalnik-Brown, 2009).

In the present study, a gold-coated split-anode design was used to examine the conductive behavior of high-power, mixed-species MFC biofilms over an extended range of anode potentials (-600 – 200 mV vs. Ag/AgCl) in both the presence and absence of an electron donor (Malvankar et al., 2011). Results demonstrated significant differences in conductivity compared to previous studies using pure cultures and provides evidence for redox driven conductivity in mixed-species biofilms of MFCs.

2.2 Materials and Methods

2.2.1 Anode preparation

A split-anode design modified from a previous study was developed for the in situ evaluation of biofilm conductivity (Malvankar et al., 2011). A water resistant adhesive (Loctite, Düsseldorf, Germany) was applied to standard weighing paper (Schleicher & Schuell, Inc., Keene, NH, USA) to provide rigidity. Adhesive laden paper was then cut into a circle with area of 7 cm^2. An electrically conductive gold film (approx. 5 μm) was then applied to the adhesive layer by an Cressington 108 auto sputter coater (Cressington Scientific, Watford, UK). The gold film layer was then cut down the center by an ESI 5330 UV Laser machine (Electro Scientific Industries, Inc., Portland, OR, USA) to create a non-conductive gap of 50 μm. Resistance measurements confirmed that the two pieces of the anode were electrically separated ($R_{gap} > 10^{10}$ Ω).

2.2.2 Microbial fuel cell design and operation

Single-chamber, air-cathode MFCs with gold-coated split-anodes were used to develop biofilms on the anode surface. Carbon cloth/activated carbon cathodes were fabricated following previously developed protocols (Janicek et al., 2015). The projected surface areas of anode and cathode were 7 cm^2 and the total MFC volume was 12 mL. The MFCs were electrically connected in one of two ways to examine the biofilm growth and conductivity (Figure 2.1.). Double anode MFCs labeled ‘DA-MFC’ contained anodes in which both halves of the split anode were connected to the closed electrical circuit, while in single anode MFCs labeled ‘SA-MFC’ only one of the two halves of the split

anode was connected to the closed electrical circuit. Reactors with neither of the two halves of the split anode connected to circuit were used as a control.

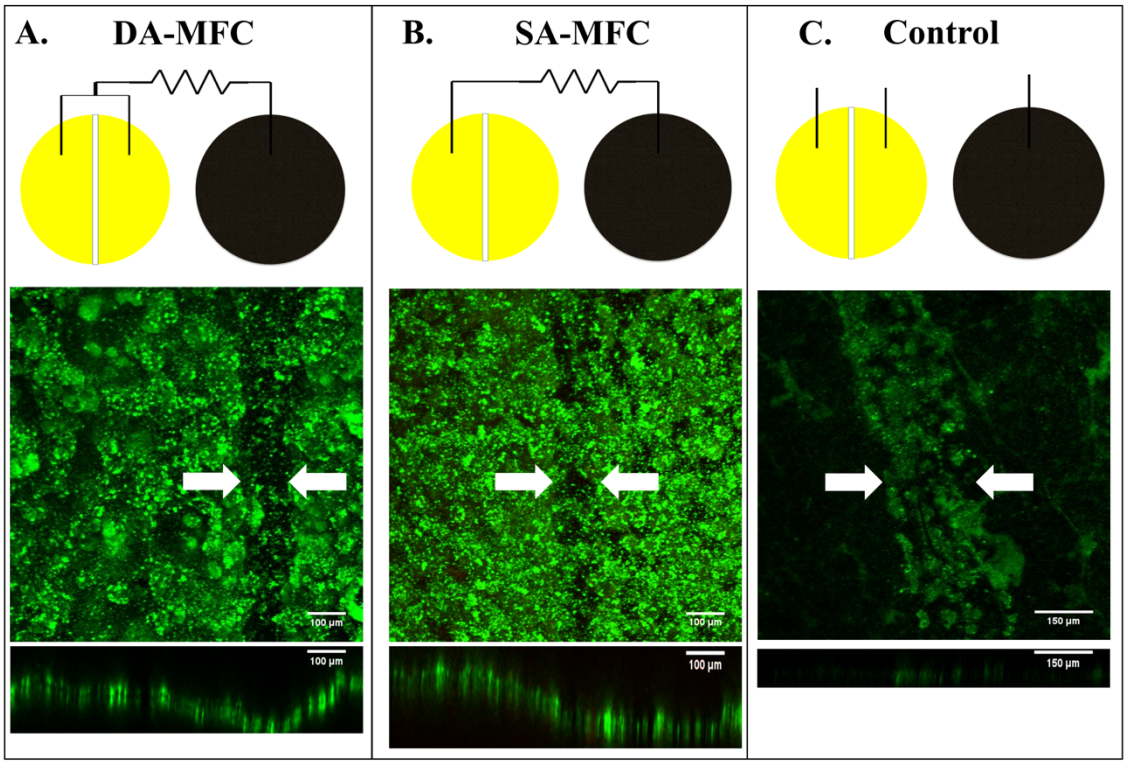

Figure 2.1. Top down CLSM images and schematic of MFC setup used for culture of exoelectrogenic biofilms. (A) Anode from DA-MFC with 50 µm non-conductive gap, (B) Anode from SA-MFC with 50 µm non-conductive gap, and (C) Electrode from control MFC with 300 µm non-conductive gap. Arrows indicate the location of non-conductive gap. Frame size = 8.1 X 10^{-3} cm^2.

Lab-maintained active MFC cultures were used as inoculum, which was originally from active sludge collected from the Corvallis Wastewater Treatment Plant (Corvallis, OR) and has been demonstrated to converge to a consistent community composition over extended periods of operation and across varying reactor designs when fed acetate (Lesnik & Liu, 2014). 30 mM of acetate was provided as the electron donor during the startup of MFCs which was increased to 60 mM after power outputs became stable. Modified *Geobacter* medium (MGM) (pH 7) was used in all experiments. The medium consists of the following ingredients (per liter): KCl, 0.13 g; NH_4Cl, 0.31 g; $NaH_2PO_4 \cdot H_2O$, 5.84 g; $Na_2HPO_4 \cdot 7H_2O$, 15.5g; vitamin, 12.5 mL; and mineral 12.5 mL solution as previously reported (Fan et al., 2012). MFCs were operated in fed-batch mode with external resistance decreased from 10,000 to 500 Ω between batches as the biofilms grew in order to maintain maximum cell voltages around 0.3 V. When voltages were under 5% of batch maximum, the media was removed and replaced with new media. The length of each batch was approximately 48 hours. Though activated carbon air-cathodes were used, anodic growth was considered to be anaerobic in nature (Cheng et al., 2006).

2.2.3 Conductivity measurements

Electrochemical analyses were performed to measure the in situ resistance/conductivity of biofilms. For all experiments a conventional three electrode configuration was used in which a split anode was used as the working electrode, a 5% platinum plate (6.45 cm^2) parallel to the split anode was used as the counter electrode, and a Ag/AgCl (3M NaCl) electrode was used as a reference. One half of the split anode

was used as the electron source and the other half of the split anode was used as electron drain (Malvankar et al., 2012c).

Initial experiments were conducted in order to evaluate biofilms over time at open circuit anode potential (OCP). In order to perform OCP conductivity measurements and to prevent interference from anodic current, the MFC anodes were temporarily disconnected from the cathode and allowed OCP to be reached. Then a voltage ramp (V_{app}) low enough to avoid the electrolysis of water or a self-heating effect was then applied between two halves of a split anode (0 – 0.075 V) in steps of 0.025 V by using a source meter (Model 2405, Keithley, USA). The potential of both halves of the split anode were then continuously measured through the use of reference electrodes (Ag/AgCl, 3M NaCl). The average of the potentials of the two anode halves was considered the midpoint potential (E_{mid}) of the biofilm, which was determined to be stable at -460 to -470 mV (vs. Ag/AgCl) in the presence of acetate containing media during open circuit conditions and when voltage ramps were applied (Figure 2.S1.A.). For each voltage step, transient ionic current related to counter-ion diffusion was allowed to decline for approximately 20 minutes until a steady state was reached (Dalton et al., 1990; Malvankar et al., 2011). Current was then recorded every 30 seconds over a period of 3 minutes. Biofilm resistance was calculated by plotting V_{app} against measured current thereby avoiding the measurement of catalytic current associated with acetate oxidation. Conductance was then calculated from the inverse of resistance. Measurements were taken approximately twice a week during operation. Measurements of conductivity conducted at OCP were performed in triplicate reactors (n=3).

To further measure biofilm resistance as a function of potential and to further examine conductive behavior of mixed-species biofilms in the presence and absence of electron donor, electrochemical gating analysis was performed based on the three electrode configuration (Malvankar et al., 2012c; Malvankar et al., 2011; Vanmaekelbergh et al., 2007). A potentiostat (References 100, Gamry Instruments Inc., Warminster, PA) in conjunction with the three electrode setup previously described was used to set the gate potential (V_g), which ranged from -600 to 200 mV (vs. Ag/AgCl) (Malvankar et al., 2011). V_g was increased in increments of 100 mV from -600 to -500 mV, 25 mV from -500 to -400 mV, 50 mV from -400 to -200 mV, and 100 mV from -200 to 200 mV. Concurrent with the setting of Vg, a source meter (Model 2405, Keithley, USA) was used to apply voltages (V_{app}) between the source and drain anode. The conducting currents at various V_{app} (0, 25, 50, and 75 mV) were measured and used to calculate resistance from the slope of the voltage-current curve as previously described in preceding paragraphs. Following changes to V_g or V_{app}, 20 minutes were waited before measurements were taken to allow the dissipation of transient ionic current. The changes of E_{mid} can be seen in Figure 2.S1.B. To measure biofilm conductivity in the absence of substrate, acetate-containing growth media was replaced with MGM containing no acetate to investigate conductive behavior in the absence of electron donor. Cell voltages of the MFCs dropped below 0.001 V within 24 hours following acetate removal and conductivity measurements were conducted by using two electrode method described above. Liquid samples were also collected and analyzed using high performance liquid chromatography (HPLC) to confirm that acetate was completely removed following

medium replacement. Additional control experiments were also conducted. These controls included experiments with a biofilm-less anode using MGM with acetate, MGM without acetate, and sterile-filtered effluent from active MFCs. For all electrochemical gating experiments, deoxygenated media were prepared by bubbling of nitrogen gas for 30 minutes. Experiments of electrochemical gating analysis were conducted using multiple reactors (n = 2).

2.2.4 Confocal laser scanning microscopy (CLSM)

Confocal laser scanning microscopy (CLSM) was used to verify biofilm growth across non-conductive gaps and on electrode surfaces in addition to measuring biofilm thickness. Following biofilm maturity, small pieces of the anodes (approximately 7 to 14 % of the total anodic surface area) were carefully cut, stained with LIVE/DEAD BacLight Bacterial Viaibility Kit (Molecular Probes, Eugene, OR, USA), and then examined with the Zeiss LSM 510 Meta confocal microscope with a 10X objective lens (Carl Zeiss AG, Oberkochen, Germany). A minimum of three fields were imaged. Images were further processed and analyzed by software ImageJ (ver. 1.49d). A minimum of ten random CLSM stacks along the y-axis were used to determine the average thickness of biofilm.

2.2.5 Fluorescent in situ hybridization (FISH)

Fluorescent in situ hybridization (FISH) was used to confirm the presence of *Geobacter* spp. within the biofilm using the Geo1A probe (Hugenholtz et al., 2002). For

FISH analysis, a small piece of biofilm containing anodes was cut out as described above. Select pieces were fixed for 1-2 hours in 4% paraformaldehyde/ phosphate buffered saline (PBS) in a 24-well cell culture plate and subsequently permeablized by treatment with lysozyme (70,000 U/ml) in buffer for 10 min at 37°C then rinsed with PBS. FISH was performed immediately after fixation following procedures previously described (Hugenholtz et al., 2002). Conditions were optimized with pure cultures of non-target strains and cultures of the target species by gradually increasing the formamide concentration in the hybridization buffer while maintaining equivalent ionic strengths and hybridization temperatures. Biofilms were first incubated in hybridization buffer consisting of 45% formamide, 20 mM Tris-HCl (pH 7.5), 0.9 M NaCl, and 0.01% SDS for 15 min at 46 °C, and then immersed in the same solution containing the Geo1A probe (2 μg/ml) for 3 hrs at 46 °C. Immediately following hybrization biofilms were soaked for 15 min at 48 °C in the washing buffer (Tris-HCl (pH 7.5), 0.03 M NaCl, 0.01% SDS, 5 mM EDTA). Biofilms were rinsed in saline, lightly dried, and then embedded in a Citiflour antifadent (London, UK) before being stored in the dark at room temperature between 3 – 48 hours prior to examination. Samples were then examined by the Zeiss LSM 510 Meta confocal microscope with 10X and 20X objectives. Images were processed using ImageJ software (ver. 1.49d). A minimum of three fields were selected to represent the whole examined area.

2.2.6 Biofilm Conductivity Calculation

Conformal mapping was used to calculate biofilm conductivity (σ) from biofilm thickness (g), determined through CLSM measurements, and biofilm resistance (R), determined through two-electrode measurements (Kankare & Kupila, 1992; Malvankar et al., 2011). The following equation was used, where D is the diameter of the electrode and a is the half of the width of the non-conductive gap:

$$\sigma = \frac{\pi}{RD} \Big/ \ln\left(\frac{8g}{\pi a}\right)$$

2.2.7 Cyclic voltammetry (CV)

Cyclic voltammetry (CV) was used to confirm direct electron transfer processes and identify major redox peaks in the mixed-species biofilms. Following growth, a three-electrode electrochemical cell setup was used. The anode containing a biofilm was used as the working electrode and a platinum plate (6.45 cm^2) was used as the counter electrode. An Ag/AgCl (3 M NaCl) was used as the reference electrode. For DA-MFCs, CV was performed in the presence and absence of acetate with substrate depletion confirmed through HPLC analysis. Biofilm-less control experiments were also conducted by filling control cells with the filtered MFC effluent. All CV experiments were performed by using a potentiostat (References 100, Gamry Instruments Inc., Warminster, PA) over a potential range from -600 to 200 mV vs. Ag/AgCl at a scan rate of 1 mV s^{-1}. For all CVs, deoxygenated media was prepared by bubbling nitrogen gas for 30 minutes.

2.3 Results

2.3.1 Growth and Spatial Distribution of Biofilms

CLSM imaging revealed that biofilms formed over the 50 μm non-conductive gaps between the two active anode surfaces connected to the circuit in DA-MFCs. Average biofilm thickness within the gap area of DA-MFCs was 38.4 ± 10.1 μm after approximately 70 days of growth (Figure 2.1.A.). Biofilm growth was also observed across the non-conductive gap in SA-MFCs with an average biofilm thickness of 52.2 ± 11.6 μm within the gap area (Figure 2.1.B.). Biofilm growth on the unconnected anode surface (~1 cm away from an active electrode surface) was observed in all anodes of SA-MFCs with less red pigment than active electrode surfaces (Figure 2.S2.). Control reactors with unconnected anodes displayed limited growth on gold-coated electrode surfaces and biofilms were too sparse for thickness to be measured (Figure 2.1.C.). *Geobacter* spp. were detected on both active and inactive anode surfaces of DA-MFCs and SA-MFCs but not detected on any electrode surfaces of control reactors (Figure 2.2.).

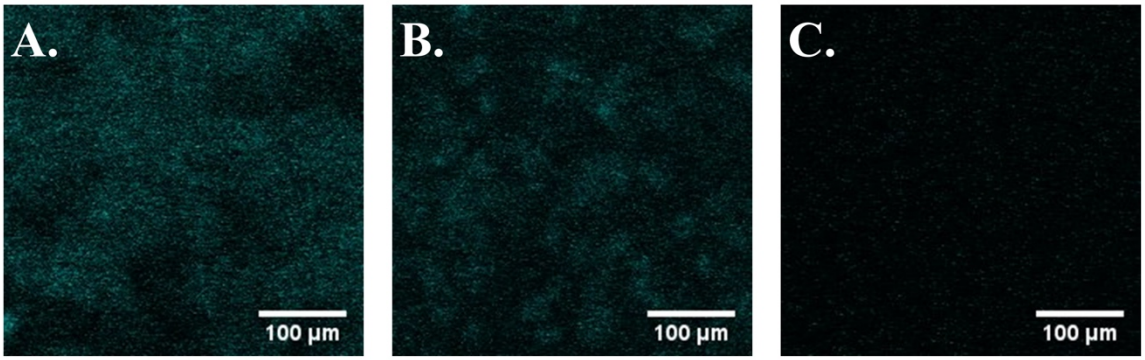

Figure 2.2. Fluorescent in situ hybridization images displaying *Geobacter* distribution. (A) On actively respired anode surface, (B) On non-actively respired surface of the same MFC, (C) On surface of control MFC. Frame size = 1.6 X 10^{-3} cm^2.

2.3.2 Current and Power Generation

Increases over time in electrical current and power generation were observed for both DA-MFCs and SA-MFCs (Figure 2.3.). When normalized to cathode surface area, power generation of SA-MFC reactors averaged 63.1% of the power generation of DA-MFC reactors, significantly greater than the 50% that would be expected if no exoelectrogenic growth was on the unconnected electrode surface (single factor t-test, α = 0.05). This observation suggests that the establishment of an electrical connection beyond the active electrode was simultaneously supported by the growth of exoelectrogens on the inactive anode surface of SA-MFCs and contributed to power generation.

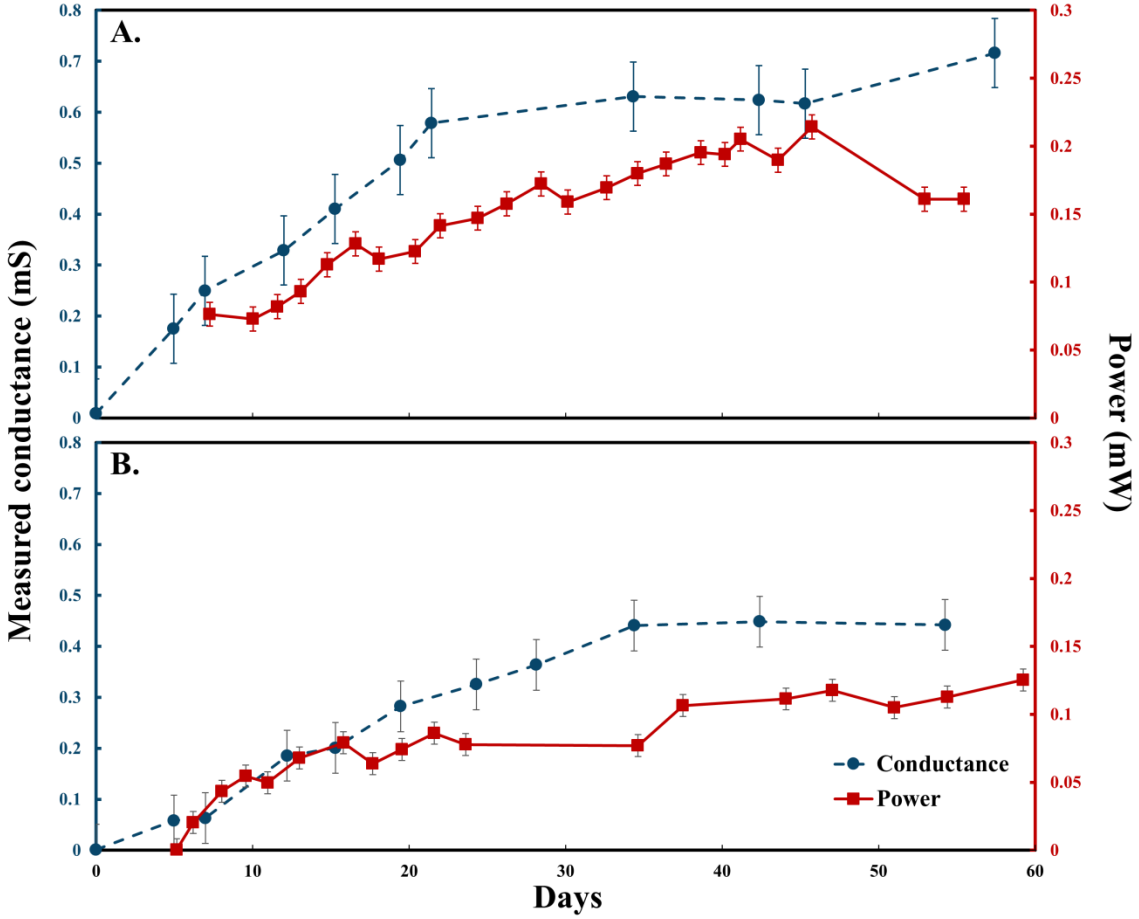

Figure 2.3. Measured conductance and power of DA-MFCs and SA-MFCs over time. (A) DA-MFC with 50 µm non-conductive gap, (B) SA-MFC with 50 µm non-conductive gap. Error bars represent standard deviation (n = 3).

2.3.3 Conductivity of Mixed-Species Biofilms

Initial conductance was calculated during growth at biofilm mid-point potentials (E_{mid}) of -470 mV (vs. Ag/AgCl) corresponding to open circuit potentials of anode.

Conductance was observed in both DA- and SA-MFC reactors and increased as biofilms grew across non-conductive gaps (Figure 2.3.). Initial increases in power were correlated to increases in conductance yet continued to increase after conductance plateaued. This is likely due to stacking of active biomass enabled by the conductivity of the inner biofilm structure. Average biofilm conductivity for DA-MFCs was 679.4 ± 15.6 μs cm^{-1}. This conductivity is significantly higher than that calculated for the open-circuit control reactor using average biofilm thickness of DA-MFCs (3.2 ± 1.5 μs cm^{-1}). Increases in conductance proceeded slower in SA-MFC setups likely due to a single point of origin for exoelectrogenic growth across the gap (Figure 2.3.B.). The average conductivity of SA-MFC reactors was 285.2 ± 52.3 μs cm^{-1} at the same E_{mid}, corresponding to a 58.2% decrease compared to DA-MFCs.

After the conductivity plateaued, conductivity was then further analyzed over a range of potentials using electrochemical gating analysis. Results revealed that the conductivity of mixed-species biofilms changed in a peak-manner based on gate potential (V_g) (Figure 2.4.A.). Maximum conductance of the mixed-species biofilms was 3437 ± 271 μS corresponding to a V_g of -350 mV (vs. Ag/AgCl). Conductance of biofilms poised at a V_g more negative than -500 mV or more positive than 0 mV were significantly decreased. Measurements in both control experiments using the same electrode geometry but without established biofilms did not exhibit a peak in conductivity and only marginal conductivity was observed (0.8 to 15.3 μS), indicating that the observed conductivity was related to the development of an exoelectrogenic biofilm.

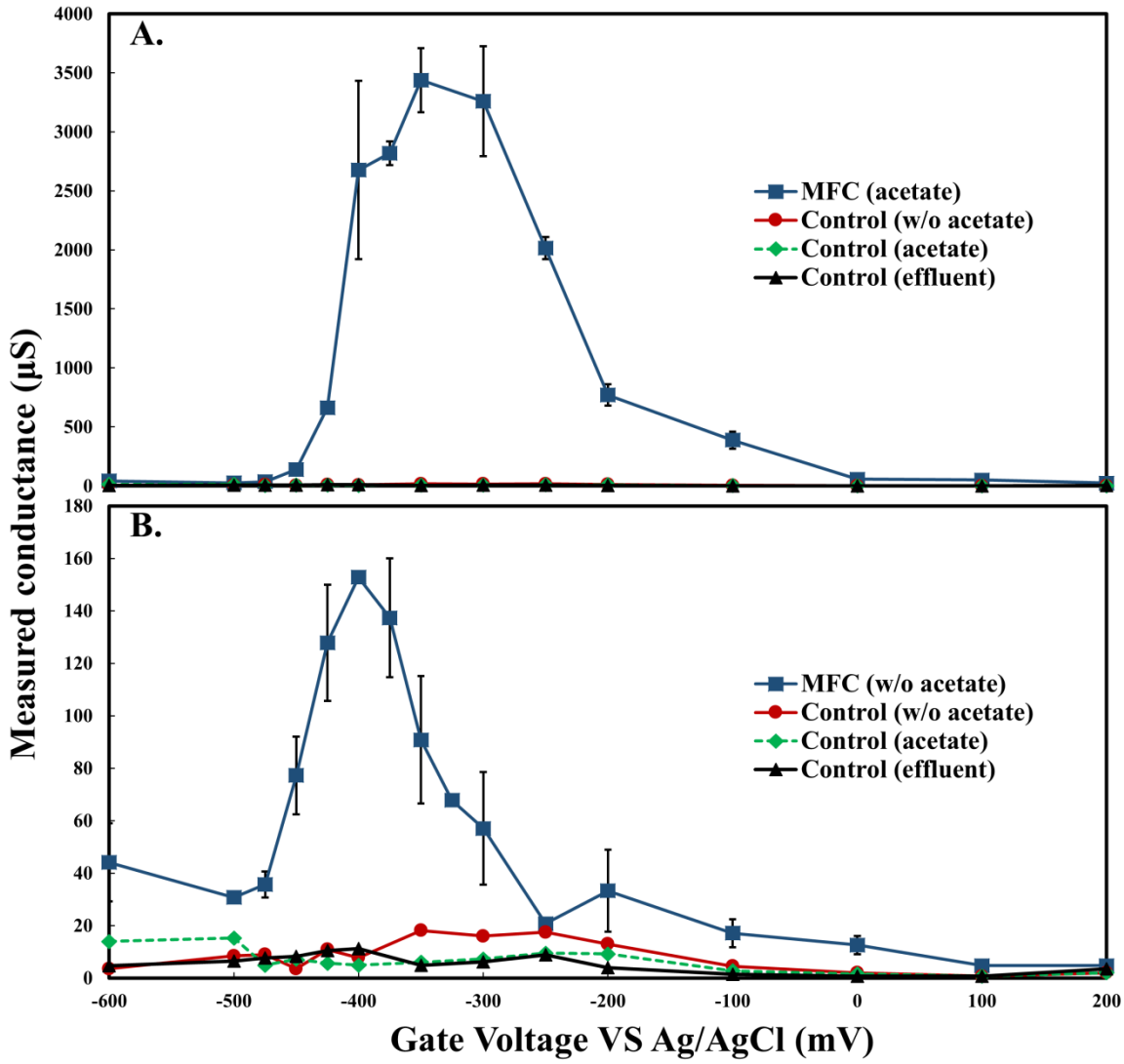

Figure 2.4. Conductivity of mixed-species biofilms and control estimated by electrochemical gating analysis. Error bars represent standard deviation (n = 2).

To investigate the effect of electron donors on biofilm conductivity, measurements were also performed in the absence of acetate. Following the removal of

acetate from the growth media, electrical current production ceased (Figure 2.S3.). Peak conductance estimated through electrochemical gating analysis shifted from -350 mV to -400 mV (vs. Ag/AgCl) while maximum conductance decreased from 3437 ± 271 μS to 153 ± 2 μS (Figure 2.4.B.). After acetate was added back to the growth media current production in each reactor recovered immediately indicating biofilms remained intact during acetate removal testing (Figure 2.S3.).

2.3.4 Cyclic Voltammetry

In the absence of electron donor, two major redox peaks were identified at potentials of -370 and -310 mV (vs. Ag/AgCl) (Figure 2.5.A.). Multiple additional peaks from -300 to -600 mV (vs. Ag/AgCl) were also detected suggesting the existence of multiple redox cofactors spanning a range around formal potentials similar to what have been observed previously (Bond et al., 2012; Fricke et al., 2008). No redox peaks were observed in the control electrochemical cell (biofilm-less anode) with filtered MFC effluent. These results indicate that observed current can be attributed to the altering of the oxidation state of these redox cofactors localized in present biofilms and electrochemical activity can be attributed to membrane-bound redox cofactors like outer membrane cytochromes (OMCs) as opposed to extracellular electron shuttles (Bond et al., 2012; Fricke et al., 2008). In the presence of acetate, the midpoint of catalytic current associated with the oxidation of acetate occurred at -360 mV (vs. Ag/AgCl) similar to the primary peaks observed in the absence of acetate (Figure 2.5.B.). In biofilm-less reactors no current response was observed.

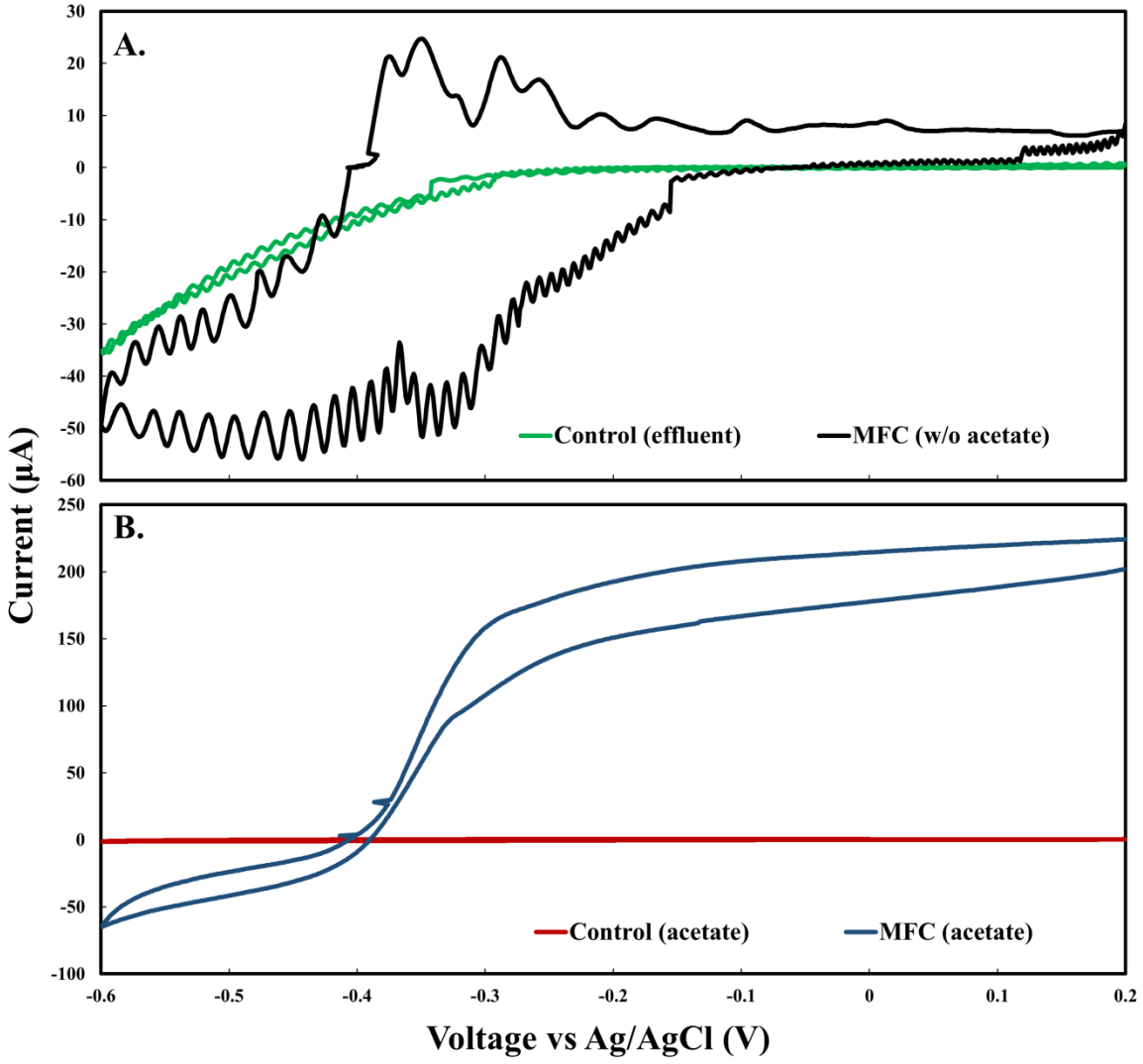

Figure 2.5. Cyclic voltammograms of mixed-species biofilm. The voltammograms were recorded (A) in the absence of electron donor and (B) in the presence of electron donor. Scan rate was 1 mV S^{-1}.

2.4 Discussion

2.4.1 Properties of Mixed-Species Biofilms

The most significant difference between previous studies featuring pure cultures and the present one featuring a mixed-species community is the response of conductivity to the removal of an electron donor. In previous studies using single species exoelectrogenic biofilms were not significantly influenced by the removal of acetate (Malvankar et al., 2011). However, in the present study, when acetate was removed from the medium decreases in peak conductivity as large as 96.6% were observed along with simultaneous -50 mV shift in biofilm potential at which maximum conductivity occurs. These differences reflect changes in the type and activity of localized redox cofactors as well as magnitude of electron accumulation within the biofilm (Bond et al., 2012; Ruhl et al., 2014). Another difference between previous studies featuring single species biofilms and the mixed-species biofilms of the present study is the ability to establish growth on an inactive electrode 1 cm away from an active electrode (Figure 2.1. & 2.2.) (Malvankar et al., 2012c; Malvankar et al., 2011). The extended growth in the mixed-species environment was possible due to the presence of alternate redox factors and the likely presence of interspecies coadhesion interactions that enable extended growth distances from active electrodes. mixed-species environments (Liu & Bond, 2012; Rotaru et al., 2014a; Rotaru et al., 2014b; Summers et al., 2010).

2.4.2 Conductive Mechanisms

Further investigation into the conduction mechanism of mixed-species exoelectrogenic biofilm was conducted by measuring biofilm conductivity as a function of potential. A conductivity peak was observed around a V_g of -360 mV (vs. Ag/AgCl), similar to the formal potential of c-type cytochromes associated with other exoelectrogenic biofilms (Richter et al., 2008). The peak-manner response observed is a characteristic of a redox molecule-mediated electron transfer mechanism like that of conductive polymers (Dalton et al., 1990; Ohsaka et al., 1987). Classically, this electron transport is considered to be driven by concentration gradients of localized reduced and oxidized redox cofactors though voltage gradients may also be responsible. Either way the fundamental electron hopping event is unchanged and can be unified under generalized thermodynamic forces (Dalton et al., 1990). Concentration gradient driven electron transfer is dependent on a mixed valent state and maximized at potentials in which the ratio of reduced and oxidized redox sites within the matrix are equal (Dalton et al., 1990). If redox sites are completely reduced or oxidized within the biofilm matrix, the biofilm will become non-conductive as observed in the present study when V_g was more positive than 0 mV or more negative than -500 mV. Overall support of a concentration gradient driven conduction mechanism in the present study is consistent with previous research presenting an electron hopping model of electron transfer in single species biofilms of *G. sulfurreducens* (Snider et al., 2012; Strycharz-Glaven et al., 2011).

2.4.3 Biofilm Conductivity Evaluation Methods

Despite the importance of constructing conductive biofilms/aggregates as direct extracellular electron transfer conduits, few studies have been published related to conductive biofilms/aggregates and their conduction mechanisms. In the present study, a practical two-electrode setup was used to allow the measurement of conductive current in microbial biofilms. Experiments were designed to ensure accurate measurements of conductivity of biofilms. First, the large conductive surface areas of the two electrodes (3.5 cm^2) combined with a thin non-conductive gap (50 um) ensured proper biofilm development on the active electrode surfaces and the nonconductive gaps, allowing the measurement of conducting current. Second, steady state experiments were used to avoid measuring transient ionic current (Dalton et al., 1990). In the case of redox gradient driven electron conduction, the self-exchange of electrons between the redox sites is accompanied with the diffusion of counter-ions for the sake of electroneutrality (Dalton et al., 1990). Third, appropriate means were employed to account for catalytic current related to acetate oxidation (Bond et al., 2012). In addition to removing the electron donor during electrochemical gating analysis, the slope of V_{app} versus current was also used in the calculation to avoid the inclusion of the catalytic current.

Additional tests to further elucidate conduction mechanisms of biological materials include examining redox potential dependency, temperature dependency, pH dependency, and behavior following exposure to several inhibitors (Malvankar et al., 2011). However, many of these experiments might induce destruction of the delicate

biofilm structure and should be carefully conducted to ensure the intactness of biofilms. Electrochemical gating analysis used in present study is relatively moderate redox gradient dependency test, and should be carried out within biological range based on previous observations (Malvankar et al., 2012c; Malvankar et al., 2011). The relationship between biofilm conductivity and electrochemical potential also suggests that biofilm conductivity should be reported along with the potential at which the measurement was performed.

2.5 Conclusions

Mixed-species communities will continue to play a critical role in many MESs. The current study provides an initial reference point for the conductive behavior of mixed-species biofilms. Differential responses were observed in the absence of an electron donor and over varying potentials suggesting redox driven conductivity of the mixed-species exoelectrogenic biofilms. The construction of these conductive biofilms is clearly one strategy that communities use to effectively take advantage of inexhaustible, insoluble electron acceptors in addition to also providing a conduit for direct electron transfer that is the foundation of many synergistic relationships. Further understanding the conductive behavior and electronic interactions of these communities will lead to improvements of power and efficiencies in MESs, and may potentially open up new bioelectronics applications.

Acknowledgements

The authors wish to acknowledge Anne-Marie Girard and the Confocal Microscopy Facility of the Center for Genome Research and Biocomputing (CGRB) and the Environmental and Health Sciences Center at Oregon State University for confocal support, Mark Dasenko at CGRB for sequencing support, Teresa Sawyer and the Electron Microscope facility at Oregon State University, and the equipment provided by Microproducts Breakthrough Institute.

Supporting Information

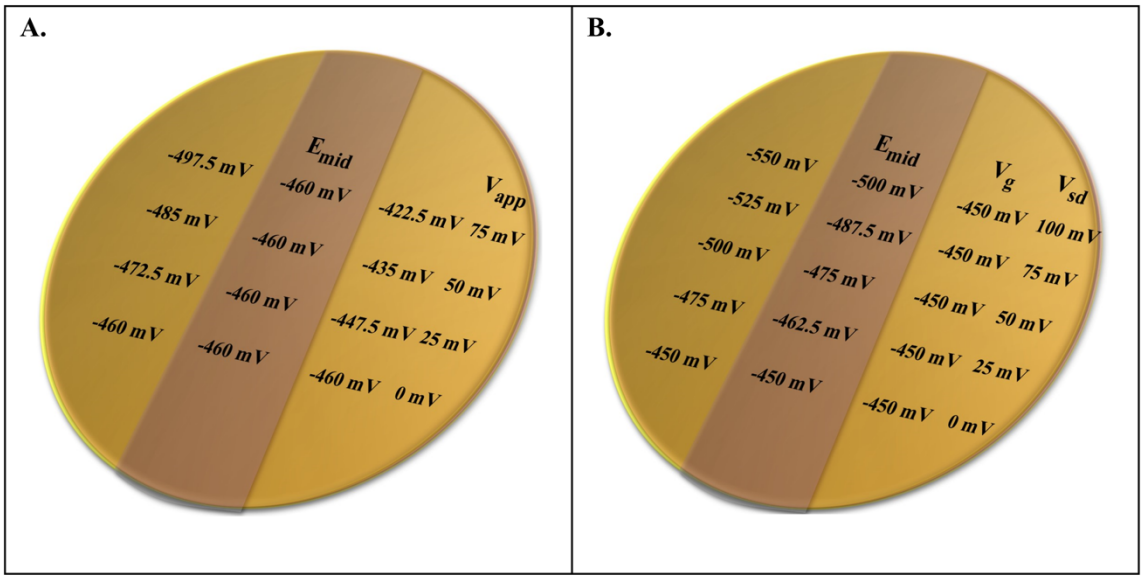

Figure 2.S1. Changes of midpoint potentials during experiments. (A) two-electrode experiment (B) electrochemical gating analysis.

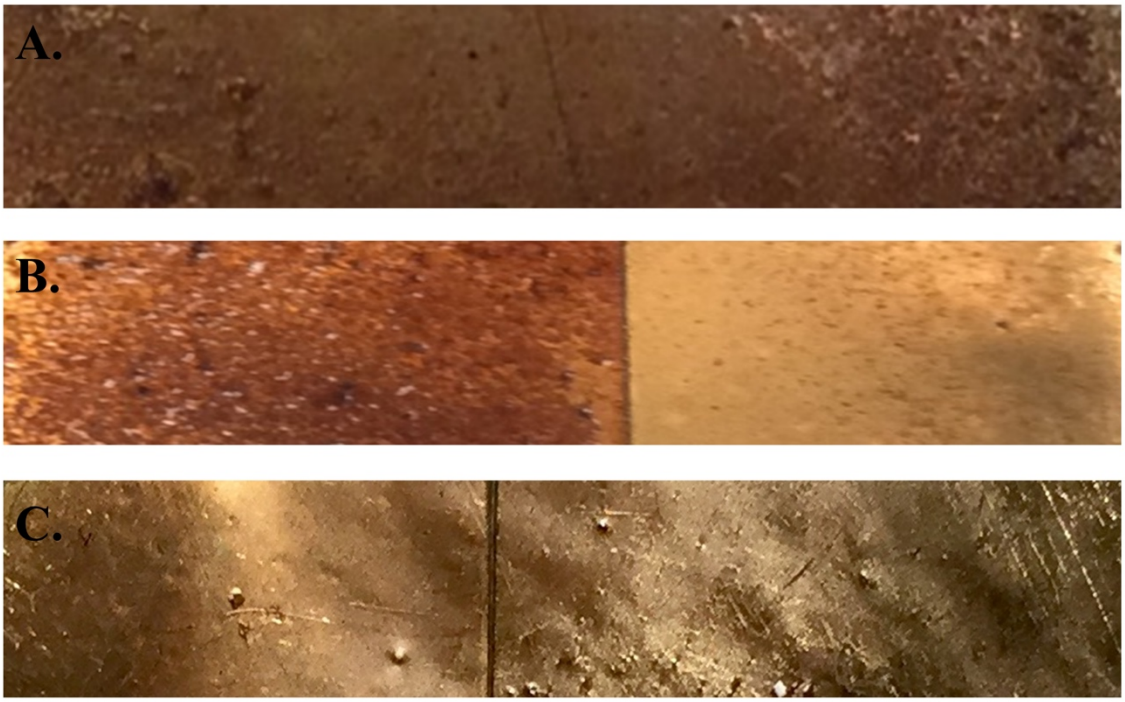

Figure 2.S2. Top down digital camera pictures. (A) Anode from DA-MFC, (B) Anode from SA-MFCs, and (C) Bare surface of gold electrode.

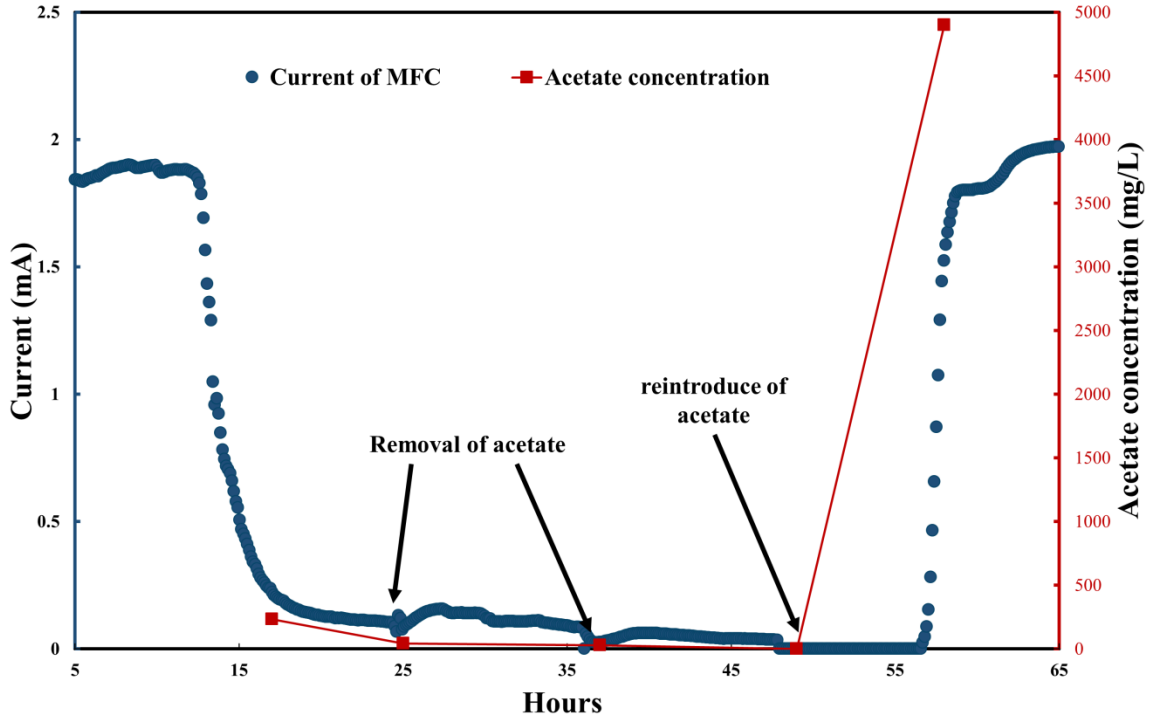

Figure 2.S3. Acetate removal experiment. Blue round dots represent the current of MFC and red solid line represents the acetate concentration detected by HPLC.

3 Millimeter Scale Electron Conduction through Exoelectrogenic Mixed-Species Biofilms

Cheng Li, Keaton Larson Lesnik, Yanzhen Fan, and Hong Liu

FEMS microbiology letters
June 7, 2016
https://doi.org/10.1093/femsle/fnw153

Abstract: The functioning of many natural and engineered environments is dependent on long distance electron transfer mediated through electrical currents. These currents have been observed in exoelectrogenic biofilms and it has been proposed that microbial biofilms can mediate electron transfer via electrical currents on the centimeter scale. However, direct evidence to confirm this hypothesis has not been demonstrated and the longest known electrical transfer distance for single species exoelectrogenic biofilms is limited to 100 μm. In the present study, biofilms were developed on electrodes with electrically nonconductive gaps from 50 μm to 1 mm and the in situ conductance of biofilms was evaluated over time. Results demonstrated that the exoelectrogenic mixed-species biofilms in the present study possess the ability to transfer electrons through electrical currents over a distance of up to 1mm, 10 times further than previously observed. Results indicate the possibility of interspecies interactions playing an important role in the spatial development of exoelectrogenic biofilms, suggesting that these biological networks might remain conductive even at longer distance. These findings have significant implications in regards to future optimization of microbial electrochemical systems.

Keywords: Microbial Fuel Cell, Biofilm, Conductivity, Exoelectrogenic bacteria, Extracellular Electron Transfer

3.1 Introduction

The average bacterium is only ~ 2 μm in length yet electron transfer over distances that are on the order of 10^3 to 10^6 fold greater are essential to the metabolism of several microorganisms (Lovley, 2011a; Lovley, 2011b; Reguera, 2012; Reguera, 2011). The efficiency with which electron transfer can be accomplished is not only critical to energy conservation within collections of cells but also vital to the performance of several microbial electrochemical systems (MESs) (Lovley, 2011a; Malkin et al., 2014). Recently, the prevalence of electron transfer over extended distances via electrical currents has been recognized in several natural and engineered environments (Lovley, 2012; Malvankar & Lovley, 2014; Reguera, 2012; Reguera, 2011). Electrical currents offer clear temporal and efficiency advantages over the diffusion of small molecules in regards to electron transfer particularly in diffusion limited environments like biofilms and anoxic sediments (Lovley, 2012; Lovley, 2011a; Lovley, 2011b). For this reason, it is not surprising that bacteria have evolved a diverse means of electrical conduction. Exoelectrogenic bacteria, capable of transferring electrons extracellularly, have been well studied due to their biotechnological relevance and are ubiquitous in anoxic sediments and other anaerobic environmental systems (Logan, 2009). The most prominent of these are *Geobacter sulfurreducens* and *Shewanella oneidensis*, used as model systems for electron transfer and recognized for their ability to conduct electrons through specialized appendages like microbial nanowires and c-type cytochromes (El-Naggar et al., 2010; Kato et al., 2012a; Kato et al., 2012b; Liu et al., 2015; Malvankar et al., 2012a; Malvankar et al., 2012c; Nakamura et al., 2010; Shrestha & Rotaru, 2014). Although no

consensus has been reached on the mechanism of electron transfer along nanowires nor the function served by the semi-conductive minerals they are central to the construction of conductive biofilm networks (Kato et al., 2012a; Kato et al., 2012b; Malvankar et al., 2012a; Malvankar et al., 2011; Snider et al., 2012; Strycharz-Glaven et al., 2011).

Another example of electron transfer through electrical currents has also been recognized in filamentous bacteria belonging to the family *Desulfobulbaceae*. In these bacteria electrons are transferred through cable-like filaments in which a charged internal environment is enclosed in an insulative outer membrane (Malkin et al., 2014; Nielsen & Risgaard-Petersen, 2015; Pfeffer et al., 2012; Risgaard-Petersen et al., 2015). The presence of these filaments putatively connects sulphide oxidation in the anoxic layer to oxygen reduction in the oxic layer separated by 1.4 – 1.8 cm, over 100 fold further than observations of biofilm mediated electrical currents. These hypotheses were established on the observations of changed rates of oxygen consumption in sediment layers rather than direct measurement of electrical current and conductivity (Malkin et al., 2014; Malvankar et al., 2014a; Pfeffer et al., 2012).

Electrical conductivity has been recognized as an important property in both single and mixed-species exoelectrogenic biofilms (Li et al., 2016b; Malvankar et al., 2012a; Malvankar et al., 2011). Electron transfer mediated by biofilm conductivity on a centimeter scale has been proposed as a means of efficient long range transfer in natural and engineered environments, but has yet to be demonstrated. Single-species biofilms of *G. sulfurreducens* were the conduit for the longest biofilm mediated electron transfer distance previously observed, but the 100 μm distance reported is significantly less than

hypothesized in many environments (Malvankar et al., 2012c; Malvankar et al., 2011). However, interspecies interactions in mixed-species communities result in differential conductive behaviors and may lead to spatial distributions that promote extended electron transfer distances over those previously observed (Kouzuma et al., 2015; Li et al., 2016b).

To evaluate the conduction distance of exoelectrogenic mixed-species biofilms the conductance of such biofilms over non-conductive gaps with various widths from 50 μm to 1 mm was measured. Results demonstrate the ability of the conductive mixed-species exoelectrogenic biofilms to transfer electrons via electrical currents on the millimeter scale, 10 fold greater than previously observed in any biofilms, with further expansion possible.

3.2 Materials and Methods

3.2.1 Electrode Preparation

A split anode design was adapted from previous study to perform in situ measurement of biofilm conductivity (Malvankar et al., 2011). To construct split anode, a water resistant adhesive (Loctite, Düsseldorf, Germany) was applied to standard weighing paper (Schleicher & Schuell, Inc., Keene, NH, USA). Adhesive laden paper was then cut into a circle with area of 7 cm^2, and an electrically conductive gold film with a thickness of 5 μm was applied onto the adhesive layer by a Cressington 108 Auto sputter coater (Cressington Scientific, Watford, UK). A ESI 5330 UV Laser machine (Electro Scientific Industries, Inc., Portland, OR, USA) was used to create nonconductive gap with various width (50, 150, 300, and 1000 μm) at the center of electrode. To ensure

electrical separation of the two halves of the split anode, resistance measurements across the gap were conducted using a source meter (Model 2405, Keithley, USA). The gap was considered electrically separated if $R_{gap} > 10^{10}$ Ω.

3.2.2 Microbial Fuel Cell (MFC) Design and Operation

Single chamber air cathode MFCs with the gold-coated split-anodes were used to develop biofilms on the anode surface. The procedure to fabricate carbon cloth/activated carbon cathode was developed similar to a previous study (Janicek et al., 2015). The projected surface areas of anode and cathode were 7 cm^2 and the total MFC liquid volume was 12 mL. To evaluate the possible distance of biofilm mediated electron transfer, both halves or only one half of the split anode were connected to cathode (Figure 3.1.). MFCs labeled 'MFC' contained anodes in which both halves of the split anode were connected to cathode by resistor, while for MFCs labeled 'SA-MFC' only one half of the split anode was connected to cathode. Replicates were used (n=3) to ensure the repeatability of experiments. Control reactors contained split electrode that neither of the two halves was connected to cathode. Sufficient replicates were used (n=3) to ensure the repeatability of experiments.

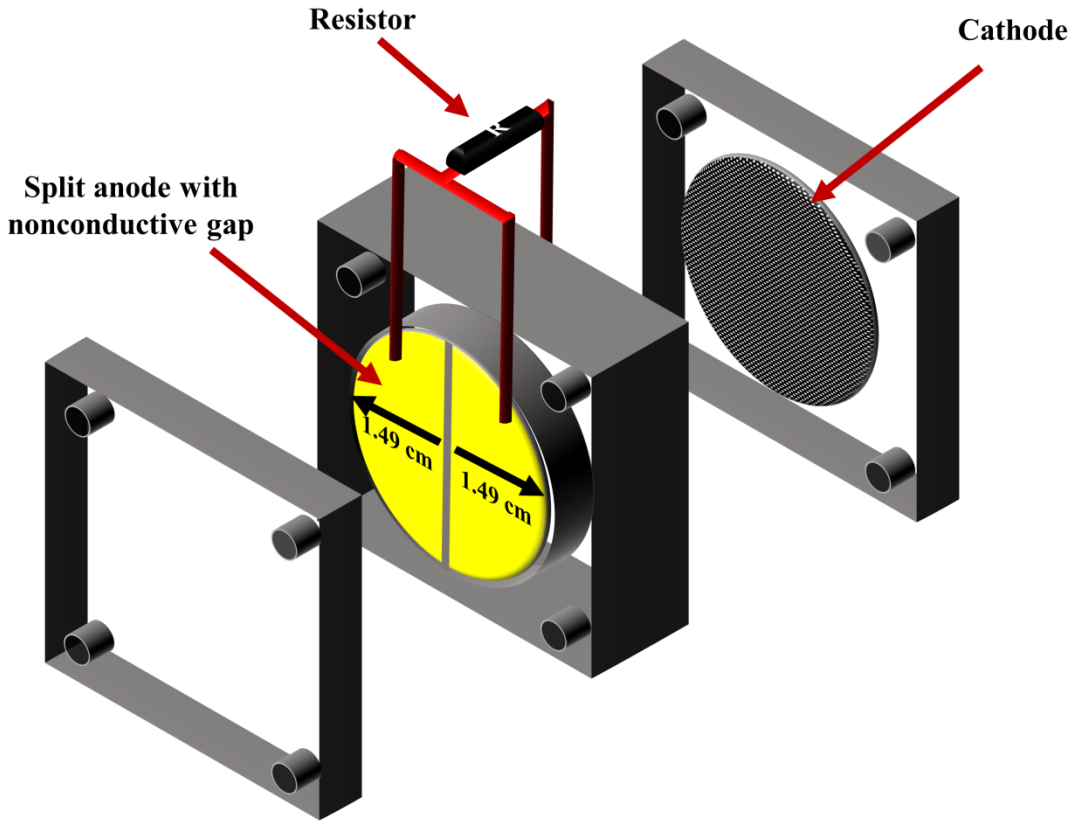

Figure 3.1. Schematics of MFC with both halves of the split anode connected by resistor to cathode.

Lab-maintained active MFC cultures enriched from active sludge of Corvallis Wastewater Treatment Plant (Corvallis, OR) were used as inoculum. This community has been demonstrated to maintain a relative consistent community composition over extended periods of operation and across reactor designs when fed with acetate (Lesnik & Liu, 2014). Modified Geobacter medium (MGM) (pH 7) containing (per liter of solution) KCl, 0.13 g; NH_4Cl, 0.31 g; $NaH_2PO_4 \cdot H_2O$, 5.84 g; $Na_2HPO_4 \cdot 7H_2O$, 15.5g; vitamin, 12.5

mL; and mineral 12.5 mL solution was used in all experiments. During the startup of MFCs, 30 mM of acetate with MGM buffer was used to avoid the substrate inhibition. When the current production became stable, the concentration of acetate was raised to 60 mM and maintained till the rest of the study. All cells were operated in fed-batch mode with external resistance decreased from 10,000 to 500 Ω. When voltages were under 5% of batch maximum, the media was removed and replaced with new media, to maintain optimal cell voltages around 0.3 V.

3.2.3 Two-Electrode Conductivity Measurement

To evaluate in situ biofilm conductance, MFC anode was temporarily disconnected from cathode and was allowed to reach open circuit potential (460 - 470 mV vs. Ag/AgCl). A voltage low enough to avoid the electrolysis of water or a self-heating effect was applied between two halves of a split anode (0 – 0.075 V) in steps of 0.025 V by using a source meter (Model 2405, Keithley, USA). For each voltage step, transient ionic current related to counter-ion diffusion was allowed to decline for approximately 20 minutes until steady state was reached. Current of each voltage step was recorded every 30 seconds over a 3 minutes period. A slope was generated by plotting average currents against applied voltages and was also used in the calculation of biofilm conductance to avoid the inclusion of the current of acetate oxidation. Measurement of conductance was performed similarly in control reactors in which biofilm growth was not supported.

3.2.4 Confocal Laser Scanning Microscopy (CLSM)

Biofilm growth on the split electrode was examined by confocal laser scanning microscope (CLSM). When the measured conductance and maximum power of MFCs plateaued for 4 weeks, biofilms were considered to be mature. Electrodes from all reactors were then carefully taken out. A small piece of the electrodes was then gently cut and stained with LIVE/DEAD BacLight Bacterial Viaibility Kit (Molecular Probes, Eugene, OR, USA) following the instructions of manufacturer. Stained specimens were then examined with the Zeiss LSM 510 Meta confocal microscope with a 10X objective lens (Carl Zeiss AG, Oberkochen, Germany). ImageJ (1.49d) was used to process images.

3.2.5 Statistical Analysis

Correlation coefficient r was generated by using analysis package in Microsoft Excel and a correlation coefficient greater than 0.8 ($n>10$) was considered as positively correlated, $P < 0.05$ was considered to be statistically significant.

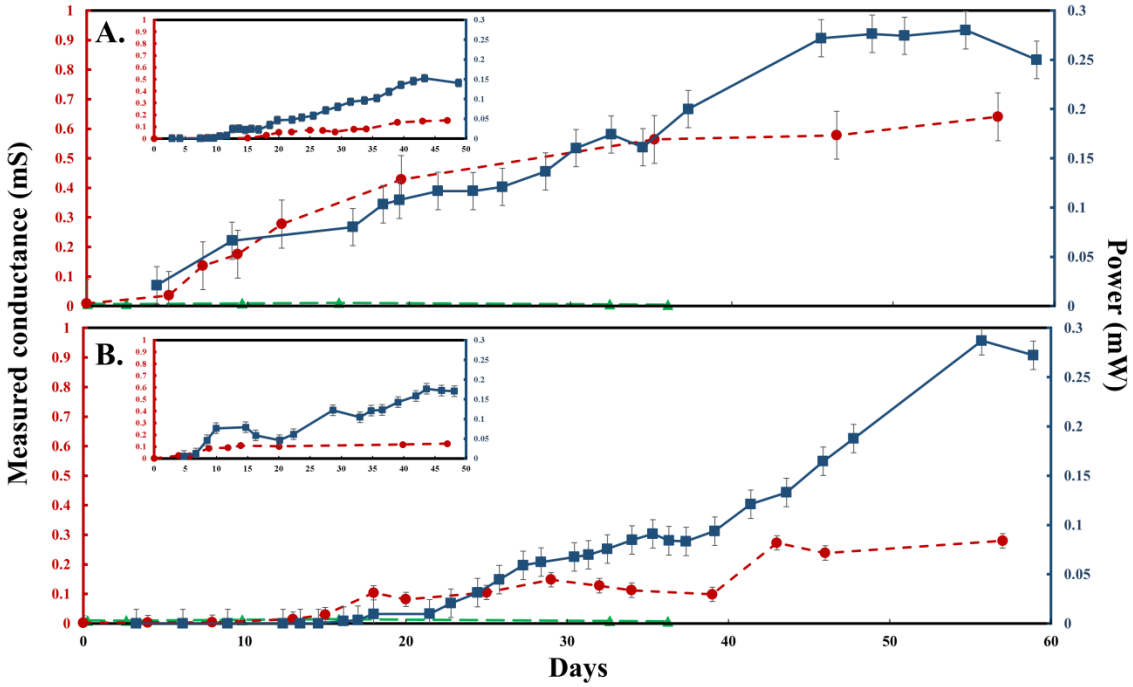

Figure 3.2. Measured conductance and power of MFCs over time: (A) from reactors with 300 µm non-conductive gap and (B) from reactors with 1000 µm non-conductive gap. Inserts: measured conductance and power of SA-MFCs over time. Red and green dash line represent the measured conductance of MFCs and control reactors, and blue solid line represents the power. Error bars indicate the standard error of individual measurements of several MFCs (n=3).

3.3 Results and Discussion

Following inoculation of the MFC reactors, measured conductance continually increased over time indicating growth of conductive biofilms across the gaps (Figure 3.2.). Conductance values of all gap width increased on the order of 100 to 300 fold from

the initial average conductance value of 0.005 mS to 0.53 mS. No increase in conductance was observed in controls without connection between anode and cathode. Starting from 150 μm, observed electron transfer distances that can be mediated by biofilms in present study are greater than previous reported for any exoelectrogenic biofilm (Malvankar et al., 2012c; Malvankar et al., 2011). When one side of the split anode was left unconnected during biofilm development in single-anode MFCs (SA-MFCs) (Table 3.1.), similar results were yield. Increases in conductance proceeded slower in SA-MFCs compared to MFCs, likely due to a single point of origin for exoelectrogenic growth (inserts of Figure 3.2.). Average biofilm conductance decreased as gap width increased (Figure 3.3.). This may be a result of lower overall concentrations of redox active sites across longer gaps, suggestive of redox concentration gradient driven electron transfer mechanism previously observed in *G. sulfurreducens* biofilms (Snider et al., 2012; Strycharz-Glaven et al., 2011). When the gap width increased, the ratio of exoeletrogenic to non-exoelectrogenic bacteria in gap area decreased possibly due to the increased hindrance of donating electron to active electrode, causing dilution to concentration of electroactive sites similar to previous observation in conductive polymer film (Ohsaka et al., 1987). Further support of this hypothesis is that conductance of SA-MFCs was significantly lower than conductance of MFCs ($P < 0.05$).

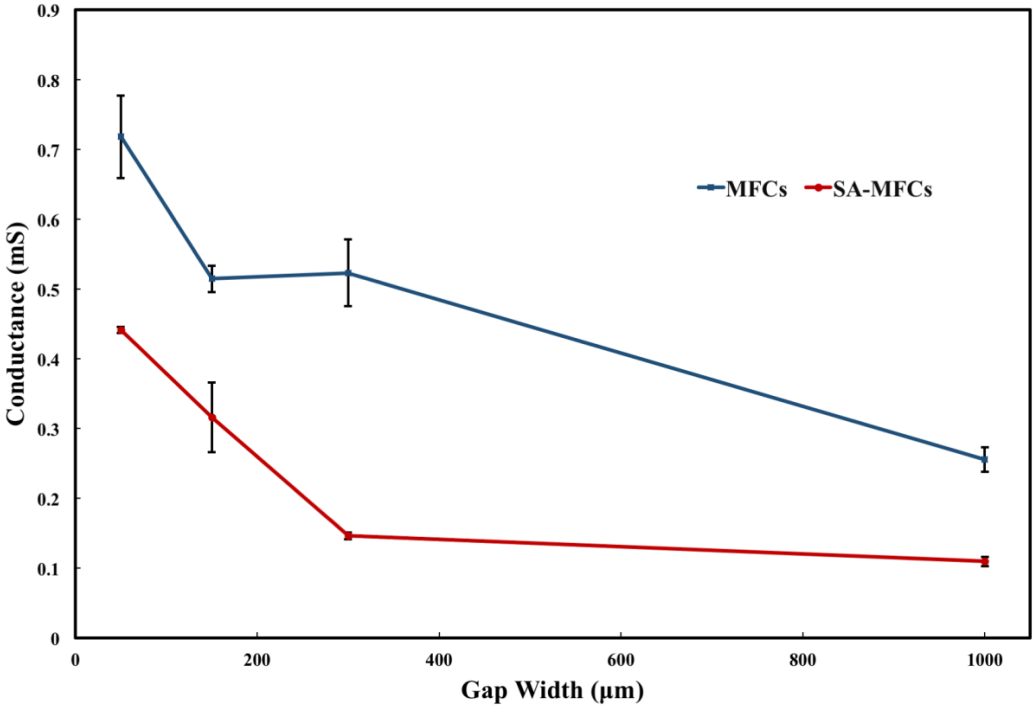

Figure 3.3. Conductance of MFCs and SA-MFCs over gap width after day 70. Error bars indicate the standard error of individual measurements of several MFCs (n=3).

TABLE 3.1. Average power and biofilm thickness in MFCs and SA-MFCs reactors.

	MFCs				SA-MFCs			
Gap Width (μm)	50	150	300	1000	50	150	300	1000
Power (mW)	0.19±0.01	0.14±0.02	0.25±0.02	0.17±0.00	0.11±0.01	0.15±0.01	0.15±0.00	0.14±0.01
Biofilm Thickness (μm)	38.4±10.1	49.3±11.7	60.3±12.9	50.0±10.3	52.2±11.6	44.1±7.4	39.5±8.7	62.3±17.7

* Error bars indicate the standard error of individual measurements of several MFCs (n=3).

Biofilm growth across the non-conductive gaps was further confirmed using CLSM (Figure 3.4.). Average biofilm thickness across the nonconductive gaps was 50.1 ± 3.5 µm. Some growth was observed on electrode of control reactors that were inoculated but without a closed circuit. However, biofilm growth of these reactors was too sparse for thickness to be measured. While results of previous studies using pure cultures of *G. sulfurreducens* indicate that exoelectrogenic singles species biofilms were unable to extend more than 100 µm from active electrodes (Malvankar et al., 2012c; Malvankar et al., 2011), exoelectrogenic mixed-species biofilms of present study were able to extend 1 mm. In mixed-species environments, coadhesion or coaggregation could be initialized by various species and further expansion of the conductive matrix on the order of centimeters may even be possible (Ruhl et al., 2014).

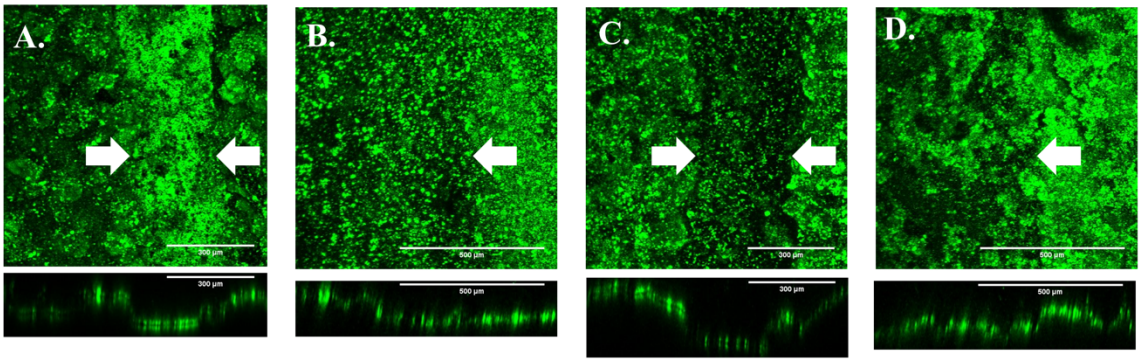

Figure 3.4. Top down CLSM images of anodes: (A) from MFCs anode with 300 µm nonconductive gap, (B) from MFCs anode with 1000 µm nonconductive gap, (C) from SA-MFCs anode with 300 µm nonconductive gap, and (D) from SA-MFCs anode with 1000 µm nonconductive gap. Arrows indicate the location of non-conductive gap. Frame size = 8.1 X 10^{-3} cm^2.

Power generation was found to be positively correlated with conductance in both MFCs and SA-MFCs ($r > 0.8$) and statistically significant ($P < 0.05$). The correlation between conductivity and power is suggestive of an increase in biomass contact with an active electrode due to conductance enabling vertical stacking and longitudinal expansion. The establishment of conductivity in three dimensional space not only enables the transfer of electrons to the anode following oxidation of the substrate from superficial biomass distal from the anode surface, but also enables electron transfer from one half of the split anode to the other.

Conductivity is undoubtedly an important property of exoelectrogenic biofilms in relation to energy conservation during electron transfer (Malvankar et al., 2012a; Malvankar et al., 2012c). However, the connection between power output and conductivity of biofilms in mixed-species settings remains unclear. Exoelectrogenic single species biofilms containing higher concentrations of redox proteins may possess higher measurable conductivity (Kato Marcus et al., 2007). In environments limited by substrate diffusion and utilization, interspecies interactions that allow for increased biomass access to a limited respirable surface area and enhanced product removal by complimentary species may lead to the observed increases in performance in regards to power output.

The results of the present study provide evidence for biofilm mediated electron transfer on the millimeter scale, 10 times greater than previously observed. In natural environments conductive biofilms are likely an essential means of facilitating long distance electron transfer that is the foundation of many biogeochemical processes (Kato

et al., 2012a; Kato et al., 2012b; Reguera, 2012). In engineered environments of MESs, interspecies interactions in exoelectrogenic mixed-species biofilms may lead to the extension of the electroactive biomass compared to pure cultures, thereby allowing microbial communities to take advantage of limited electrode surface area. Such extension is beneficial in regards to optimizing the ratio of active biomass to electrode surface area and should be considered in future electrode designs. Further deciphering the conductive behavior of exoelectrogenic bacteria may lead to increased understanding of global carbon cycling in natural environments as well as opening up new applications of bioelectronics, therefore warranting additional research.

Acknowledgements

This publication was made possible in by grant CBET 0955124 and PFI 1312301 from the U.S. National Science Foundation and in part by grant number 1S10RR107903-01 from the National Institutes of Health. The authors wish to acknowledge Anne-Marie Girard and the Confocal Microscopy Facility of the Center for Genome Research and Biocomputing (CGRB) and the Environmental and Health Sciences Center at Oregon State University for confocal support, Teresa Sawyer and the Electron Microscope facility at Oregon State University, and the equipment provided by Microproducts Breakthrough Institute.

4 Conductive Properties of Methanogenic Biofilms

Cheng Li, Keaton Larson Lesnik and Hong Liu

Bioelectrochemistry
Submitted

Abstract: Extracellular electron transfer between syntrophic partners needs to be efficiently maintained in methanogenic environments. Direct extracellular electron transfer as the form the electrical current is an alternative to indirect hydrogen transfer and requires construction of conductive extracellular structure. However, the conductive mechanism and the relationship between conductivity and the community composition in mixed-species methanogenic biofilms are not well understood. The present study investigated conductive behaviors of methanogenic biofilms and examined the correlation between biofilm conductivity and community composition between different anaerobic biofilms enriched from the same inoculum. Highest conductivity observed in methanogenic biofilms was 71.8 ± 4.0 μS/cm, twice more conductive than preious reported number. Peak-manner response of conductivity upon changes over a range of electrochemical potentials suggests that electron transfer in methanogenic biofilms occurs through redox driven super-exchange. The strong correlation observed between biofilm conductivity and *Geobacter* spp. in the metabolically diverse anaerobic communities suggests that the efficiency of DEET may provide pressure for microbial communities to select for species that can produce electrical conduits. Results indicate a means by which efficiency and start-up times may be improved in anaerobic microbial electrochemical technologies.

Keywords: Mathenogenic biofilms, electrical conductivity, *in situ* conductivity measurements

4.1 Introduction

Methanogenesis is a vital process in regards to biofuel production and the global carbon cycle. Extracellular electron transfer (EET) regulates much of methanogenesis and is of energetic importance in many microbial communities (Kouzuma et al., 2015; Thauer et al., 2008). Recently, direct transfer models of the EET process have emerged in contrast to the more established indirect EET models involving transfer of small redox intermediates. The existence of an alternative direct extracellular electron transfer (DEET) may enable transfer of electrons as electrical current at high efficiency (Liu et al., 2012; Malvankar & Lovley, 2014; Rotaru et al., 2014a; Rotaru et al., 2014b).

In order to transfer electrons directly in the form of electrical current, microbes need to establish electrical connections with extracellular electron acceptors. This physical adaption can often be evident from construction of conductive extracellular structures, as has been observed in single species *Geobacter* biofilms (Malvankar et al., 2011). The conductive mechanism of single species *Geobacter* biofilms is currently not well understood. Some evidences suggest that the conductivity can be attributed to proteinaceous filament (pili) possessing "metallic-like" conductivity that can be attributed to overlapping π-π orbital of aromatic amino acids residues (Malvankar et al., 2012b; Malvankar et al., 2011). Other studies have indicated that electron transfer within conductive biofilms occurs through redox driven electron self-exchange within a network of localized redox cofactors like outer membrane cytochromes (OMCs) (Li et al., 2016b; Snider et al., 2012; Strycharz-Glaven et al., 2011; Strycharz-Glaven & Tender, 2012).

Electrical conductivity is also a recognized property of many methanogenic granules (Morita et al., 2011; Shrestha et al., 2014). *Ex situ* investigation of granule conductivity upon changes of temperature suggests the existence of "metallic-like" conductivity in these granules, though dehydration of granules and bias towards measured area might affect the appropriate elucidation (Phan et al., 2016). Direct *In situ* investigation of conductive mechanism in methanogenic granules and other types of methanogenic aggregates such as biofilm, that might potentially avoid those misinterpretations, has not previously been conducted before.

Additionally, the relationship between the community composition and conductivity in anaerobic mixed-species aggregates (biofilms and granules) has not been elucidated. In both methanogenic and exoelectrogenic communities *Geobacter* spp. are often highly metabolically active, however, microbial aggregates originating from these communities often possess conductivities varying by orders of magnitude (Li et al., 2016b; Malvankar et al., 2012a; Morita et al., 2011; Shrestha et al., 2014). For example, conductivity values of 250 and 680 μS/cm have been respectively reported in exoelectrogenic anodic biofilms containing 52% and 16 % *Geobacter* spp., while electrical conductivity of methanogenic aggregates has been observed in the range of 0.8 to 36.7 μS/cm (2 - 29% *Geobacter* spp.) (Li et al., 2016b; Malvankar et al., 2012a; Morita et al., 2011; Shrestha et al., 2014). Previous studies have suggested that the difference of conductivities may be due to longer electron transfer distance to acceptors (electrodes) in exoelectrogenic biofilms. However, recent research focusing DEET in methanotrophic granules indicates that distance of DEET in granules composed by

archaea and bacterial species is longer than previous recognition and should not be not limited to cells that are in adjacent to each other (McGlynn et al., 2015), and thus opposing the previous assumption. As the future enhancement of methane-related bioenergy strategies such as anaerobic digester and methane microbial electrolysis cells (MECs) could depend on the elucidation and optimization of methanogenesis via DEET (Malvankar & Lovley, 2014; Rotaru et al., 2014a; Ruhl et al., 2014; Shrestha et al., 2014), conductive mechanism and relationship between conductivity and community membership in methanogenic biofilms needs to be further investigated.

In the present study, methanogenic biofilms, another form of methanogenic aggregates that possess similar metabolic activities to granules, were examined in *in situ* conditions using a gold-coated split-anode design adapted from previous studies (Li et al., 2016b; Malvankar et al., 2011). Exoelectrogenic and fermentative biofilms enriched from the same inoculum were used for comparison. The exoelectrogenic capabilities of mature methanogenic communities were also examined. All communities were sequenced and analyzed in order to determine the relationship between conductivity and community structure. Results provide evidence for a redox driven conductivity mechanism in methanogenic biofilms and suggest important roles in regards to methanogenic community conductivity for exoelectrogens such as *Geobacter* spp.

4.2 Materials and Methods

4.2.1 Preparation of Split Electrodes

A split-electrode design modified from a previous study (Malvankar et al., 2011) was used for anaerobic biofilm development and *in situ* measurement of biofilm conductivity (Figure 4.S1.). A water resistant adhesive (Loctite, Düsseldorf, Germany) was pasted to standard weighing paper (Schleicher & Schuell, Inc., Keene, NH, USA) to provide rigidity. Adhesive laden paper was then cut into circle with area of 7 cm^2, and an electrically conductive gold film (approx. 5 μm) was applied to the adhesive layer by an Cressington 108 Auto sputter coater (Cressington Scientific, Watford, UK). The gold coated surface was then cut down at the center by an ESI 5330 UV Laser machine (Electro Scientific Industries, Inc., Portland, OR, USA) to create a 50 μm non-conductive gap. Resistance measurements confirmed that two pieces of electrodes were electrically well separated.

4.2.2 Biofilm Development

Anaerobic sludge collected from the Corvallis Wastewater Treatment Plant (Corvallis, OR) was used as inoculum for developing anaerobic biofilms. Methanogenic and fermentative biofilms were developed in continuous-flow reactors (12 ml liquid volume) modified from single chamber MFCs by enclosing the cathode opening to provide anaerobic condition. The methanogenic reactors were fed with a modified medium solution amended with 50 mM phosphate buffer (Morita et al., 2011) with sodium acetate trihydrate (1.8 g/L), sodium propionate (0.72 g/L), and ethanol (1.96 g/L)

as the carbon source with pH maintained around 7.0. The fermentative reactors were fed with the same medium containing except with glucose as carbon source (9 g/L) and the pH was maintained around 5 to inhibit methane production. The flow rates for methanogenic and fermentative reactors were 0.1 mL/min and 2.8 mL/min, respectively. The exoelectrognenic biofilms were developed in single-chamber air-cathode MFCs as reported previously (Li et al., 2016a; Li et al., 2016b). The MFCs were operated in fed-batch mode using the same medium solution for methanogenic reactors with external resistance gradually decreased from 10,000 to 500 Ω in between batches in order to maintain the maximum cell voltages around 0.3 V. When voltages were under 5% of batch maximum, medium was replaced with fresh medium. When the conductance measurement of methanogenic biofilms was plateau, electrodes containing methanogenic biofilms were placed into single-chamber air-cathode MFCs to serve as anodes. Methanogenic biofilms MFCs were operated in the same manner as described above. All experiments were conducted in triplicate at 37.0 ℃.

4.2.3 Confocal Laser Scanning Microscopy (CLSM)

After maturation of biofilms (120 days for both methanogenic and exoelectrogenic biofilms, 20 days for fermentative biofilms), reactors were opened and small pieces of biofilm-containing electrodes (approximately 15 to 30 % of the total surface area) were carefully cut. Specimens containing biofilms were first stained with LIVE/DEAD BacLight Bacterial Viaibility Kit (Molecular Probes, Eugene, OR, USA)

following the instructions of manufacturer. The stained biofilms were then examined with the Zeiss LSM 780 NLO confocal microscope with a 10X objective lens (Carl Zeiss AG, Oberkochen, Germany), and a minimum of three fields were imaged. Images were further processed and analyzed by software ImageJ (ver. 1.49d) to estimate the thickness of biofilm. A minimum of ten random CLSM stacks along the y axis were used to determine the average thickness of biofilm. The thickness of fermentative biofilm in the gap area was estimated by using fractional caliper due to the excess thickness of biofilms compared to methanogenic and exoelectrogenic biofilms.

4.2.4 Conductivity Measurement (Two-Electrode Method)

To measure the *in situ* conductivity of biofilms, two electrode method was used as described previously (Li et al., 2016b). A voltage ramp (0 – 0.075 V) that is low enough to avoid the electrolysis of water or a self-heating effect was applied between two sides of a gapped electrode in steps of 0.025 V by using a source meter (Model 2401, Keithley, USA). For each voltage step, transient ionic current related to the charge transport was allowed to decay until a steady state was reached. Current was then measured every 30 seconds over a 3-minute period. For measuring the conductivity of exoelectrogenic biofilms, MFC anodes were temporarily disconnected from the cathode and allowed open circuit potential (OCP) to be reached. Resistances were calculated by plotting average currents of each step and applied voltages to calculate the current-voltage linear curve. Biofilm conductivity (σ) was calculated incorporating biofilms thickness measurements using the following equation where R is the measured resistance, D is diameter of the

electrode, *g* is the biofilm thickness, and a is the half of the width of the non-conductive gap (Kankare & Kupila, 1992):

$$\sigma = \frac{\pi}{RD} \Big/ \ln\left(\frac{8g}{\pi a}\right)$$

4.2.5 Electrochemical Gating Analysis

Electrochemical gating analysis was performed to measure the biofilm conductivity as a function of poised potential. A conventional three-electrode configuration was used with the anode as working electrode, a platinum plate (6.45 cm^2) as the counter electrode, and an Ag/AgCl (3 M NaCl) electrode as the reference electrode. A potentiostat (References 100, Gamry Instruments Inc., Warminster, PA) was used to set a range of potential (-600 to 600 mV) on one half of the split electrode with respect to the reference electrode. A source meter (Model 2405, Keithley, USA) was used to apply voltages (0, 25, 50, and 75 mV) between two halves of the split electrode (source and drain) to measure conductance as described in previous study (Li et al., 2016b). For current measurement at each potential, transient current related to the macrodiffusion of counterions was allowed to decay until the steady state was reach. Experiments of electrochemical gating analysis were conducted in duplicate.

4.2.6 DNA Extraction

Samples of methanogenic, exoelectrogenic, and fermentative biofilms were collected prior to examination of CLSM (120 days for both methanogenic and exoelectrogenic biofilms, 20 days for fermentative biofilms) for DNA extraction. And the converted methanogenic biofilms were harvest after 40 days of serving as anodic biofilms in MFCs. DNA extraction was performed using the MoBio PowerBiofilm DNA Isolation Kit (Carlsbad, CA) following the protocol suggested by the manufacture. The quality of the DNA extraction was checked on an agarose gel and further verified through use of spectrophotometer (NanoDrop, Wilmington, DE, USA).

4.2.7 Metagenomic Sequencing

DNA from each community was amplified using gene-specific primer pairs targeting the 16S V3 and V4 region (Klindworth et al., 2012). Illumina adapter sequences were added before the gene-specific sequences for full length primer sequences of TCGTCGGCAGCGTCAGATGTGTATAAGAGACAGCCTACGGGNGGCWGCAG (forward primer, 5' to 3') and GTCTCGTGGGCTCGGAGATGTGTATAAGAGACAGGACTACHVGGGTATCTAATCC (reverse primer, 5' to 3'). Twenty-five microliter PCR reaction volumes were used for amplication consisting of 2.5 µl genomic DNA, 5 µl forward primer (1 µM), 5 µl reverse primer (1 µM), and 12.5 µl of the KAPA HiFi HotStart Ready Mix (Kapa Biosystems, Wilmington, Massachusetts, USA). For the amplication PCR, an initial 3-

min step at 95 °C was followed by 25 cycles of 95 °C (30 s), 55 °C (30 s), and 72 °C (30 s) with a final 5 min extension at 72 °C. PCR products were checked using an Agilent Bioanalyzer 2100 (Santa Clara, California) and purified using Agencourt AMPure XP beads (Brea, California). Another PCR reaction using the same polymerase was then performed using Nextera XT index primers (Illumina, San Diego, CA) following provided protocol. Indexed PCR products were cleaned up and validated using the same method as the previous round. Libraries were then quantified using Qubit fluorometer quantification (Thermo Fisher Scientific, Waltham, MA), normalized, and pooled. The Illumina MiSeq was used for sequencing with MiSeq v.3 reagents for a paired end 2x300 bp run.

4.2.8 Sequence and Data Analysis

Initial quality filtering and demultiplexing was performed by Illumina MiSeq Reporter. Further sequence processing was performed using QIIME (Caporaso et al., 2010). The UClust algorithm was used for OTU assignment using the GreenGenes database (Edgar, 2010). The relative abundance of sequences was represented as a percentage of total sequences in each metagenome. Principle component analysis using UniFrac metrics was performed using QIIME (Hamady et al., 2010). Distance matrices were also calculated for *Geobacter* spp. percentage and conductivity (mS). The Pearson statistic calculated using the Mantel test was used to compare community structure (per determined principle components), conductivity, and relative abundance of *Geobacter spp*. Results are defined to be significant at $p < 0.05$ and marginally significant at $0.05 <$

$p < 0.1$. All metagenomes were submitted to the GenBank Sequence Read Archives (www.ncbi.nlm.nih.gov/Traces/sra/) and assigned the accession number SRP.

4.3 Results and Discussion

4.3.1 Structure and Community Composition of Methanogenic Biofilms

Following the inoculation of a known methanogenic sludge community, biofilms began to form over the 50 μm non-conductive gaps of the split electrodes in all reactors. Mature methanogenic biofilms following 120 days of growth possessed an average thickness of 26.0 ± 2.0 μm (n=3) (Figure 4.1.A.). Sparse spherical granule-like structures (0.2 to 1 mm in width) were observed in methanogenic biofilms (Figure 4.1.B.) and were not observed in reactors with either exoelectrogenic or fermentative communities. Substantial methane production was detected 7 days following the inoculation of the sludge under conditions supporting methanogenic growth, but not detected throughout the experiment in control (fermentative and exoelectrogenic) reactors. This result indicates the formation of an active methanogenic community. The primary constituents of the methanogenic community were members of the *Nocardiaceae* (23.0%), *Porphyromonadaceae* (7.90%), and *Camplyobacterceae* (7.5%) families which are typically associated with sewage sludge but do not appear to play central roles in regards to methanogenesis. The only prominent methanogenic archaea family was Methanobacteriaceae which composed 2.20% of the community (Figure 4.S2.). The archaeal sequences recovered in methanogenic biofilms was respectively 6 and 45 times

higher compared to exoelectrogenic and fermentative biofilms, indicating the substantial activity of methanogenic archaea in methanogenic biofilms.

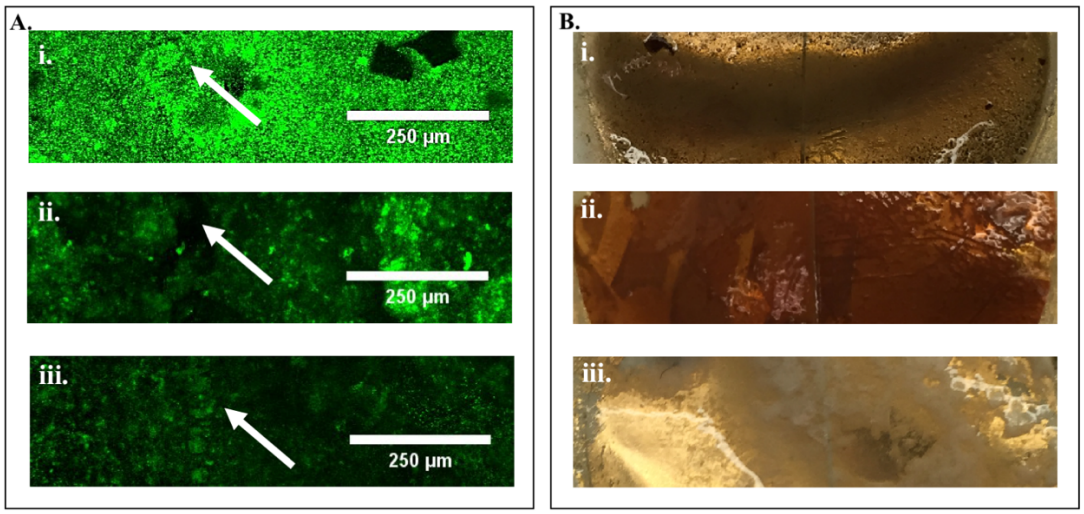

Figure 4.1. (A.) Top down Confocal laser scanning microscopy images of i) methane-producing biofilms, ii) current-producing biofilms, iii) fermentative biofilms. Frame size = 7.22 X 10^{-3} cm^2. (B.) Digital camera images of i) methane-producing biofilms, ii) current-producing biofilms, iii) fermentative biofilms.

4.3.2 Conductivity and Conductive Mechanism of Methanogenic Biofilms

Conductance of the methanogenic biofilm increased gradually over time with final conductance reaching a plateau after 113 days (Figure 4.2.). Increases in conductance were 80 fold that of the initial average conductance values, from 0.2 to 15.9 µS. Conductivity was able to be determined following biofilm thickness measurements

and an average conductivity of 33.7 ± 16.9 µS/cm (n = 3) was obtained in the methanogenic biofilms (Figure 4.3.), comparable to conductivities of methanogenic granules (0.8 to 36.7 µS/cm) in anaerobic digester treating brewery wastewater (Shrestha et al., 2014).

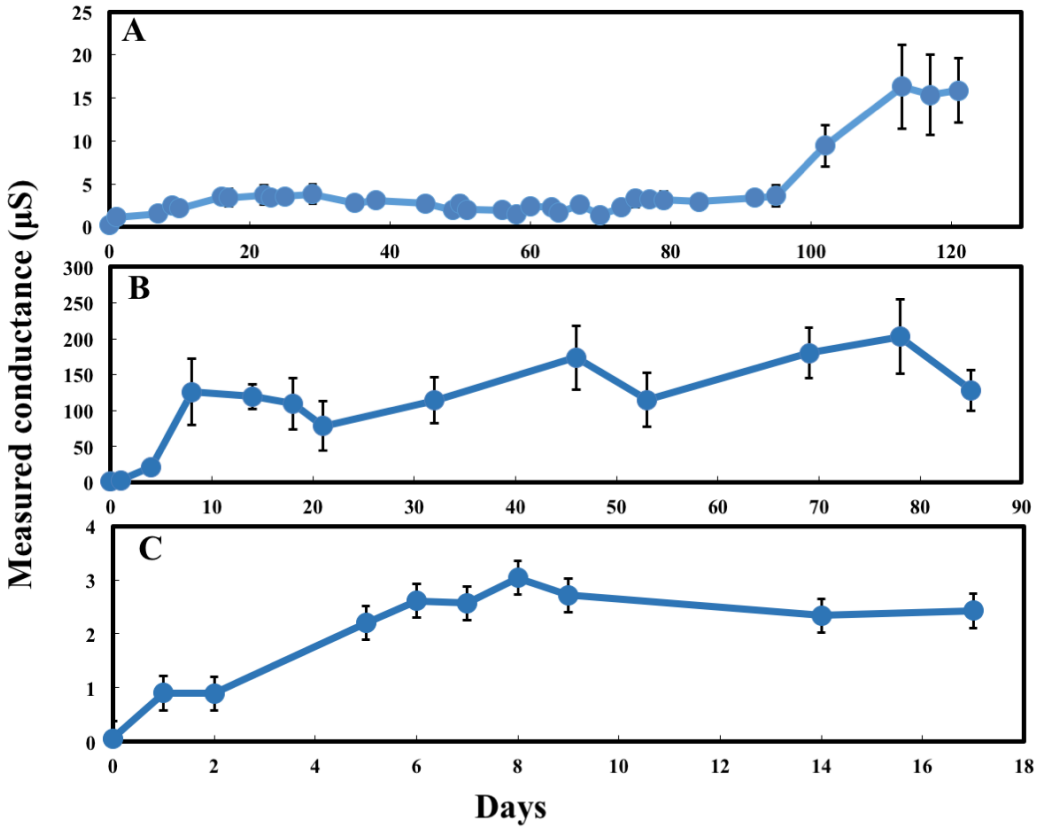

Figure 4.2. Measured conductance over time. (A.) methane-producing biofilms, (B.) current-producing biofilms, (C.) fermentative biofilms. Measurements for fermentative biofilms were stopped after day 20 due to excess growth of biomass. Error bars represent standard error obtained with 3 replicates.

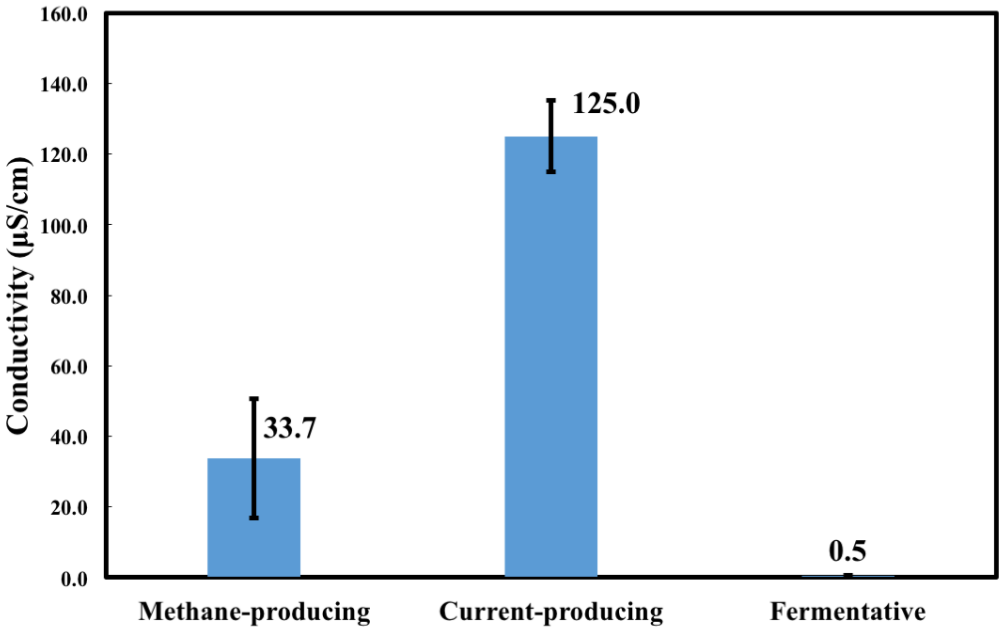

Figure 4.3. Conductivity of methanogenic biofilms, exoelectrogenic biofilms, and fermentative biofilms. Error bars represent standard error obtained with 3 replicates.

Conductivity of methanogenic biofilms was measured as a function of biofilm potential in order to elucidate conductive mechanisms (Figure 4.4.). The biofilm conductivity displayed a peak-manner response with the highest conductivity (71.8 ± 4.0 µS/cm) observed at gate voltage (V_g) of -175 mV (vs. Ag/AgCl). Two smaller secondary peaks were observed at V_g of -50 and 100 mV with conductivities 52.1 ± 1.8 and 43.6 ± 7.4 µS/cm, respectively. All of three peak conductivity number were higher than any other reported number of methanogenic granule conductivity (Morita et al., 2011; Shrestha et al., 2014). Conductance at V_g more negative than -450 mV or more positive than 200 mV were limited ranging from 5.0 to 18.0 µS/cm. Control experiments using

split electrode that had no biofilm growth did not exhibit any recognizable pattern conductance, indicating that the observed response in conductance was biofilm related. The potentiodynamic peak-manner response observed in the present study, a characteristic of redox driven conductivity, has never been reported in aggregates associated with methanogenic communities. When the hydration state of biofilms allows sufficient mobility of counterions, application of a small voltage bias between contacting electrodes will result in electrolysis of redox cofactors near electrode surface till the concentration gradient of reduce/oxidized redox cofactors achieves steady state (Dalton et al., 1990; Strycharz-Glaven et al., 2011). This gradient also provide the driving force for electron transport as occurs in redox conducting polymer such as viologen, in which electrons diffuse from areas of high to low concentration (Dalton et al., 1990; Snider et al., 2012). The conductive peak represents the potential at which the ratio of reduced and oxidized redox cofactors within the matrix are equal (Dalton et al., 1990).

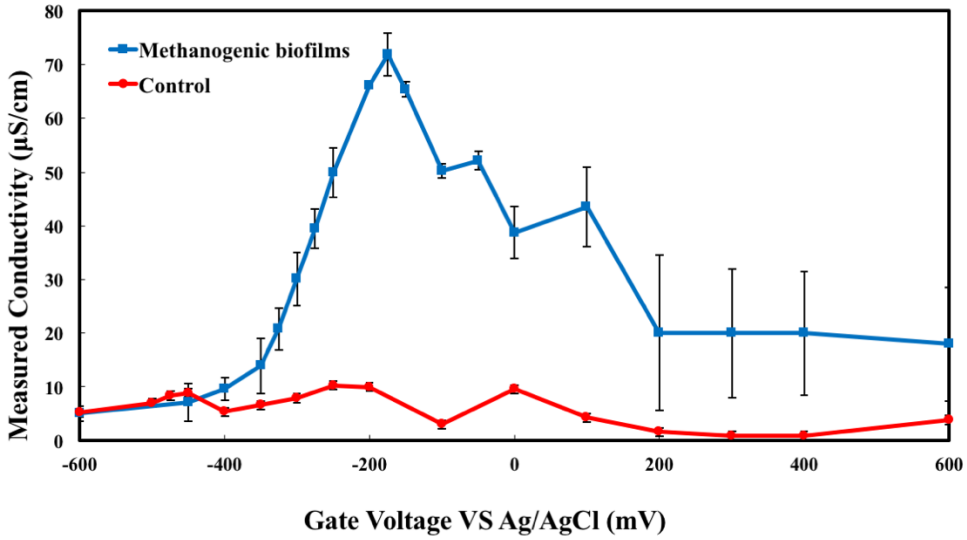

Figure 4.4. Conductivity of mixed-species methanogenic biofilms estimated by electrochemical gating analysis. Error bars represent standard deviation (n = 2).

The finding of a redox driven conductivity in methanogenic biofilms is consistent with previous researches presenting an superexchange model of electron transfer in single species biofilms of *G. sulfurreducens* and mixed-species exoelectrogenic biofilms containing *Geobacter* spp. (Li et al., 2016b; Phan et al., 2016; Snider et al., 2012; Strycharz-Glaven et al., 2011; Strycharz-Glaven & Tender, 2012; Yates et al., 2015), but differs from a "metallic-like" conductivity previously proposed for methanogenic granules (Morita et al., 2011). The different understandings of the nature of conductivity could be due to the different approaches used for elucidating the conductive mechanism. In the previous study featuring methanogenic granules, the response of conductivity upon changes of temperature was obtained under *ex situ* condition in which water content

within the granules and in the ambient environments was not specifically controlled (Morita et al., 2011; Phan et al., 2016). Water content, however, is an important parameter affecting the mobility of counterion within network of reduced/oxidized redox cofactors. This mobility is essential in the maintaining of electroneutrality during the super-exchange of electrons and if not maintained at physiologically relevant conditions it may affect result interpretations (Dalton et al., 1990; Phan et al., 2016). In the presence study, *in situ* measurements were directly conducted avoiding dehydration of the methanogenic biofilms.

4.3.3 Exoelectrogenic Capability of Methanogenic Biofilms

Split gold electrodes containing methanogenic biofilms were put into MFCs to serve as the anodes in order to further investigate electron exchange capabilities within the methanogenic biofilms. Immediately upon switching growth modes the methanogenic biofilms were able to spontaneously produce significant levels of electrical current (Figure 4.5.). Increases in electrical current outputs to stable levels were significantly faster in methanogenic anode biofilms compared to MFC anode communities that were enriched directly from anaerobic sludge. It took 48 hours for the MFCs with methanogenic biofilms to reach a power density of 0.5 A/m^2, while it took about 19 days for the MFCs with sludge as inoculum to reach similar power densities. This is likely due to the enrichment of exoelectrogenic biomass from the sludge during methanogenic growth. Likewise, previous studies have identified *Geobacter* spp. as one of the predominant and most metabolically active microbes in methanogenic granules and

suggests that some members of *Methanosaeta* spp. and *Methanosarcin*a spp. can directly accept extracellular electrons from *Geobacter metallireducens* (Rotaru et al., 2014a; Rotaru et al., 2014b; Shrestha et al., 2014).

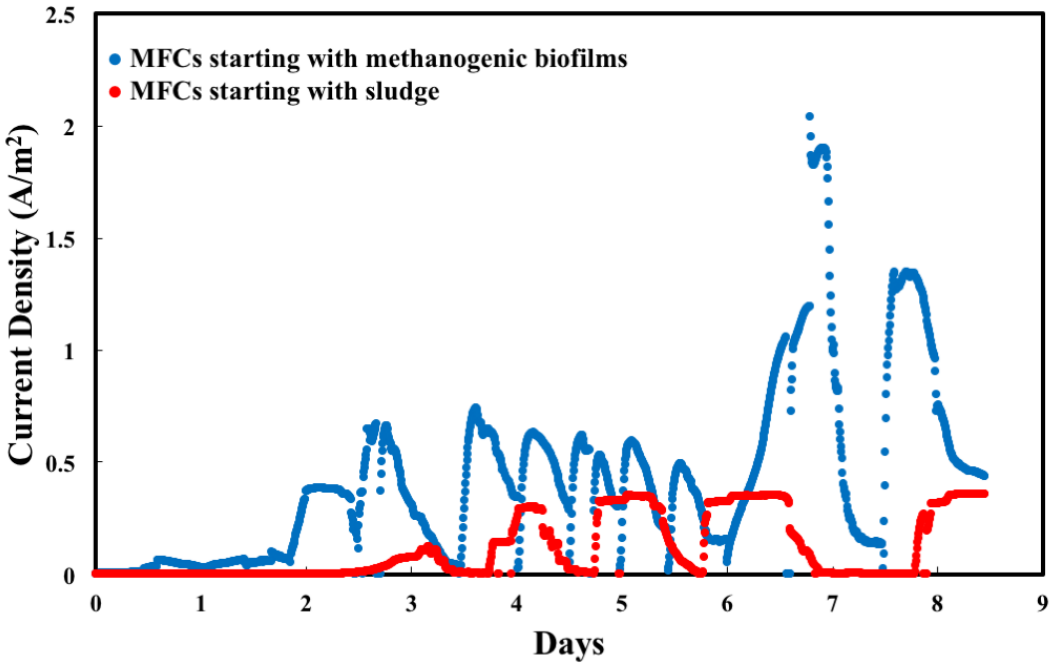

Figure 4.5. Current densities of MFCs starting with methanogenic biofilms and sludge.

Further increases in methanogenic biofilm conductivity were observed following the switch to exoelectrogenic growth. After 15 days of exoelectrogenic growth, the converted biofilm conductivity was 307.4 ± 72.6 μS/cm, almost 2.5 times higher than the final biofilm conductivity in exoelectrogenic biofilms directly enriched from sludge. This is likely the result of increases in the abundance of *Geobacter* spp. when a more favourable electron acceptor (MFC anode) was introduced into the system. This results

suggests that substantial percentage of exoelectrogens can be maintained in cultures outside of bioelectrochemical reactors like MFCs, thereby providing a means to achieve faster and more consistent start-up times and address one of the many challenges in the pratical application of MFCs (Liu et al., 2011).

4.3.4 Correlation between Conductivity and Biofilm Community Composition

The conductive properties and microbial composition of the methanogenic biofilm community were compared with exoelectrogenic and fermentative biofilm communities enriched from the same sludge in order to correlate differences in conductive characteristics to community structure. Conductivity of the methanogenic biofilms (33.7 ± 16.9 μS/cm) was significantly greater than the thicker (863 ± 75 μm) fermentative biofilms (0.5 ± 0.1 μS/cm), but significantly less than exoelectrogenic biofilms (125.0 ± 10.1 μS/cm) of similar biofilm thickness (32.7 ± 4.4 μm). Biofilms that were initially methanogenic then switched to exoelectrogenic growth mode had a conductivity of 307.4 ± 72.6 μS/cm (Figure 4.6.). The relatively high conductivity of methanogenic communities indicates that the energetic favourability of DEET likely provides a selective pressure biased towards microbial species capable of establishing conductive extracellular structures.

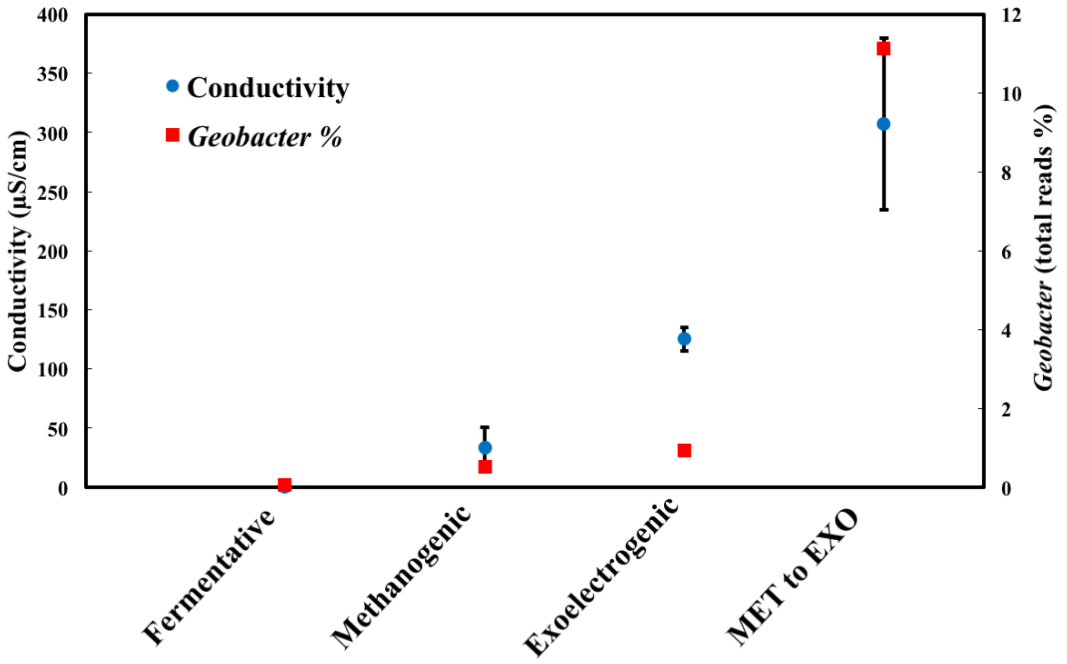

Figure 4.6. Correlation between biofilm conductivity and abundance of genus *Geobacter*. Error bars represent standard error obtained with 3 replicates.

Between the phylogenetically distinct communities (Figure 4.7.), *Geobacter* spp. percentage was significantly positively correlated (r = 0.90) with conductivity of biofilms ($P < 0.05$). No correlation at any level between community composition and conductivity was found following control of *Geobacter* spp. abundance (SI data spreadsheet). This is similar to the moderate linear correlation (r = 0.67) previously observed between conductivity and *Geobacter* abundance in methanogenic granules. *Geobacter* spp., recognized as electron donating partners in syntrophic methanogenesis and a dominant, metabolically-active component of exoelectrogenic communities, accounted for 0.50% of the total reads in methanogenic biofilms while accounting for 0.93% in exoelectrogenic

communities, 0.04% fermentative communities, and 11.13% of the total reads in communities that were transitioned from methanogenic to exoelectrogenic growth modes. The strong correlation between *Geobacter* spp. and conductivity reinforces the notion that *Geobacter* spp. are the major constructer of conductive extracellular structures that enables conductivity in mixed-species biofilms. While evidence for the existence of "metallic-like" conductivity in pili filaments produced by *Geobacter* spp. seems to be overwhelming, results of the present study may indicate that redox conduction may still be the rate limiting step in anaerobic biofilms containing *Geobacter* spp. This suggests a shared model by which a network of supramolecular cytochrome arrangements interconnected by semiconducting pili fibers provide equipotential conditions within physical distant points of localized redox cofactors (Ordòñez et al., 2016). The presence of other microbial species may provide advantageous features for biofilms such as allowing biofilms to build and maintain conductivity over an extended distances (Li et al., 2016a). Additionally, many of these microbial species can produce localized redox cofactors other than cytochromes such as Fe-S proteins (Yates et al., 2016a), which may further decorate the semi-redox conductive relay network to suit the needs of these communities.

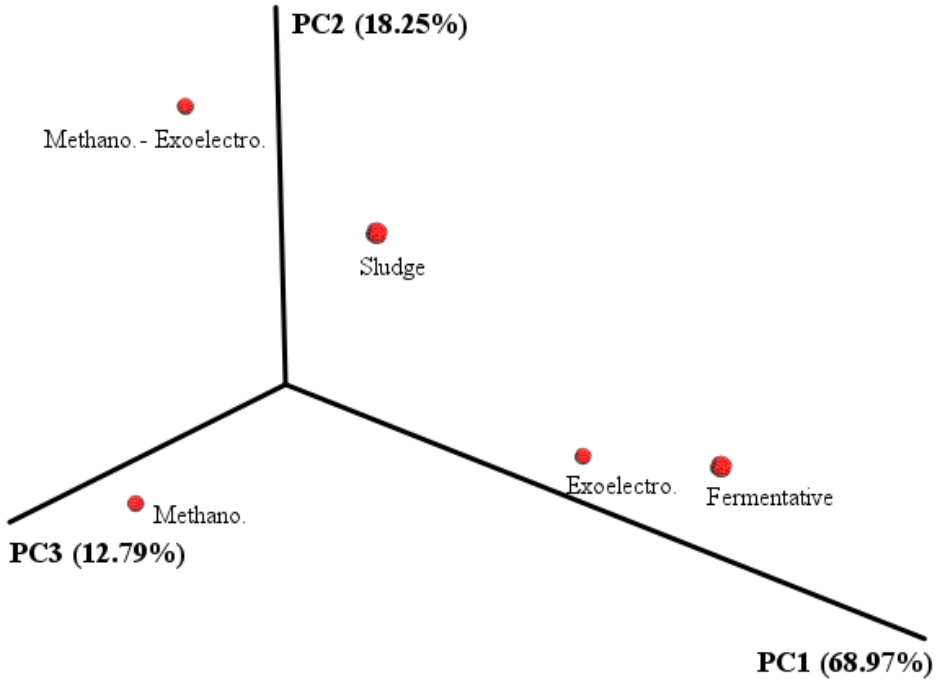

Figure 4.7. Principle components analysis of microbial community composition including sludge inoculum (Sludge), methanogenic community (Methano.), exoelectrogenic community (Exoelectro.), fermentative community (Fermentative), and methanogenic-enriched exoelectrogenic community (Methano.-Exoelectro.).

4.4 Implications

In the present study, results feature a conductivity of methanogenic biofilms twice higher than previous recorded conductivity of methanogenic granules and demonstrate that electron transfer within methanogenic aggregates may occur through redox driven electron conduction for the first time. The abundance of *Geobacter* spp. was found to

positively correlate with the conductivity of metabolically diverse microbial aggregates. Additionally, supplementing conductive nanoparticles of magnetite, analogizing outer membrane cytochromes, may enhance methanogenesis through conferring the needs of electrical connection of DEET and can stimulate the growth of *Geobacter* spp. (Kato et al., 2012a; Kato et al., 2012b). Given the ubiquity of these conductive nanoparticles in natural methanogenic environments such as sediments and soils, these results suggest that methanogenic communities in such environments may have acquired the ability to effective utilize the superexchange to transfer electron extracellularly. These findings expand the understanding of extracellular electron transfer within anaerobic communities and the construction of conductive extracellular structure. Results from the present study suggest a new possibility of optimizing the extracellular electron transfer process through connection to the microbial community structure. Further investigation into this phenomenon is important for future exploration of bioenergy production as well as enhancing current understanding of many biogeochemical processes in anaerobic environments.

Acknowledgements

This publication was made possible in by grant CBET 0955124 from the U.S. National Science Foundation and in part by grant number 1S10RR107903-01 from the National Institutes of Health. The authors wish to acknowledge Anne-Marie Girard and the Confocal Microscopy Facility of the Center for Genome Research and Biocomputing

(CGRB) and the Environmental and Health Sciences Center at Oregon State University for confocal support, Teresa Sawyer and the Electron Microscope facility at Oregon State University for electrode coating, and Ningshengjie Gao for helpful discussions about electrochemical tests.

Supporting Information:

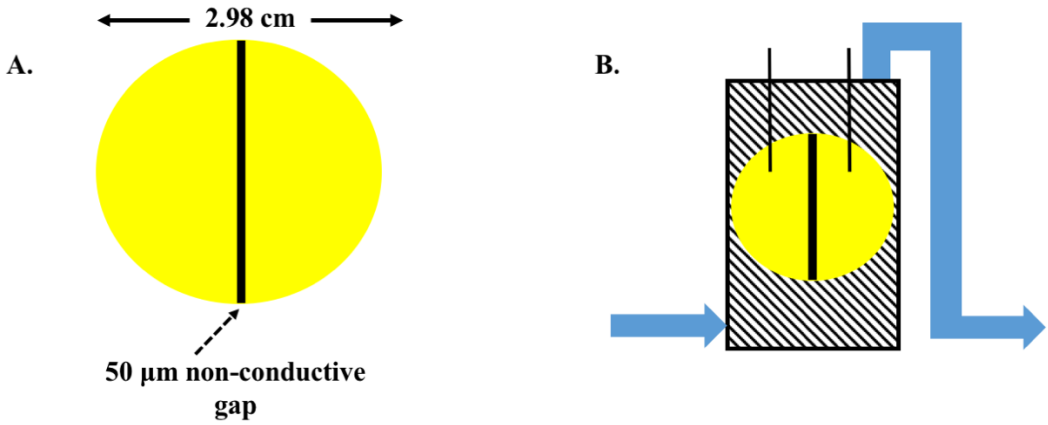

Figure 4.S1. Schematic setup of electrode and continuous flow reactors for in situ conductivity measurement. (A.) Gold-coated electrode with 50 µm nonconductive gap. (B.) continuous flow reactors modified from single chamber Microbial fuel cell.

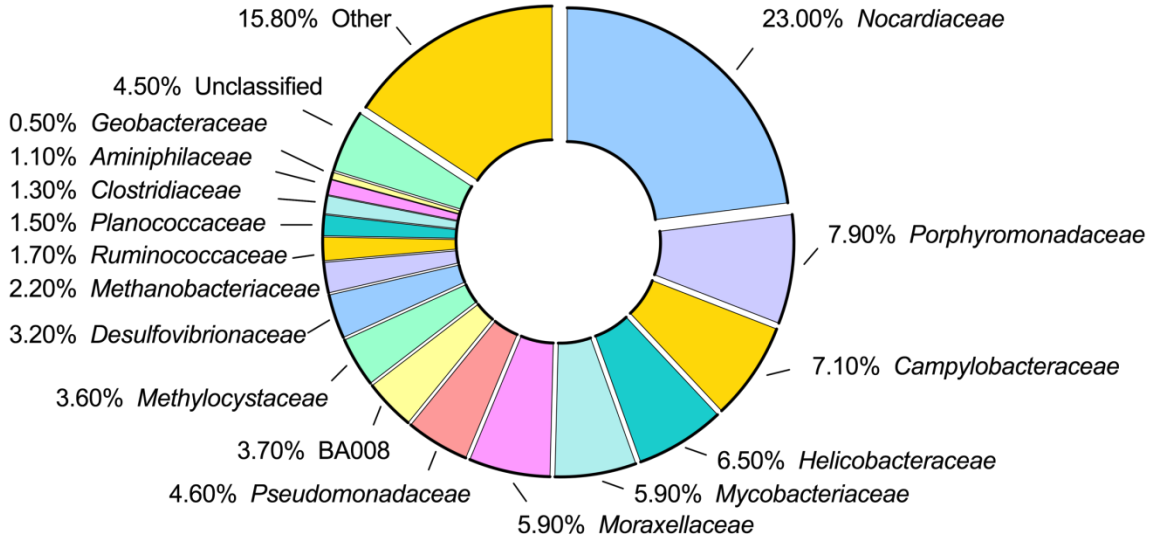

Figure 4.S2. Community composition of methanogenic biofilms.

5 Enhanced Current Production and Redox Conductivity of Anodic Biofilm by Applying Static Magnetic Field to Microbial Fuel Cells

Cheng Li and Hong Liu

Bioresource Technology
To be submitted

Abstract: A possible approach to enhance the performance of microbial fuel cells (MFCs) is to increase the conductivity of anodic biofilms and thereby the extracellular electron transfer. In the present study, we evaluated the impact of static low intensity magnetic field on current production and conductive behaviors of anodic biofilms. Results demonstrated that the application of a magnetic field can shorten the startup time of MFCs and enhance the power and current output by 140-300%, reaching 4.5 W/m^2 and 20 A/m^2, respectively. The maximum conductance of the anodic biofilms in the presence of magnetic field was 150% higher than that in the control MFCs, in accordance with the increase in current density. The positive response of biofilm conductance to magnetic field, which is similar to the negative magnetoresistance of some polymer films, has never been observed in biofilms and also confirmed the redox conduction mechanism of the exoelectrogenic biofilms.

Keywords: Extracellular Electron Transfer, Conductive Biofilms, Magnetic Field, Magnetoresistance, Microbial Fuel Cells

5.1 Introduction

Microbial fuel cells (MFC) technology uses exoelectrogenic microorganisms on anode to convert the chemical energy stored in organic substance to electricity. It has the potential to be used for wastewater treatment, bioenergy production, and bioremediation (Logan, 2009). However, low power/current output has prevented this technology from practical applications (Logan, 2009; Malvankar et al., 2012c). Many previous studies have attempted to enhance the power/current production of MFCs through developing novel electrode materials and improving reactor designs (Fan et al., 2012; Fan et al., 2011). An alternative is to enhance the unique ability of anodic exoelectrogenic microbial communities in directly transferring extracellular electrons to electrode (Leang et al., 2013).

Critical to direct extracellular electron transfer (DEET) to electrode is the establishment of electrical connections facilitated through conductivity of anodic exoelectrogenic biofilms (Lovley, 2011a; Lovley, 2011b). The detailed conduction mechanisms of anodic exoelectrogenic biofilms are still under investigation and diverged into two distinct theories, the model of redox conductivity (Phan et al., 2016; Yates et al., 2015; Yates et al., 2016b) and the model of metallic-like conductivity (Malvankar et al., 2016; Malvankar et al., 2012b; Malvankar et al., 2015; Malvankar et al., 2011). Despite the controversy of conduction mechanisms, conductivity of anodic exoelectrogenic biofilms supports the long distance electron transfer beyond the molecular scale and conserves energy during electron transfer, and therefore is critical to the ability of anodic

exoelectrogenic microbial communities in directly transferring extracellular electrons to electrode (Lovley, 2011a; Lovley, 2011b). Previous study demonstrated that the conductivity of anodic exoelectrogenic biofilms directly correlates with current density of MFCs (Lee et al., 2016; Malvankar et al., 2012c). Increasing the conductivity of anodic exoelectrogenic biofilms through manipulating of the pilus expression of *Geobacter sulfurreducens* (Leang et al., 2013) and reductively depositing iron conductive nanoparticles in *Shewanella oneidensis* biofilms (Jiang et al., 2014) has been suggested as effective approaches to increase the power/current production of MFCs using pure cultures. However, low-cost strategies with low environmental impact are preferred for practical applications of MFCs, especially those using mixed cultures.

Recently, static low intensity magnetic field (SLIMF) had been applied to the anode side of MFCs and demonstrated enhancement on power/current output of MFCs (Li et al., 2011; Tao & Zhou, 2014; Yin et al., 2013; Zhao et al., 2016). It has been hypothesized that the observed enhancement of current production was a result of biological effects of SLIMF had on the anodic exoelectrogenic community including stimulating enzyme activity (Zhao et al., 2016) and enhancing oxidation stress (Yin et al., 2013). While it is a well-known phenomenon that the resistivity of conductive materials can vary in the presence of magnetic field (Nalwa, 2001), the impact of SLIMF on the conductivity of mixed-species anodic biofilms has not been investigated.

In the present study, we first investigated the magnitude and persistency of the impact of SLIMF on the power/current production of single chamber MFCs and then

examined the changes of conductive behaviors of the anodic biofilms in the presence of SLIMF. Our results have demonstrated that SLIMF can shorten the startup time and enhance the current production more than 300% in the typical current density range of 4-20 A/m^2. We also, for the first time, demonstrated that the conductance of anodic biofilms correlated with the intensity of applied magnetic field that resembles the negative magnetoresistance (NMR). Observed increase in anodic biofilm conductivity in the presence of SLIMF not only provided an explanation for the enhanced performance of MFCs, but also confirmed the redox conductive mechanism of the biofilms.

5.2 Materials and Methods

5.2.1 Microbial Fuel Cells Design and Operation

Single chamber MFCs (total volume of 12 mL) were constructed according to the design of previous studies (Fan et al., 2007; Fan et al., 2008). Carbon cloth (Type B, fuelcellearth.com) with a projected surface area of 3 cm^2 was used as the anode of the MFCs (labelled as CCA-MFC) to evaluate the effect of magnetic field on the performance of anodic biofilms. Gold foil sheet (projected surface area of 7 cm^2, Alfa Aesar, Haverhill, MA, USA) was used as the anode of the MFCs (labelled as GA-MFC) to evaluate the effect of SLIMF on the conductivity of anodic biofilms. A nonconductive gap in the middle of the gold electrode was created according to our previous studies (Li et al., 2016a; Li et al., 2016b). Carbon cloth/activated carbon air cathode (projected surface area of 7 cm^2) was fabricated following a previously developed protocol (Janicek

et al., 2015) and used in both the CCA-MFCs and GA-MFCs. Magnets (2.54 cm diameter, K&J Magnetics, Inc. Pipersville, PA, USA) were applied to the anode side of the MFCs (0.2 cm away from anode (Figure 5.1.A. & B.)) to create SLIMF with intensities of 105 and 150 mT at the surface of anodes. The intensity of magnetic field was determined using a Gauss meter (7010, Sypris Solution, Inc. Louisville, KY, USA). Control CCA-MFCs and GA-MFCs were constructed but were not subjected to the impact of SLIMF. Magnets were applied to the magnetic CCA-MFCs right after the inoculation of a mixed exoelectrogenic culture. After 100 days of operation, the magnets were removed from the magnetic CCA-MFCs to investigate the persistency of the SLIMF effects. The GA-MFCs were operated in two ways to evaluate the effects of SLIMF on the conductance of anodic biofilms at different growth stages: 1) applying magnets right after the inoculation, and 2) applying magnets after power production became stable and biofilms were mature.

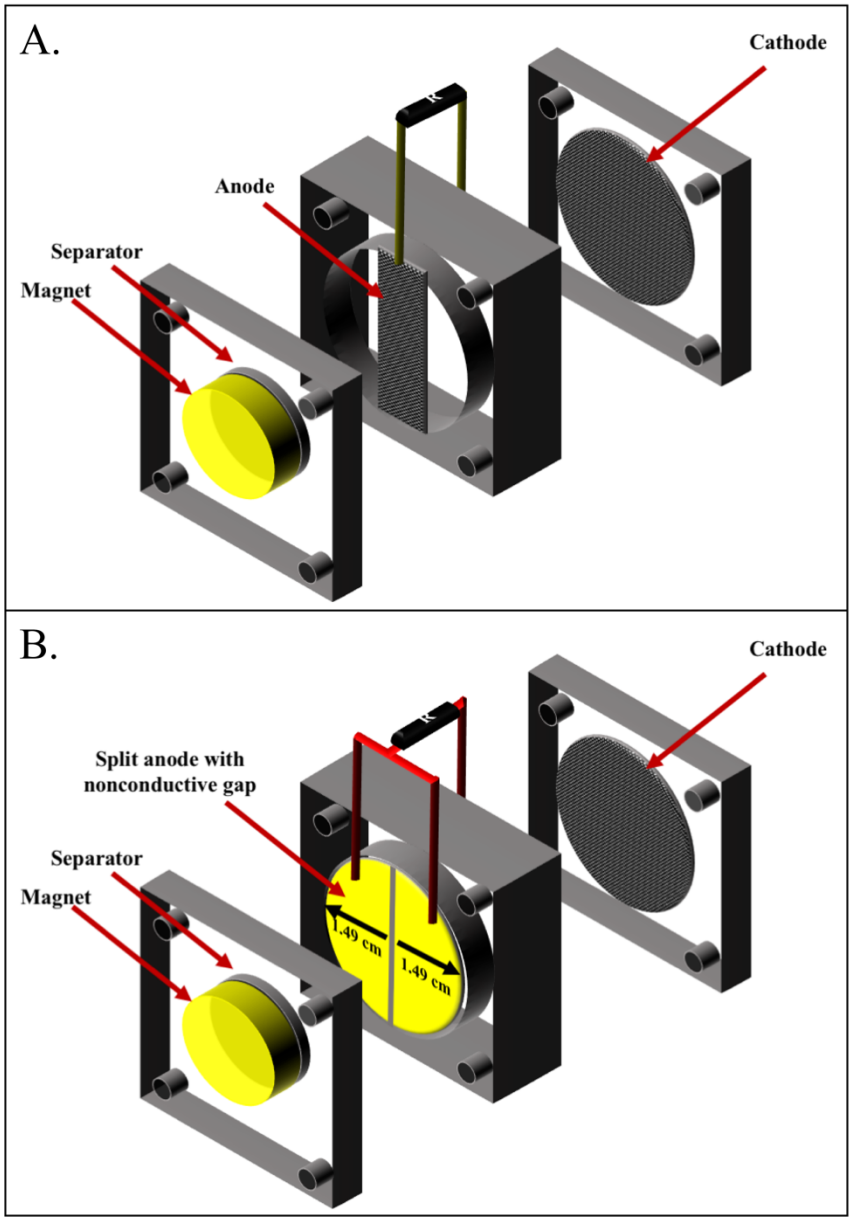

Figure 5.1. Schematic of MFC setup: A. CCA-MFC and B. GA-MFC with 50 µm non-conductive gap in the middle of anode.

A lab-maintained active MFC culture was used as inoculum for all the MFCs. The culture was originally enriched from active sludge collected from the Corvallis Wastewater Treatment Plant (Corvallis, OR). This anodic exoelectrogenic community has been demonstrated to produce one of the highest reported power densities (Fan et al., 2007). Acetate (30 mM) was used as the electron donor during the startup of MFCs and the concentration increased to 60 mM after power outputs became stable. Modified *Geobacter* medium (MGM) (pH 7) was used in all experiments (Fan et al., 2012). The medium consists of the following ingredients (per liter): KCl, 0.13 g; NH_4Cl, 0.31 g; $NaH_2PO_4 \cdot H_2O$, 5.84 g; $Na_2HPO_4 \cdot 7H_2O$, 15.5g; vitamin, 12.5 mL; and mineral 12.5 mL solution as previously reported. MFCs were operated in fed-batch mode with external resistance decreased from 10,000 to 75 Ω for CCA-MFCs and from 10,000 to 500 Ω for GA-MFCs between batches as the biofilms grew in order to maintain maximum cell voltages around 0.3 V. When voltages were under 10% of batch maximum, the media was removed and replaced with new media.

When power/current production of all CCA-MFCs became stable (after day 14), polarization curves was made by changing external resistance from 1000 to 33 ohms with interval time of 20 mins. Internal resistance was calculated according to a previous study (Fan et al., 2008). Power/current density was calculated by normalizing to the surface area of anode.

5.2.2 In situ Measurement of Biofilm Conductance

5.2.2.1 Two probe conductivity measurement

Two probe method adapted from previous studies (Li et al., 2016a; Li et al., 2016b; Malvankar et al., 2011) was used to evaluate the *in situ* biofilm conductance during growth period at open circuit potential (OCP). GA-MFC anodes were temporarily disconnected from the cathode and allowed OCP (-470 mV vs. Ag/AgCl) to be reached. Then a voltage bias (V_{app}) was straddled between two halves of a split anode (0, 25, and 50 mV) in steps of 25 mV by using a source meter (Model 2405, Keithley, USA). For each voltage step, transient ionic current was allowed to decline until a steady state was reached. Conducting current flowing between the two halves of split anode was then recorded every 30 seconds over a period of 3 minutes by using the same source meter. Biofilm resistance was calculated by plotting V_{app} against measured current. Conductance was then calculated from the inverse of resistance. Measurements were taken approximately twice a week during MFC operation. Measurements of conductance conducted at OCP were performed in duplicate reactors.

5.2.2.2 Electrochemical gating analysis

To further examine the conductive behavior of the mixed-species exoelectrogenic biofilms under the impact of SLIMF, electrochemical gating analysis *in situ* measures biofilm conductance as a function of redox potential, was performed based on the three electrode configuration described previously (Li et al., 2016b; Malvankar et al., 2012b). A potentiostat (References 100, Gamry Instruments Inc., Warminster, PA) was used to

apply a series of gate potentials (V_g) from -500 to -300 mV with increments of 50 mV (vs. Ag/AgCl) (Li et al., 2016b). Concurrent with the setting of V_g, a source meter (Model 2405, Keithley, USA) was used to apply voltages (V_{app}) between the source and drain anode. The conducting currents at various V_{app} (0, 25, and 50 mV) were measured and used to calculate resistance from the slope of the voltage-current curve.

Electrochemical gating analysis was also conducted to investigate the conductive behavior of the mixed-species exoelectrogenic biofilms in the absence of substrate as described previously (Li et al., 2016b). To remove substrate, acetate-containing growth media was replaced with MGM containing no acetate. Cell voltages of the MFCs dropped below 0.001 V within 24 hours following acetate removal. Liquid samples were also collected and analyzed using high performance liquid chromatography (HPLC) to confirm that acetate was completely removed following medium replacement. To prevent potential of damage to biofilms, all electrochemical gating analysis was limited with 48 hours and deoxygenated media were used. Experiments of electrochemical gating analysis were conducted using duplicate reactors with 6 replicates.

5.2.3 Statistical Analysis

Single factor analysis of variance (ANOVA) was performed by using data analysis package in Microsoft Excel and numbers were considered statistically different when $P < 0.05$.

5.3 Results and Discussion

5.3.1 Effects of Magnetic Field on MFC Performance

In the present study, an MFC configuration with reduced cathode limitation was used to investigate the impact of SLIMF on high-current producing biofilms. Increases in power density over time were observed for all CCA-MFC reactors during startup period (Figure 5.2.A.). While CCA-MFC reactors amended with 105 mT and 150 mT SLIMF generated more than 3 W/m^2 power density (normalized to anodic surface area) in less than 8 days, the power density generated by the control CCA-MFC reactors was still less than 1 W/m^2 after 12 days even similar approach (maintaining output voltage of 0.3 V) was used to operate MFCs. Polarization experiment was conducted at day 20 when power production became stable. The average maximum current densities of 105 mT and 150 mT CCA-MFCs were 18.4 ± 1.0 and 20.1 ± 0.4 A/m^2, respectively, which were significantly greater than the control CCA-MFCs (4.8 ± 0.2 A/m^2) (P<0.05) (Figure 2.B.). The average maximum power densities of 105 mT and 150 mT CCA-MFCs were also greater than that of control CCA-MFCs (4.31 ± 0.16 and 4.56 ± 0.07 W/m^2 compared to 1.90 ± 0.45 W/m^2) (P<0.05) (Figure 5.2.B.). The internal resistances (R_{int}) of MFCs, calculated from the linear sections of polarization curves, were similar for the CCA-MFCs amended with 105 (70.7 ± 8.2 ohm) and 150 (68.2 ± 2.0 ohm) mT SLIMF, but were two times higher for the control CCA-MFCs (155.6 ± 17.8 ohms).

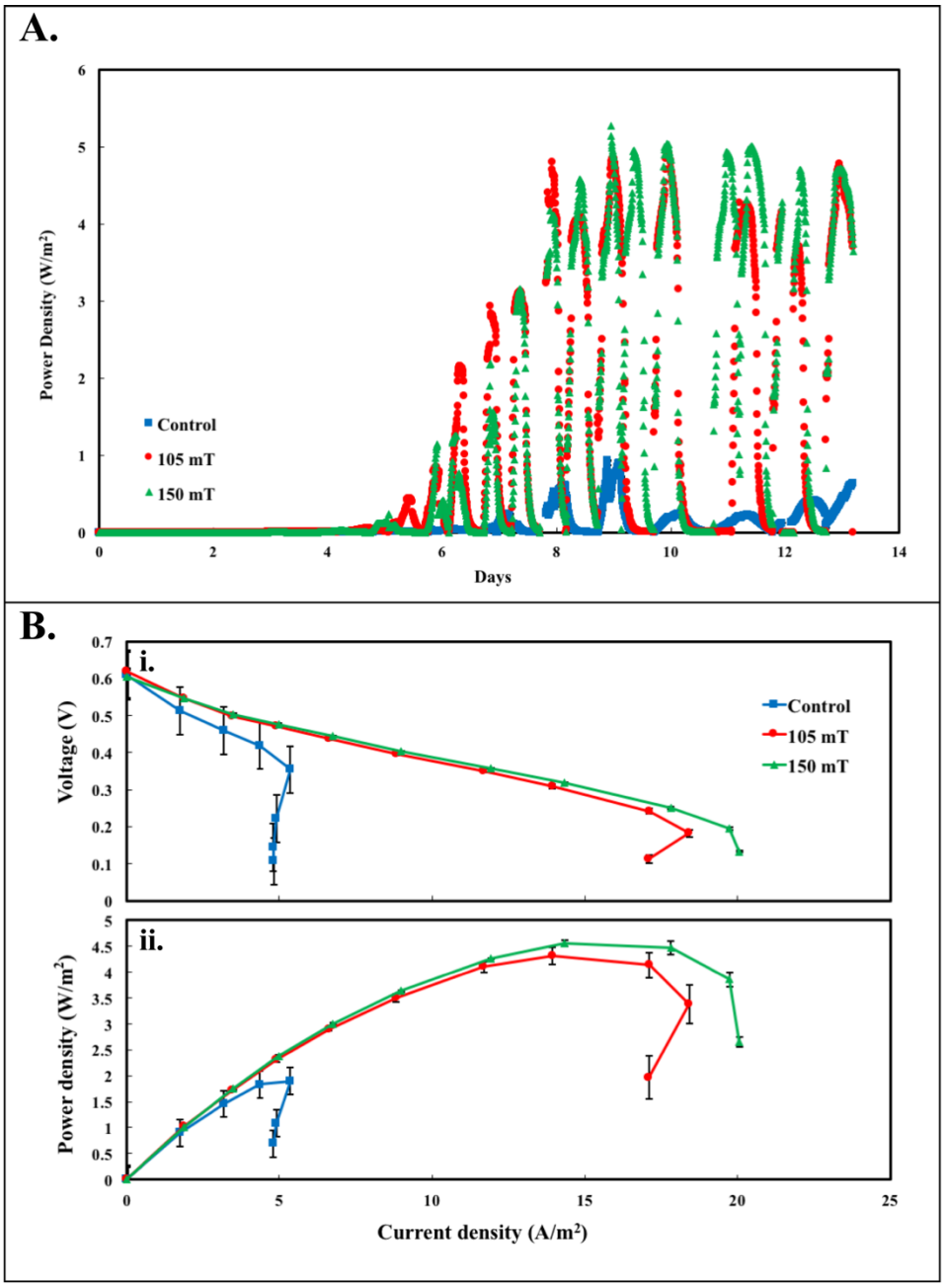

Figure 5.2. A. Changes of MFC power density at the startup period. B. i) Polarization and ii) power density curve of CCA-MFC reactors. Batch figure represents the performance from one reactor in triplicate setting. Error bar represent the standard deviation (n=3).

SLIMF has been suggested as a beneficial factor to overall performance of MFCs (Li et al., 2011; Tao & Zhou, 2014; Yin et al., 2013; Zhao et al., 2016). The reported enhanced current densities in these studies ranged from 0.005 mA/m^2 to 8.5 A/m^2, corresponding to a current increase of 10% -50% (compared to control MFCs). In the present study, we observed a much greater increase in current (over 300%) to even higher current densities (18 to 20 A/m^2). The significant enhancement suggests that the SLIMF impact can be more significant than previous observation and this enhancement can be extended to a higher current density range, indicating the potential of this approach for practical application. While the impact of SLIMF on MFC may not be limited to the anode of the MFCs, previous studies have demonstrated that the effects of SLIMF on cathodic and solution resistance was insignificant compared to its impact on anodic resistance (Yin et al., 2017; Yin et al., 2013). In addition, the magnetic field at the cathode surface was less than 20% of the intensity on the anode surface in this study. Therefore, it is reasonable to believe that the enhanced performance of MFCs was mainly due to the impact of SLIMF on anodic biofilms.

To evaluate the persistency of magnetic effects on MFC performance, magnets were removed from the magnetic CCA-MFCs after 100 days of operation. Removal of SLIMF did not significantly affect the power production ($P<0.05$, Figure 5.3.). The difference in peak power density around day 100 compared to the startup period was likely due to the aging effects of cathode (Zhang et al., 2014). Enhanced performance of MFCs by SLIMF was suggested to be reversible (Li et al., 2011; Tao & Zhou, 2014).

However, in the present study enhancements of power and current output did not regress after the removal of magnetic field when the magnetic field was applied right after the inoculation. This persistency may be related to the improved ability of extracellular electron transfer of anodic biofilms over time.

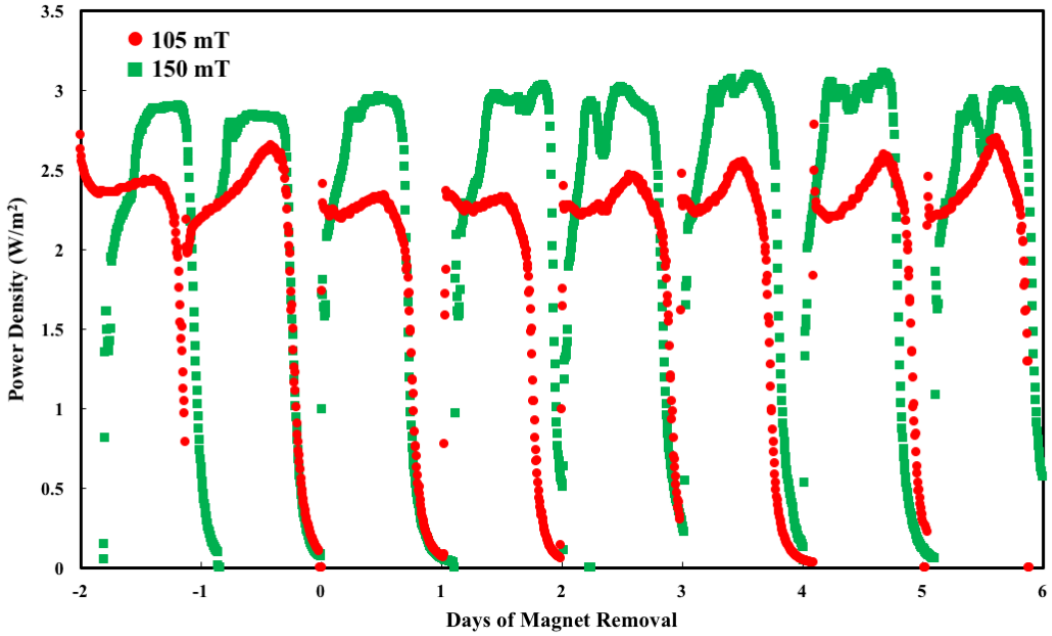

Figure 5.3. Power density changes upon the removal of SLIMF in CCA-MFC reactors (Magnets were removed from MFCs at day 0). Similar results were obtained in triplicate CCA-MFCs but only the performance of one MFC was shown here.

5.3.2 Effects of Magnetic Field on the Development of Anodic Biofilm Conductivity

The changes of biofilm conductance overtime in the presence and absence of SLIMF were monitored by using gold anode with a nonconductive gap in the middle. The conductance increased as biofilms grew across non-conductive gaps in both control and

magnetic GA-MFCs (Figure 5.4.A.). However, the conductance of anodic biofilms in the magnetic GA-MFCs became higher than in the control GA-MFCs starting from days 12, which may due to the faster development of conductive structure under the influence of SLIMF. It has been reported that certain *Geobacter* spp. and *Shewanella* spp. possess the ability to produce and utilize extracellular magnetite particles (Konhauser, 2009; Lovley et al., 1987; Vali et al., 2004). The presence of magnetic field may affect the metabolisms and growth of these exoelectrogens, leading to the faster construction of conductivity of the anodic biofilms in the magnetic MFCs.

After the conductance plateaued, conductance was then further analyzed over a range of potentials. Results demonstrated that the conductivity of anodic biofilms in both magnetic and control GA-MFCs changed in a peak-manner based on gate potential (V_g) (Figure 5.4.B.). The peak conductance of the anodic biofilms was 1516.1 ± 23.0 μS at V_g of -400 mV (vs. Ag/AgCl) in the magnetic GA-MFCs, which was approximately 150% higher than that in control GA-MFCs (613.3 ± 1.0 μS). No significant difference of conductance can be observed between the GA-MFCs with 105 and 150 mT SLIMF (P>0.05).

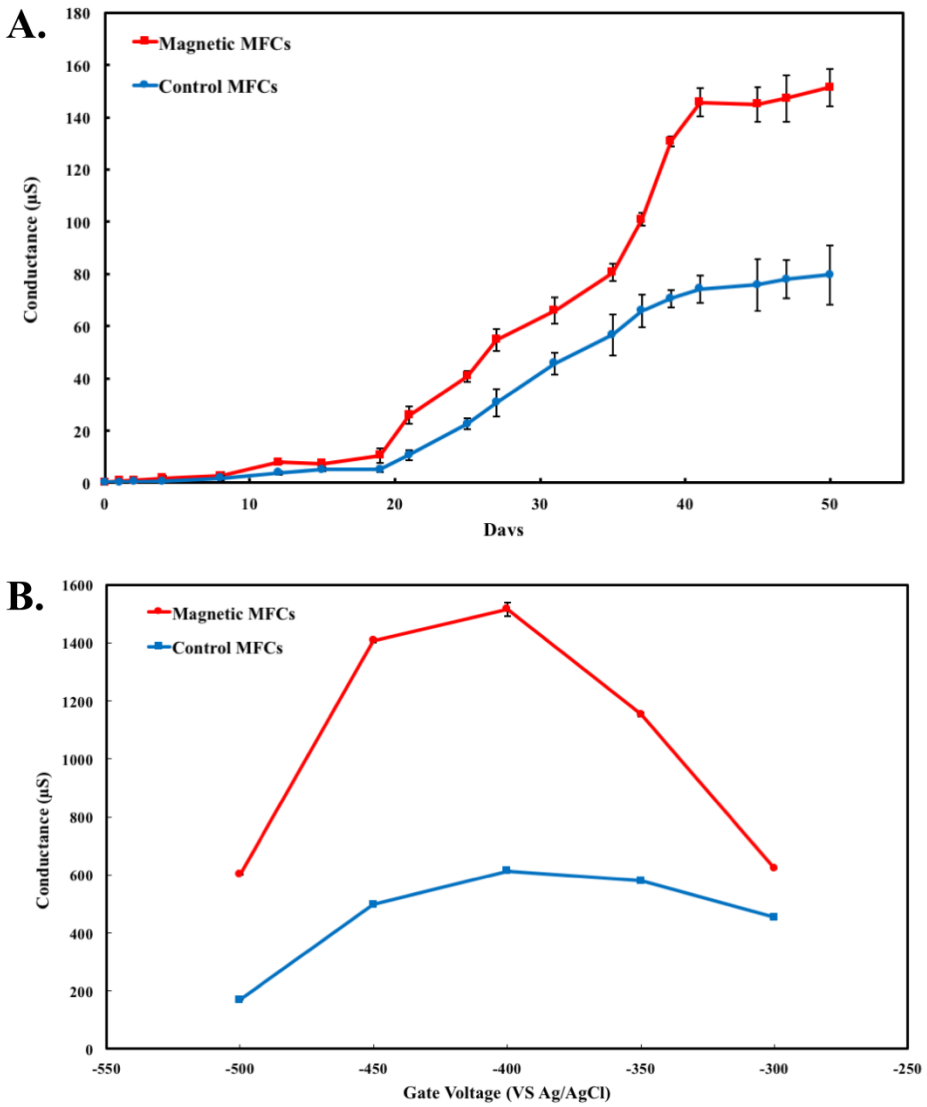

Figure 5.4. A. Measured conductance of magnetic and control GA-MFC reactors over times. Error bar represent the standard deviation (n=2). B. Electrochemical gating analysis of anodic biofilms in magnetic and control GA-MFC reactors. Error bar represent the standard deviation (n=6). Average conductance of the biofilms from the magnetic GA-MFCs under two magnetic intensities (105 and 150 mT) was used in this figure.

It is well-known that SLIMF can influent certain metabolic activities of microbial communities (Moore, 1979; Xu et al., 2009) and may alter the conductivity of thin polymer films (Nalwa, 2001). Previous studies have also suggested that SLIMF could affect the electricity generation of MFCs through decreasing anodic activation loss (Yin et al., 2013) and encouraging growth of anodic exoelectrogenic biofilms (Zhao et al., 2016). While all of these factors can affect or be affected by the increase of the conductivity of anodic biofilms (Kato Marcus et al., 2007; Malvankar et al., 2012a), our present study clearly demonstrated the correlation between the enhanced current density and biofilm conductivity caused by the application of SLIMF. The of similar magnitude of increase in biofilm conductivity and the current density confirms that the biofilm conductivity is a limiting factor for the current generation of anodic biofims in MFCs (Lee et al., 2016; Malvankar et al., 2012c).

The peak-manner response of conductivity over gate potentials confirmed our previous observation that the mixed-species anodic biofilms possess redox conduction as the major conductive mechanism (Li et al., 2016b). The model of redox conductivity describes the conduction network within anodic exoelectrogenic biofilms as a matrix composed by localized reduced and oxidized redox cofactors, in which electrons transfer through via multi-steps hopping process (Li et al., 2016b; Phan et al., 2016; Snider et al., 2012; Yates et al., 2016a; Yates et al., 2015; Yates et al., 2016b). Previous studies have suggested that the presence of SLIMF can stimulate the production of redox cofactors such as flavins in anodic biofilms in *Geobacter*- and *Shewanella*-inoculated MFCs (Li et

al., 2011; Yin et al., 2017; Yin et al., 2013) and the major exoelectrogens in the current anodic communities was *Geobacter* spp. (Lesnik & Liu, 2014). Although some previous studies have suggested that *Geobacter* spp. was unable to utilize redox cofactors like flavin to perform DEET (Bond & Lovley, 2003; Malvankar et al., 2012b), a recent study indicates that *G. sulfurreducens* can secrete and utilize flavins as a bound redox cofactor along with outer membrane c-type cytochromes to facilitate DEET (Okamoto et al., 2014). The significant difference of the maximum conductivity (Figure 4B) in the presence and absence of SLIMF in this study suggests that the observed increase in conductivity of anodic biofilms may be a result of increased production of redox cofactors (Okamoto et al., 2014; Oyama et al., 1986; Snider et al., 2012).

5.3.3 Effects of Magnetic Field on the Conductivity of Mature Biofilms

To evaluate the effect of SLIMF on the conductivity of mature biofilms, SLIMF (105 mT) was applied to the GA-MFCs containing mature biofilms that had not been affected by magnetic field prior. Upon the application of SLIMF, biofilm conductance at OCP increased from 77 to 150 - 176 μS along with the increase of power production (Figure 5.5.). The lower power output observed in GA-MFCs compared with CCA-MFCs was likely due to the use of gold foil anode, which contains less effective surface area than carbon cloth anode with similar projected surface area.

Further electrochemical gating analysis demonstrated that the peak conductivity of anodic exoelectrogenic biofilms in GA-MFCs was also affected by the intensity of

applied SLIMF with the highest conductance (680.0 ± 1.3 μS) observed at the field intensity of 150 mT followed by 655.3 ± 4.6 μS at the intensity of 105 mT (Figure 5.6.A.). Although these conductances were 10% and 6% higher than that of the control (613.3 μS), they were much lower than the 1516.1 μS observed in the biofilms with SLIMF applied from the startup of MFCs. This was possible due to the lower production of localized redox cofactors caused by shorter period of exposure to the magnetic field. In the absence of electron donor (acetate), the conductance still increased with the increase of SLIMF intensity, but the conductance (less than 130 μS) of all biofilms was much lower than that in the presence of electron donors (Figure 5.6.B.). The differences in biofilm conductance may reflect changes of electron accumulation within the biofilm, as has been suggested previously (Li et al., 2016b; Liu & Bond, 2012).

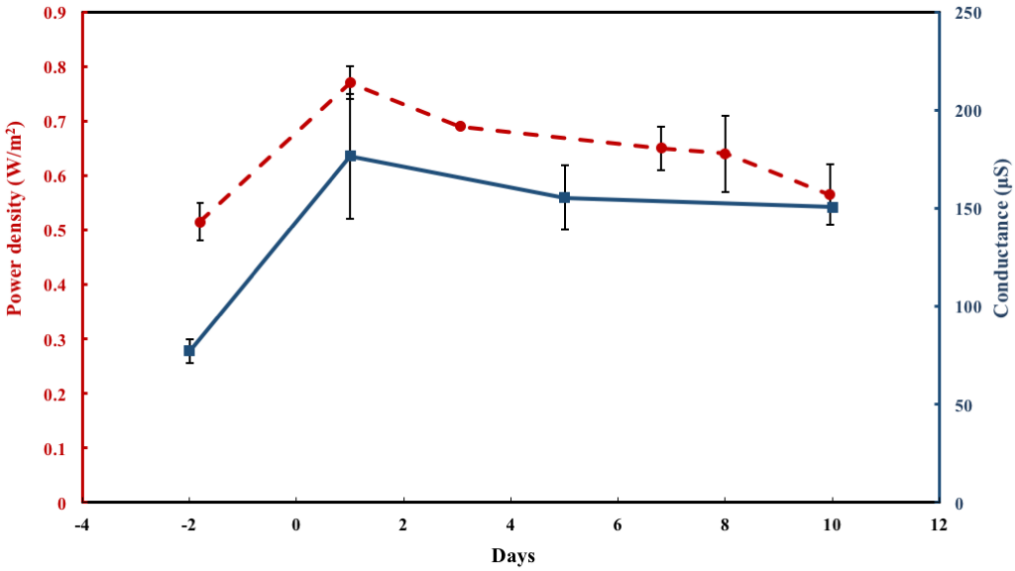

Figure 5.5. Measured conductance and power density of the GA-MFCs with mature biofilms upon the application of SLIMF. Error bar represent the standard deviation (n=2). Average conductance of the biofilms from the magnetic GA-MFCs under two magnetic intensities (105 and 150 mT) was used in this figure.

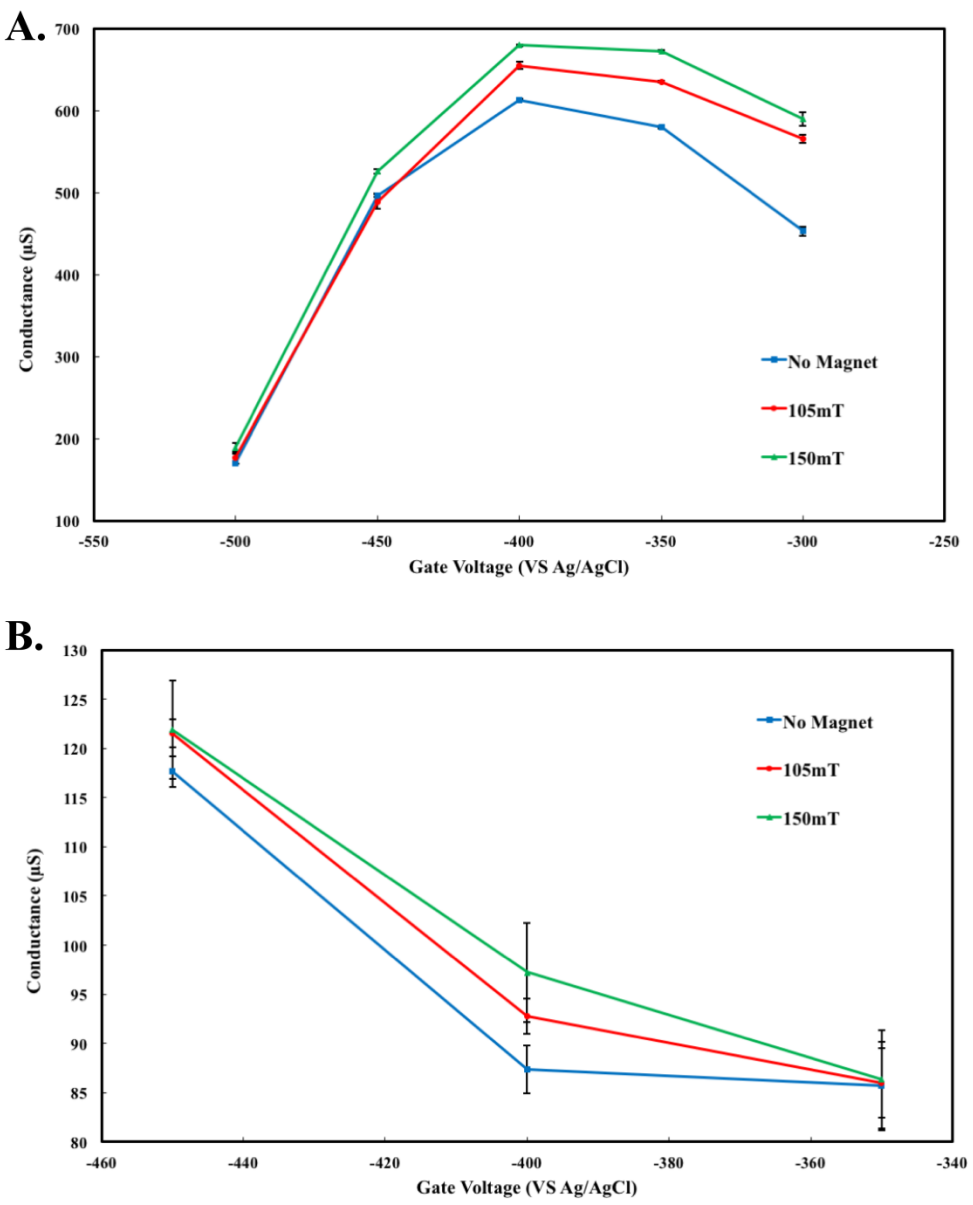

Figure 5.6. Electrochemical gating analysis of anodic biofilms in control GA-MFC reactors under different intensities of SLIMF: A. with substrate and B. without substrate. Error bar represent the standard deviation (n=6).

The impact of magnetic field on biofilm conductivity also confirms the model of redox conduction from an angle different with previous studies that were based on temperature dependency of conductance (Phan et al., 2016; Yates et al., 2016a; Yates et al., 2015) and double potential step chronoamperometry (Zhang et al., 2017). The increase of conductance in mature anodic exoelectrogenic biofilms when being exposed to SLIMF resembles a conductive behavior of thin polymer films called "negative magnetoresistance (NMR)", which has not been observed in conductive biofilms before. NMR describes the resistivity of a conductive material decrease as the magnetic field strength increases (Hu & Wu, 2007). The causes of NMR in conductive materials where electron conduction depends on hopping could be various, from reducing the shrinkage of wave function to decreasing the activation energy of hopping (Raikh, 1990; Raikh et al., 1992). On the other hand, the model of metallic-like conductivity suggests that conductivity of anodic exoelectrogenic biofilms is conferred by the special type of pilus filaments produced by *Geobacter* spp. which possess π-π delocalized electronic state similar to organic metal polymer such as polyaniline (Holmes et al., 2016; Malvankar et al., 2012b; Malvankar et al., 2015; Malvankar et al., 2011; Tan et al., 2016; Vargas et al., 2013). This NMR-like behavior of anodic biofilms is distinct from the conductive behavior of polyaniline polymers, which display positive magnetoresistance (the resistivity of a conductive material increases as the field strength increases) in the presence of magnetic field (Gu et al., 2014).

5.4 Conclusions

Results in this study demonstrate that applying SLIMF can greatly (300%) enhance the current density in high-current producing biofilms and this enhancement seems irreversible, possible due to the significant increase in biofilm conductivity. The observed magnetic field dependence of biofilm conductance confirms the redox conduction mechanism of exoelectrogenic assemblages and represents the first direct observation of NMR behavior in conductive biofilms. Further investigations on the influence of SLIMF on biofilm structure and community, expression of genes related DEET, and metabolic pathways will greatly enhance our understanding of conductive biofilms, leading to their broader applications.

Acknowledgements

This publication was made possible in by grant CBET 0955124 and PFI 1312301 from the U.S. National Science Foundation. The authors would like to acknowledge Keaton Larson Lesnik and Ningshengjie Gao for their valuable discussion.

6 Conclusion & Outlook

6.1 Conclusion

In this dissertation, we aim to further understanding the conductive features of mixed-species microbial assemblages with an ultimate goal of enhancing the performance of engineered anaerobic microbial systems for energy generation from renewable resources. These conductive features include electrical conductivity, conductive behaviors, and conductive mechanism of these assemblages.

The construction of electrical conductivity is one strategy that microbial communities use to effectively take advantage of inexhaustible, insoluble electron acceptors in addition to also providing a conduit for direct electron transfer that is the foundation of many synergistic relationships. The need to perform DEET may provide selective pressure for mixed species microbial communities to choose species that can produce electrical conduits, and thereby shapes conductivity of community assemblage. The present dissertation has demonstrated that the mixed-species exoelectrogenic and methanogenic biofilms possess electrical conductivity. Peak conductivities of mixed-species exoelectrogenic and methanogenic biofilms are respectively 2651 and 71.8 μS/cm at gate potentials of -360 and -175 mV vs Ag/AgCl. The correlation observed between conductivity and community membership has suggested a new possibility of optimizing the extracellular electron transfer process in engineered anaerobic microbial systems. In this dissertation, we also observed about 250% and 300% increases in respectively power and current productions of MFC when SLIMF was applied to MFCs from the inoculation

of mixed species exoelectrogenic culture, suggesting the potential of a nonintrusive approach for practical application of MFCs. Taken together, these results propose feasible approaches by which energy generation may be enhanced in engineered anaerobic microbial systems such as MFC and AD.

Understanding of conductive behaviors may facilitate the development of strategies to effectively optimize the reactor design and overcome various metabolic disruptions encountered during operation of anaerobic microbial systems (Morita et al., 2011). In the present dissertation, we have also provided an initial reference point for the conductive behaviors of mixed-species biofilms. Results provide evidence for biofilm mediated electron transfer on the millimeter scale, 10 times greater than previously observed. In engineered environments of MESs, microbially constructed conductive structures over long conduction distance may lead to the extension of the electroactive biomass, thereby allowing microbial communities to take advantage of limited electrode surface area or reaction space (Malvankar & Lovley, 2014). In natural environments, these conductive structures are likely an essential means of facilitating long distance electron transfer that is the foundation of many biogeochemical processes (Kato et al., 2012a; Kato et al., 2012b; McGlynn et al., 2015; Pfeffer et al., 2012; Reguera, 2012). Shift of conductivity observed in exoelectrogenic biofilms during deprivation of substrate suggests that such deprivation should be avoided during actual operation in order to maintain a steady performance of MFC.

Identification of the conductive mechanism of mixed species biofilms is critical to development of feasible engineering approaches to enhance the energy generation in

anaerobic microbial systems relying on these biofilms. The present dissertation has demonstrated that the mechanism of redox conduction confers the need of electrical connections in both exoelectrogenic biofilms and methanogenic biofilms based on the electrochemical gating analysis. Although an increasing number of studies have identified redox conduction in various kinds of microbial assemblages (Leung et al., 2013; Li et al., 2016b; Pirbadian & El-Naggar, 2012; Xu et al., 2016; Yates et al., 2016a), one main aspect for validating this conduction model remains unexplored. No attempts to enhance the biofilm conductivity has ever succeeded based on the redox conduction theory (Malvankar & Lovley, 2014). In this dissertation, increased of biofilm conductivity in the presence of a static low intensity magnetic field was demonstrated based on the understanding of redox conduction. Therefore, this observation not only may confirm the redox conduction model from a different angle, but also may represent the first direct observation of magnetoresistance behavior in conductive biofilms. Evidences presented in this dissertation together with evidences from other studies have suggested that the conductive features of community assemblages are more often associated with redox conduction (McGlynn et al., 2015; Meysman et al., 2015; Yates et al., 2016a; Yates et al., 2015; Yates et al., 2016b), which is the rate limiting step of direct EET in microbial assemblages containing mixed conduction mechanisms.

6.2 Outlook

Assemblages of microorganisms exist throughout various natural and engineered environments in the form of biofilms, granules, and multicellular filaments. The

systematic study of these microbial assemblages has provided insight into energy interactions and syntrophic relationships of various microbial communities. The recent discovery of electrical conductivity in several of these communities has challenged the traditional understanding of microbial extracellular polymers and extracellular electron transfer (Aulenta et al., 2013; Kato et al., 2012a; Morita et al., 2011; Rotaru et al., 2014a; Yates et al., 2015). The continued discovery of new conductive communities and the relative infancy of the field suggest that other conductive assemblages are yet to be discovered (Li et al., 2016b; Meysman et al., 2015; Pfeffer et al., 2012; Snider et al., 2012; Yates et al., 2016a). The continued survey for conductive microbial assemblages and interactions enabled by their presence will increase the understanding of this phenomenon holding environmental and engineering significance (Lovley, 2016; Malvankar et al., 2012a). Coupling measurements of conductivity with genetic, microscopic, and isotopic tools will provide further insights into the detailed electron transfer pathways in these systems.

This novel means of energy transfer and communication enabled by microbially constructed conductivity has the potential for a far reaching impact beyond engineered anaerobic microbial systems and biogeochemical studies that range from material science to cellular communication, and even to human health. Further understanding biological redox conductivity may provide inspiration for the design that underlines the sustainable production of synthetic tunable redox conducting polymers that have gained enormous attention towards for protein-based bioelectronics applications like biomedical devices, microscale power units, and biosensors (Altamura et al., 2016; Holzinger et al., 2012; Le

Goff et al., 2011). Insights on cell-to-cell communication may also be greatly enhanced by broadening our understanding of microbial interactions as recent studies have demonstrated that bacterial cells are attracted to electrical signals released by biofilms (Humphries et al., 2017). The discovery of electrical interactions between anaerobic microbes in human guts and human cells in the gut epithelium may even lead to advancements in medicine and human health (Ericsson et al., 2015). The interconnected nature of small has and will continue to have a large impact on all.

7 Bibliography

Adhikari, R.Y., Malvankar, N.S., Tuominen, M.T., Lovley, D.R. 2016. Conductivity of individual Geobacter pili. *RSC Advances*, **6**(10), 8354-8357.

Altamura, L., Horvath, C., Rengaraj, S., Rongier, A., Elouarzaki, K., Gondran, C., Maçon, A.L.B., Vendrely, C., Bouchiat, V., Fontecave, M., Mariolle, D., Rannou, P., Goff, A., Duraffourg, N., Holzinger, M., Forge, V. 2016. A synthetic redox biofilm made from metalloprotein–prion domain chimera nanowires. *Nature Chemistry*, **9**, 157-163.

Anderson, L.B., Reilley, C.N. 1965. Thin-layer electrochemistry: steady-state methods of studying rate processes. *Journal of Electroanalytical Chemistry* **10**(4), 295-305.

Aulenta, F., Rossetti, S., Amalfitano, S., Majone, M., Tandoi, V. 2013. Conductive magnetite nanoparticles accelerate the microbial reductive dechlorination of trichloroethene by promoting interspecies electron transfer processes. *ChemSusChem*, **6**(3), 433-436.

Bond, D.R., Lovley, D.R. 2003. Electricity production by Geobacter sulfurreducens attached to electrodes. *Applied and Environmental Microbiology*, **69**(3), 1548-1555.

Bond, D.R., Strycharz-Glaven, S.M., Tender, L.M., Torres, C.I. 2012. On electron transport through Geobacter biofilms. *ChemSusChem*, **5**(6), 1099-1105.

Bryant, M.P., Wolin, E.A., Wolin, M.J., Wolfe, R.S. 1967. Methanobacillus omelianskii, a symbiotic association of two species of bacteria. *Archiv für Mikrobiologie*, **59**(1-3), 20-31.

Caporaso, J.G., Kuczynski, J., Stombaugh, J., Bittinger, K., Bushman, F.D., Costello, E.K., Fierer, N., Pena, A.G., Goodrich, J.K., Gordon, J.I. 2010. QIIME allows analysis of high-throughput community sequencing data. *Nature methods*, **7**(5), 335-336.

Chen, S., Rotaru, A.E., Liu, F., Philips, J., Woodard, T.L., Nevin, K.P., Lovley, D.R. 2014a. Carbon cloth stimulates direct interspecies electron transfer in syntrophic co-cultures. *Bioresource Technology*, **173**, 82-86.

Chen, S., Rotaru, A.E., Shrestha, P.M., Malvankar, N.S., Liu, F., Fan, W., Nevin, K.P., Lovley, D.R. 2014b. Promoting interspecies electron transfer with biochar. *Scientific Reports*, **4**, 5019.

Cheng, S., Liu, H., Logan, B.E. 2006. Increased performance of single-chamber microbial fuel cells using an improved cathode structure. *Electrochemistry Communications*, **8**(3), 489-494.

Chidsey, C.E., Feldman, B.J., Lundgren, C., Murray, R.W. 1986. Micrometer-spaced platinum interdigitated array electrode: fabrication, theory, and initial use. *Analytical Chemistry*, **58**(3), 601-607.

Dalton, E.F., Surridge, N.A., Jernigan, J.C., Wilbourn, K.O., Facci, J.S., Murray, R.W. 1990. Charge transport in electroactive polymers consisting of fixed molecular redox sites. *Chemical Physics*, **141**(1), 143-157.

Edgar, R.C. 2010. Search and clustering orders of magnitude faster than BLAST. *Bioinformatics*, **26**(19), 2460-2461.

El-Naggar, M.Y., Wanger, G., Leung, K.M., Yuzvinsky, T.D., Southam, G., Yang, J., Lau, W.M., Nealson, K.H., Gorby, Y.A. 2010. Electrical transport along bacterial nanowires from Shewanella oneidensis MR-1. *Proceedings of the National Academy of Sciences of the United States of America*, **107**(42), 18127-18131.

Ericsson, A., Davis, D., Franklin, C., Hagan, C. 2015. Exoelectrogenic capacity of host microbiota predicts lymphocyte recruitment to the gut. *Physiological Genomics*, **47**(7), 243-252.

Fan, Y., Han, S.-K., Liu, H. 2012. Improved performance of CEA microbial fuel cells with increased reactor size. *Energy & Environmental Science*, **5**(8), 8273-8280.

Fan, Y., Hu, H., Liu, H. 2007. Enhanced Coulombic efficiency and power density of air-cathode microbial fuel cells with an improved cell configuration. *Journal of Power Sources*, **171**(2), 348-354.

Fan, Y., Sharbrough, E., Liu, H. 2008. Quantification of the internal resistance distribution of microbial fuel cells. *Environmental science & technology*, **42**(21), 8101-8107.

Fan, Y., Xu, S., Schaller, R., Jiao, J., Chaplen, F., Liu, H. 2011. Nanoparticle decorated anodes for enhanced current generation in microbial electrochemical cells. *Biosensors and Bioelectronics*, **26**(5), 1908-1912.

Fricke, K., Harnisch, F., Schröder, U. 2008. On the use of cyclic voltammetry for the study of anodic electron transfer in microbial fuel cells. *Energy & Environmental Science*, **1**, 144-147.

Gorby, Y.A., Yanina, S., McLean, J.S., Rosso, K.M., Moyles, D., Dohnalkova, A., Beveridge, T.J., Chang, I.S., Kim, B.H., Kim, K.S., Culley, D.E., Reed, S.B., Romine, M.F., Saffarini, D.A., Hill, E.A., Shi, L., Elias, D.A., Kennedy, D.W., Pinchuk, G., Watanabe, K., Ishii, S.i., Logan, B., Nealson, K.H., Fredrickson, J.K. 2006. Electrically conductive bacterial nanowires produced by Shewanella oneidensis strain MR-1 and other microorganisms. *Proceedings of the National Academy of Sciences of the United States of America*, **103**(30), 11358-11363.

Gu, H., Guo, J., Yan, X., Wei, H., Zhang, X., Liu, J., Huang, Y., Wei, S., Guo, Z. 2014. Electrical transport and magnetoresistance in advanced polyaniline nanostructures and nanocomposites. *Polymer*, **55**(17), 4405-4419.

Hamady, M., Lozupone, C., Knight, R. 2010. Fast UniFrac: facilitating high-throughput phylogenetic analyses of microbial communities including analysis of pyrosequencing and PhyloChip data. *The ISME journal*, **4**(1), 17-27.

Heeger, A.J. 2001. Semiconducting and metallic polymers: the fourth generation of polymeric materials. *The Journal of Physical Chemistry*, **105**(36), 8475-8491.

Holmes, D.E., Dang, Y., Walker, D.J.F. 2016. The Electrically Conductive Pili of Geobacter Species are a Recently Evolved Feature for Extracellular Electron Transfer. *Microbial Genomics*.

Holzinger, M., Goff, A., Cosnier, S. 2012. Carbon nanotube/enzyme biofuel cells. *Electrochimica Acta*, **82**, 179-190.

Hu, B., Wu, Y. 2007. Tuning magnetoresistance between positive and negative values in organic semiconductors. *Nature materials*, **6**, 985-991.

Hugenholtz, P., Tyson, G.W., Blackall, L.L. 2002. Design and evaluation of 16S rRNA-targeted oligonucleotide probes for fluorescence in situ hybridization. in: *Gene Probes*, Springer, pp. 29-42.

Humphries, J., Xiong, L., Liu, J., Prindle, A., Yuan, F., Arjes, H.A., Tsimring, L., Süel, G.M. 2017. Species-Independent Attraction to Biofilms through Electrical Signaling. *Cell*, **168**(1-2), 200-209.

Inzelt, G. 2012. Classification of Electrochemically Active Polymers. in: *Conducting Polymers: A New Era in Electrochemistry*, Springer Berlin Heidelberg. Berlin, Heidelberg, pp. 7-82.

Janicek, A., Fan, Y., Liu, H. 2015. Performance and Stability of Different Cathode Base Materials for Use in Microbial Fuel Cells. *Journal of Power Sources*, **280**, 159-165.

Jiang, X., Hu, J., Lieber, A.M., Jackan, C.S., Biffinger, J.C., Fitzgerald, L.A., Ringeisen, B.R., Lieber, C.M. 2014. Nanoparticle facilitated extracellular electron transfer in microbial fuel cells. *Nano Letters*, **14**(11), 6737-6742.

Kankare, J., Kupila, E.-L. 1992. *In-situ* conductance measurement during electropolymerization. *Journal of Electroanalytical Chemistry*, **322**(1), 167-181.

Kato Marcus, A., Torres, C.I., Rittmann, B.E. 2007. Conduction-based modeling of the biofilm anode of a microbial fuel cell. *Biotechnology and Bioengineering*, **98**(6), 1171-1182.

Kato, S. 2015. Biotechnological aspects of microbial extracellular electron transfer. *Microbes and Environments*, **30**(2), 133-139.

Kato, S., Hashimoto, K., Watanabe, K. 2012a. Methanogenesis facilitated by electric syntrophy via (semi)conductive iron-oxide minerals. *Environmental Microbiology*, **14**, 1646-1654.

Kato, S., Hashimoto, K., Watanabe, K. 2012b. Microbial interspecies electron transfer via electric currents through conductive minerals. *Proceedings of the National Academy of Sciences of the United States of America*, **109**(25), 10042-10046.

Kiely, P., Regan, J., Logan, B. 2011. The electric picnic: synergistic requirements for exoelectrogenic microbial communities. *Current opinion in biotechnology*, **22**(3), 378-385.

Klindworth, A., Pruesse, E., Schweer, T., Peplies, J., Quast, C., Horn, M., Glöckner, F.O. 2012. Evaluation of general 16S ribosomal RNA gene PCR primers for classical and next-generation sequencing-based diversity studies. *Nucleic acids research*, gks808.

Konhauser, K.O. 2009. *Introduction to geomicrobiology*. John Wiley & Sons.

Kouzuma, A., Kato, S., Watanabe, K. 2015. Microbial interspecies interactions: recent findings in syntrophic consortia. *Frontiers in microbiology*.

Le Goff, A., Holzinger, M., Cosnier, S. 2011. Enzymatic biosensors based on SWCNT-conducting polymer electrodes. *The Analyst*, **136**(7), 1279-1287.

Leang, C., Malvankar, N., Franks, A., Nevin, K., Lovley, D. 2013. Engineering Geobacter sulfurreducens to produce a highly cohesive conductive matrix with enhanced capacity for current production. *Energy & Environmental Science*, **6**(6), 1901-1908.

Lee, H.-S., Dhar, B., An, J., Rittmann, B.E., Ryu, H., Domingo, J.W., Ren, H., Chae, J. 2016. The Roles of Biofilm Conductivity and Donor Substrate Kinetics in a Mixed-Culture Biofilm Anode. *Environmental Science & Technology*, **50**(23), 12799-12807.

Lesnik, K.L., Liu, H. 2014. Establishing a core microbiome in acetate-fed microbial fuel cells. *Applied microbiology and biotechnology*, **98**(9), 4187-4196.

Leung, K., Wanger, G., El-Naggar, M., Gorby, Y., Southam, G., Lau, W., Yang, J. 2013. Shewanella oneidensis MR-1 Bacterial Nanowires Exhibit P-type, Tunable Electronic Behaviour. *Nano Letters*, **13**(6), 2407-2411.

Leung, K., Wanger, G., Guo, Q., Gorby, Y., Southam, G., Lau, W., Yang, J. 2011. Bacterial nanowires: conductive as silicon, soft as polymer. *Soft Matter*, **7**(14), 6617.

Li, C., Lesnik, K.L., Fan, Y., Liu, H. 2016a. Millimeter scale electron conduction through exoelectrogenic mixed species biofilms. *FEMS Microbiology Letters*, **363**(15), fnw153.

Li, C., Lesnik, K.L., Fan, Y., Liu, H. 2016b. Redox conductivity of current-producing mixed species biofilms. *PloS One*, **11**(5), e0155247.

Li, W.W., Sheng, G.P., Liu, X.W., Cai, P.J., Sun, M. 2011. Impact of a static magnetic field on the electricity production of Shewanella-inoculated microbial fuel cells. *Biosensors and Bioelectronics*, **26**(10), 3987-3992.

Liu, F., Rotaru, A.-E., Shrestha, P.M., Malvankar, N.S., Nevin, K.P., Lovley, D.R. 2015. Magnetite compensates for the lack of a pilin-associated c-type cytochrome in extracellular electron exchange. *Environmental Microbiology*, **17**(3), 648-655.

Liu, F., Rotaru, A.E., Shrestha, P.M., Malvankar, N.S., Nevin, K.P., Lovley, D.R. 2012. Promoting direct interspecies electron transfer with activated carbon. *Energy & Environmental Science*, **5**(10), 8982-8989.

Liu, G., Yates, M.D., Cheng, S., Call, D.F., Sun, D., Logan, B.E. 2011. Examination of microbial fuel cell start-up times with domestic wastewater and additional amendments. *Bioresource Technology*, **102**(15), 7301-7306.

Liu, X., Tremblay, P.-L., Malvankar, N., Nevin, K., Lovley, D., Vargas, M. 2013. Geobacter sulfurreducens Strain Expressing Pseudomonas aeruginosa Type IV Pili Localizes OmcS on Pili but is Deficient in Fe(III) Oxide Reduction and Current Production. *Applied and Environmental Microbiology*, **80**(3), 1219-1224.

Liu, Y., Bond, D.R. 2012. Long-distance electron transfer by G. sulfurreducens biofilms results in accumulation of reduced c-type cytochromes. *ChemSusChem*, **5**(6), 1047-1053.

Logan, B.E. 2009. Exoelectrogenic bacteria that power microbial fuel cells. *Nature Reviews Microbiology*, **7**(5), 375-381.

Lovley, D.R. 2012. Electromicrobiology. *Annual review of microbiology*, **66**, 391-409.

Lovley, D.R. 2016. Happy together: microbial communities that hook up to swap electrons. *The ISME Journal*, **11**(2), 327-336.

Lovley, D.R. 2011a. Live wires: direct extracellular electron exchange for bioenergy and the bioremediation of energy-related contamination. *Energy & Environmental Science*, **4**(12), 4896-4906.

Lovley, D.R. 2011b. Reach out and touch someone: potential impact of DIET (direct interspecies energy transfer) on anaerobic biogeochemistry, bioremediation, and bioenergy. *Reviews in Environmental Science and Bio/Technology*, **10**(2), 101-105.

Lovley, D.R., Malvankar, N.S. 2015. Seeing is believing: novel imaging techniques help clarify microbial nanowire structure and function. *Environmental Microbiology*, **17**(7), 2209-2215.

Lovley, D.R., Stolz, J.F., Nord, G.L., Phillips, E.J.P. 1987. Anaerobic production of magnetite by a dissimilatory iron-reducing microorganism. *Nature*.

Malkin, S.Y., Rao, A.M.F., Seitaj, D., Vasquez-Cardenas, D. 2014. Natural occurrence of microbial sulphur oxidation by long-range electron transport in the seafloor. *The ISME Journal*, **8**, 1843-1854.

Malvankar, N.S., King, G.M., Lovley, D.R. 2014a. Centimeter-long electron transport in marine sediments via conductive minerals. *The ISME Journal*, **9**(2), 527-531.

Malvankar, N.S., Lau, J., Nevin, K.P., Franks, A.E., Tuominen, M.T., Lovley, D.R. 2012a. Electrical conductivity in a mixed-species biofilm. *Applied and Environmental Microbiology*, **78**(16), 5967-5971.

Malvankar, N.S., Lovley, D.R. 2014. Microbial nanowires for bioenergy applications. *Current Opinion in Biotechnology*, **27**, 88-95.

Malvankar, N.S., Rotello, V.M., Tuominen, M.T., Lovley, D.R. 2016. Reply to 'Measuring conductivity of living Geobacter sulfurreducens biofilms'. *Nature Nanotechnology*, **11**(11), 913-914.

Malvankar, N.S., Tuominen, M.T., Lovley, D.R. 2012b. Lack of cytochrome involvement in long-range electron transport through conductive biofilms and nanowires of Geobacter sulfurreducens. *Energy & Environmental Science*, **5**(9), 8651-8659.

Malvankar, N.S., Tuominen, T.M., Lovely, R.D. 2012c. Biofilm conductivity is a decisive variable for high-current-density Geobacter sulfurreducens microbial fuel cells. *Energy & Environmental Science*, **5**, 5790-5797.

Malvankar, N.S., Vargas, M., Nevin, K., Tremblay, P.L., Evans-Lutterodt, K., Nykypanchuk, D., Martz, E., Tuominen, M.T., Lovley, D.R. 2015. Structural basis for metallic-like conductivity in microbial nanowires. *MBio*, **6**(2), e00084-15.

Malvankar, N.S., Vargas, M., Nevin, K.P., Franks, A.E., Leang, C., Kim, B.C., Inoue, K., Mester, T., Covalla, S.F., Johnson, J.P., Rotello, V.M., Tuominen, M.T., Lovley, D.R. 2011. Tunable metallic-like conductivity in microbial nanowire networks. *Nature Nanotechnology*, **6**(9), 573-579.

Malvankar, N.S., Yalcin, S.E., Tuominen, M.T., Lovley, D.R. 2014b. Visualization of charge propagation along individual pili proteins using ambient electrostatic force microscopy. *Nature Nanotechnology*, **9**, 1012-1017.

McCarty, P.L., Bae, J., Kim, J. 2011. Domestic wastewater treatment as a net energy producer–can this be achieved? *Environmental Science & Technology*, **45**(17), 7100-7106.

McDuffie, B., Anderson, L.B., Reilley, C.N. 1966. Twin-Electrode Thin-Layer Electrochemistry. Determination of Chemical Reaction Rates by Decay of Steady-State Current. *Analytical Chemistry*, **38**(7), 883-890.

McGlynn, S.E., Chadwick, G.L., Kempes, C.P., Orphan, V.J. 2015. Single cell activity reveals direct electron transfer in methanotrophic consortia. *Nature*, **526**, 531-535.

McInerney, M.J., Sieber, J.R., Gunsalus, R.P. 2009. Syntrophy in anaerobic global carbon cycles. *Current Opinion in Biotechnology*, **20**(6), 623-632.

McInerney, M.J., Struchtemeyer, C.G., Sieber, J., Mouttaki, H., Stams, A.J.M., Schink, B., Rohlin, L., Gunsalus, R.P. 2008. Physiology, Ecology, Phylogeny, and Genomics of Microorganisms Capable of Syntrophic Metabolism. *Annals of the New York Academy of Sciences*, **1125**(1), 58-72.

Meysman, F.J.R., Risgaard-Petersen, N., Malkin, S.Y., Nielsen, L.P. 2015. The geochemical fingerprint of microbial long-distance electron transport in the seafloor. *Geochimica et Cosmochimica Acta*, **152**(1), 122-142.

Moore, R.L. 1979. Biological effects of magnetic fields: studies with microorganisms. *Canadian Journal of Microbiology*, **25**(10).

Morita, M., Malvankar, N.S., Franks, A., Summers, Z., Giloteaux, L., Rotaru, A., Rotaru, C., Lovley, D. 2011. Potential for direct interspecies electron transfer in methanogenic wastewater digester aggregates. *mBio*, **2**(4), e00159-11.

Nakamura, R., Okamoto, A., Tajima, N., Newton, G.J., Kai, F., Takashima, T., Hashimoto, K. 2010. Biological iron-monosulfide production for efficient electricity harvesting from a deep-sea metal-reducing bacterium. *Chembiochem*, **11**(5), 643-645.

Nalwa, H.S. 2001. *Handbook of Thin Films, Five-Volume Set*. Academic Press.

Nielsen, L.P., Risgaard-Petersen, N. 2015. Rethinking sediment biogeochemistry after the discovery of electric currents. *Annual Review of Marine Science*, **7**, 425-442.

Ohsaka, T., Yamamoto, H., Oyama, N. 1987. Thermodynamic parameters for charge-transfer reactions in pendant viologen polymers coated on graphite electrodes and at electrode/pendant viologen polymer film interfaces. *Journal of Physical Chemistry*, **91**(14), 3775-3779.

Okamoto, A., Saito, K., Inoue, K., Nealson, K.H., Hashimoto, K., Nakamura, R. 2014. Uptake of self-secreted flavins as bound cofactors for extracellular electron transfer in Geobacter species. *Energy & Environmental Science*, **7**(4), 1357-1361.

Ordòñez, M., Schrott, G., Massazza, D., Busalmen, J. 2016. The relay network of Geobacter biofilms. *Energy & Environmental Science*, **9**, 2677-2681.

Oyama, N., Ohsaka, T., Yamamoto, H., Kaneko, M. 1986. Charge-transfer reactions in pendant viologen polymers coated on graphite electrodes and at electrode/pendant viologen polymer film interfaces. *The Journal of Physical Chemistry*, **90**(16), 3850-3856.

Pfeffer, C., Larsen, S., Song, J., Dong, M., Besenbacher, F. 2012. Filamentous bacteria transport electrons over centimetre distances. *Nature*, **491**(7423), 218-221.

Phan, H., Yates, M.D., Kirchhofer, N.D., Bazan, G.C., Tender, L.M., Nguyen, T.-Q. 2016. Biofilm as a redox conductor: a systematic study of the moisture and temperature dependence of its electrical properties. *Physical Chemistry Chemical Physics*, **18**(27), 17815-17821.

Pirbadian, S., Barchinger, S.E., Leung, K., Byun, H., Jangir, Y., Bouhenni, R.A., Reed, S.B., Romine, M.F., Saffarini, D.A., Shi, L. 2014. Shewanella oneidensis MR-1 nanowires are outer membrane and periplasmic extensions of the extracellular electron transport components. *Proceedings of the National Academy of Sciences of the United States of America*, **111**(35), 12883-12888.

Pirbadian, S., El-Naggar, M.Y. 2012. Multistep hopping and extracellular charge transfer in microbial redox chains. *Physical Chemistry Chemical Physics*, **14**(40), 13802-13808.

Pokkuluri, R.P., Londer, Y.Y., Duke, N.E.C., Long, C.W., Schiffer, M. 2004. Family of cytochrome c7-type proteins from Geobacter sulfurreducens: structure of one cytochrome c7 at 1.45 A resolution. *Biochemistry*, **43**(4), 849-859.

Rabaey, K., Boon, N., Höfte, M. 2005. Microbial phenazine production enhances electron transfer in biofuel cells. *Environmental Science & Technology*, **39**(9), 3401-3408.

Raikh, M.E. 1990. Incoherent mechanism of negative magnetoresistance in the variable- range-hopping regime. *Solid State Communications*, **75**(11), 935-938.

Raikh, M.E., Czingon, J., Ye, Q.-y., Koch, F., Schoepe, W., Ploog, K. 1992. Mechanisms of magnetoresistance in variable-range-hopping transport for two-dimensional electron systems. *Physical Review B*, **45**(11), 6015.

Reguera, G. 2012. Microbiology: Bacterial power cords. *Nature*, **491**(7423), 201-202.

Reguera, G. 2011. When microbial conversations get physical. *Trends in Microbiology*, **19**(3), 105-113.

Richter, H., McCarthy, K., Nevin, K.P., Johnson, J.P., Rotello, V.M., Lovley, D.R. 2008. Electricity Generation by Geobacter sulfurreducens Attached to Gold Electrodes. *Langmuir*, **24**(8), 4376-4379.

Risgaard-Petersen, N., Kristiansen, M., Frederiksen, R.B., Dittmer, A., Bjerg, J., Trojan, D., Schreiber, L., Damgaard, L., Schramm, A., Nielsen, L. 2015. Cable bacteria in freshwater sediments. *Applied and Environmental Microbiology*, **81**(17), 6003-6011.

Rotaru, A.E., Shrestha, P.M., Liu, F., Markovaite, B., Chen, S., Nevin, K.P., Lovley, D.R. 2014a. Direct interspecies electron transfer between Geobacter metallireducens and Methanosarcina barkeri. *Applied and Environmental Microbiology*, **80**(15), 4599-4605.

Rotaru, A.E., Shrestha, P.M., Liu, F., Shrestha, M., Shrestha, D., Embree, M., Zengler, K., Wardman, C., Nevin, K.P., Lovley, D.R. 2014b. A new model for electron flow during anaerobic digestion: direct interspecies electron transfer to Methanosaeta for the reduction of carbon dioxide to methane. *Energy & Environmental Science*, **7**(1), 408-415.

Ruhl, S., Eidt, A., Melzl, H., Reischl, U., Cisar, J.O. 2014. Probing Microbial Biofilm Communities for Coadhesion Partners. *Applied and Environmental Microbiology*, **80**(21), 6583-6590.

Sanderson, D.G., Anderson, L.B. 1985. Filar electrodes: steady-state currents and spectroelectrochemistry at twin interdigitated electrodes. *Analytical Chemistry*, **57**(12), 2388-2393.

Shrestha, P.M., Malvankar, N.S., Werner, J.J., Franks, A.E., Rotaru, A.E., Shrestha, M., Liu, F., Nevin, K., Angenent, L.T., Lovely, R.D. 2014. Correlation between microbial community and granule conductivity in anaerobic bioreactors for brewery wastewater treatment. *Bioresource Technology*, **174**, 306-310.

Shrestha, P.M., Rotaru, A.E. 2014. Plugging in or going wireless: strategies for interspecies electron transfer. *Frontiers in microbiology*, **5**.

Sieber, J.R., Le, H.M., McInerney, M.J. 2014. The importance of hydrogen and formate transfer for syntrophic fatty, aromatic and alicyclic metabolism. *Environmental Microbiology*, **16**(1), 177-188.

Sieber, J.R., McInerney, M.J., Gunsalus, R.P. 2012. Genomic insights into syntrophy: the paradigm for anaerobic metabolic cooperation. *Annual Review of Microbiology*, **66**, 429-452.

Snider, R.M., Strycharz-Glaven, S.M., Tsoi, S.D., Erickson, J.S., Tender, L.M. 2012. Long-range electron transport in Geobacter sulfurreducens biofilms is redox gradient-driven. *Proceedings of the National Academy of Sciences of the United States of America*, **109**(38), 15467-15472.

Stams, A.J., de Bok, F.A., Plugge, C.M., van Eekert, M.H., Dolfing, J., Schraa, G. 2006. Exocellular electron transfer in anaerobic microbial communities. *Environmental Microbiology*, **8**(3), 371-382.

Stams, A.J., Plugge, C.M. 2009. Electron transfer in syntrophic communities of anaerobic bacteria and archaea. *Nature Reviews Microbiology*, **7**(8), 568-577.

Strycharz-Glaven, S.M., Snider, R.M., Guiseppi-Elie, A., Tender, L.M. 2011. On the electrical conductivity of microbial nanowires and biofilms. *Energy & Environmental Science*, **4**(11), 4366-4379.

Strycharz-Glaven, S.M., Tender, L.M. 2012. Reply to the 'Comment on "On electrical conductivity of microbial nanowires and biofilms"'by NS Malvankar, MT Tuominen and DR Lovley, Energy Environ. Sci., 2012, 5, DOI: 10.1039/c2ee02613a. *Energy & Environmental Science*, **5**(3), 6250-6255.

Summers, Z.M., Fogarty, H.E., Leang, C., Franks, A.E., Malvankar, N.S., Lovley, D.R. 2010. Direct exchange of electrons within aggregates of an evolved syntrophic coculture of anaerobic bacteria. *Science*, **330**(6009), 1413-5.

Tan, Y., Adhikari, R.Y., Malvankar, N.S., Ward, J.E., Nevin, K.P., Woodard, T.L., Smith, J.A., Snoeyenbos-West, O., Franks, A., Lovley, D.R. 2016. The Low Conductivity of Geobacter uraniireducens Pili Suggests a Diversity of Extracellular Electron Transfer Mechanisms in the Genus Geobacter. *Frontiers in Microbiology*, **7**.

Tao, Q., Zhou, S. 2014. Effect of static magnetic field on electricity production and wastewater treatment in microbial fuel cells. *Applied microbiology and biotechnology*, **98**(23), 9879-9887.

Thauer, R.K., Kaster, A.-K.K., Seedorf, H., Buckel, W., Hedderich, R. 2008. Methanogenic archaea: ecologically relevant differences in energy conservation. *Nature reviews. Microbiology*, **6**(8), 579-591.

Torres, C.I., Krajmalnik-Brown, R. 2009. Selecting anode-respiring bacteria based on anode potential: phylogenetic, electrochemical, and microscopic characterization. *Environmental Science & Technology*, **43**(24), 9519-9524.

Tschirhart, T., Kim, E., McKay, R., Ueda, H., Wu, H.-C., Pottash, A., Zargar, A., Negrete, A., Shiloach, J., Payne, G.F., Bentley, W.E. 2017. Electronic control of gene expression and cell behaviour in Escherichia coli through redox signalling. *Nature Communications*, **8**, 14030.

Vali, H., Weiss, B., Li, Y.-L., Sears, S.K., Kim, S.S., Kirschvink, J.L., Zhang, C.L. 2004. Formation of tabular single-domain magnetite induced by Geobacter metallireducens GS-15. *Proceedings of the National Academy of Sciences of the United States of America*, **101**(46), 16121-16126.

Vanmaekelbergh, D., Houtepen, A.J., Kelly, J.J. 2007. Electrochemical gating: a method to tune and monitor the (opto) electronic properties of functional materials. *Electrochimica Acta*, **53**(3), 1140-1149.

Vargas, M., Malvankar, N.S., Tremblay, P.L., Leang, C., Smith, J.A., Patel, P., Synoeyenbos-West, O., Nevin, K.P., Lovley, D.R. 2013. Aromatic amino acids required for pili conductivity and long-range extracellular electron transport in Geobacter sulfurreducens. *mBio*, **4**(2), e00105-13.

Wagner, M. 2015. Microbiology: Conductive consortia. *Nature*, **526**(7574), 513-514.

Xu, S., Jangir, Y., El-Naggar, M.Y. 2016. Disentangling the roles of free and cytochrome-bound flavins in extracellular electron transport from Shewanella oneidensis MR-1. *Electrochimica Acta*, **198**, 49-55.

Xu, Y.B., Duan, X.J., Yan, J.N., Du, Y.Y., Sun, S.Y. 2009. Influence of magnetic field on activity of given anaerobic sludge. *Biodegradation*, **20**(6), 875-883.

Yates, M.D., Eddie, B.J., Kotloski, N.J., Lebedev, N., Malanoski, A.P., Lin, B., Strycharz-Glaven, S.M., Tender, L.M. 2016a. Toward understanding long-distance extracellular electron transport in an electroautotrophic microbial community. *Energy & Environmental Science*, **9**(11), 3544-3558.

Yates, M.D., Golden, J.P., Roy, J., Strycharz-Glaven, S.M., Tsoi, S., Erickson, J.S., El-Naggar, M.Y., Calabrese Barton, S., Tender, L.M. 2015. Thermally activated long range electron transport in living biofilms. *Physical Chemistry Chemical Physics*, **17**(48), 32564-32570.

Yates, M.D., Strycharz-Glaven, S.M., Golden, J.P., Roy, J., Tsoi, S., Erickson, J.S., El-Naggar, M.Y., Barton, S., Tender, L.M. 2016b. Measuring conductivity of living Geobacter sulfurreducens biofilms. *Nature Nanotechnology*, **11**(11), 910-913.

Yin, Y., Huang, G., Di, M., Xue, C., Li, W., Zhang, L., Liu, Y. 2017. Increased electroactive species concentration in anodic biofilm of Geobacter-inoculated microbial fuel cells under static magnetic field. *Research on Chemical Intermediates*, **43**(2), 873-883.

Yin, Y., Huang, G., Tong, Y., Liu, Y., Zhang, L. 2013. Electricity production and electrochemical impedance modeling of microbial fuel cells under static magnetic field. *Journal of Power Sources*, **237**, 58-63.

Yuen, J.D., Dhoot, A.S., Namdas, E.B., Coates, N.E., Heeney, M., McCulloch, I., Moses, D., Heeger, A.J. 2007. Electrochemical doping in electrolyte-gated polymer transistors. *Journal of the American Chemical Society*, **129**(46), 14367-14371.

Zhang, X., Philips, J., Roume, H., Guo, K., Rabaey, K., Prévoteau, A. 2017. Rapid and quantitative assessment of redox conduction across electroactive biofilms via double potential step chronoamperometry. *ChemElectroChem*.

Zhang, X., Xia, X., Ivanov, I., Huang, X., Logan, B.E. 2014. Enhanced activated carbon cathode performance for microbial fuel cell by blending carbon black. *Environmental science & technology*, **48**(3), 2075-2081.

Zhao, Y.N., Li, X.F., Ren, Y.P., Wang, X.H. 2016. Effect of static magnetic field on the performances of and anode biofilms in microbial fuel cells. *RSC Advances*, **6**(85), 82301-82308.

8 APPENDIX: Microbial Conversion of Waste Glycerol from Biodiesel Production into Value-Added Products

Cheng Li, Keaton L. Lesnik, and Hong Liu

Energies
September 4, 2013
doi:10.3390/en6094739

Energies **2013**, *6*, 4739-4768; doi:10.3390/en6094739

OPEN

energies

ISSN 1996-1073

www.mdpi.com/journal/energies

Review

Microbial Conversion of Waste Glycerol from Biodiesel Production into Value-Added Products

Cheng Li, Keaton L. Lesnik and Hong Liu *

Department of Biological and Ecological Engineering, Oregon State University, 116 Gilmore Hall, Corvallis, OR 97331, USA; E-Mails: lichen@onid.orst.edu (C.L.); lesnikk@onid.orst.edu (K.L.L.)

* Author to whom correspondence should be addressed; E-Mail: liuh@engr.orst.edu; Tel.: +1-541-737-6309; Fax: +1-541-737-2082.

Received: 6 June 2013; in revised form: 19 July 2013 / Accepted: 4 September 2013 / Published: 10 September 2013

Abstract: Biodiesel has gained a significant amount of attention over the past decade as an environmentally friendly fuel that is capable of being utilized by a conventional diesel engine. However, the biodiesel production process generates glycerol-containing waste streams which have become a disposal issue for biodiesel plants and generated a surplus of glycerol. A value-added opportunity is needed in order to compensate for disposal-associated costs. Microbial conversions from glycerol to valuable chemicals performed by various bacteria, yeast, fungi, and microalgae are discussed in this review paper, as well as the possibility of extending these conversions to microbial electrochemical technologies.

Keywords: biodiesel waste glycerol; microbial conversion; 1,3-propanediol; ethanol; lactic acid; hydrogen; citric acid; microbial electrochemical technologies

1. Introduction

Consumption of fossil energy is the foundation of modern society, from moving vehicles to lighting

bulbs. However, many concerns have been raised about refining efficiency, effects on climate change, air pollution, and diminishing fossil fuel deposits [1]. Biodiesel is a fast growing alternative fuel that can be applied to a conventional diesel engine. The biodiesel demand is clearly increasing in the United States as annual production of biodiesel in 2012 (969 million gallons) was 2.83 times higher than in 2010 (343 million gallons) [2]. Furthermore, under a mandate by the renewable fuels standard (RFS2) of the U.S. Energy Independence and Security Act of 2007, biomass-based diesel production is expected to increase to 36 billion by 2022 [3].

The flow chart of biodiesel production is shown in Figure 1. Biodiesel is an environmentally attractive alternative fuel, which compared to petro-diesel, holds technical advantages like inherent lubricity, low toxicity, biodegradability, renewability, *etc*. Biodiesel itself is composed of mono-alkyl esters of vegetable oils or animal fats and is produced by transesterification with a monohydric alcohol (methanol) [3]. During the transesterification reaction, the glycerol backbone of triacylglycerol is substituted by methanol in the presence of a catalyst at elevated temperature, leaving fatty acid alkyl esters and glycerol as the major liquid products. Waste glycerol, the liquid content after methanol recovery, has a pH around 10 and viscosity from 1213 to 1515 mPa·s [4]. The glycerol content in waste glycerol is from 27 wt% to 28 wt% with a methanol concentration that can vary from 6.2 wt% to 12.6 wt%. Trace amounts of soap formed in an undesirable saponification reaction can also be found in waste glycerol [4]. Previously, commercial glycerol synthesis was primarily performed by propylene chlorine hydrolyzation in caustic environments [5]. Nowadays, the chemical synthesis of glycerol only accounts for about 10% of the current market because of the increasing cost of petrochemical precursors and decreasing price of pure glycerol [6]. In the past few years, the price of refined glycerol had dropped from $1.15 per kilogram to $0.66 per kilogram while the price of waste glycerol has also dropped from $0.44 to $0.11 per kilogram [1,7]. The expansion of the biodiesel industry has thus created a surplus of glycerol, resulting in an inevitable abundance of waste glycerol now considered as a waste stream with associated disposal costs [6]. Therefore, the need to find efficient approaches to convert waste glycerol into more desirable products is urgent and necessary.

Figure 1. Scheme of biodiesel production and waste glycerol (adapted from [6]).

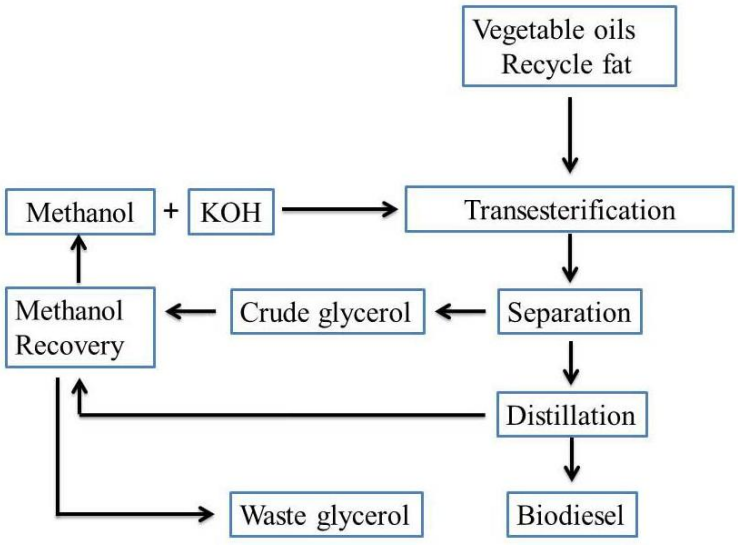

Value-added transformation processes of waste glycerol can be accomplished by direct application, chemical transformation, or microbial conversion [1,8–10]. Direct application refers to processes without any catalytic reaction, instead treating waste glycerol as a simple carbon source. One particular example of direct application is using biodiesel waste glycerol in animal feed [1,11]. However, some impurities within waste glycerol like methanol and potassium may result in harmful effects to animals, and thus concentrations need to be controlled [1]. Chemical transformation can be understood through three major approaches: (1) oxidation/reduction of glycerol into other 3-carbon compounds; (2) synthesis of higher carbon compounds with glycerol and other substrates; and (3) industrial combustion [9]. These traditional chemical catalytic processes often include expensive metal catalysts, toxic intermediates, and low conversion rates [9]. Moreover, it is difficult to combust glycerol efficiently due to its low energy density, high viscosity, high auto-ignition temperature, and potential emission problems [8]. Compared to direct application and chemical transformation, microbial conversion is a viable alternative that avoids certain disadvantages such as low product specificity, high energy input (pressure/temperature) and intensive pretreatment requirements [1,6]. On the other hand, compared to conventional biorefinery substrates, such as glucose and sucrose, waste glycerol presents a class of substrates that are inexpensive, sustainable, and not considered a suitable human food source. In addition, glycerol has a higher degree of reductant and NADH generation rate than other common microbial feedstocks. Consuming one mole of glycerol generates two additional moles of NADH, while consuming a half mole of glucose (equally on a 3-carbon basis) only generates one additional mole of NADH [12,13].

With the development of the biodiesel industry, new breakthroughs have been made each year using different microbial species and bioengineering techniques to convert waste glycerol to value-added products. There are several excellent reviews published in the past several years with a focus on specific products, microbial species, or chemical catalytic processes [1,6,9,14,15]. In this review, the glycerol metabolic pathways of representative bacterial and yeast species will be comprehensively discussed. This includes the capability of various microbial species to convert glycerol to value-added chemicals addressed in terms of yield, productivity and final concentration. We also introduced and discussed microbial electrochemical technologies that may be used as a strategy for generating value-added chemicals as well as electrical energy directly from glycerol.

2. Microbial Conversion of Glycerol

2.1. Fermentation of Glycerol by Enterobacteriaceae *Family*

Enterobacteriaceae is a large family of gram-negative bacteria that includes *Escherichia*, *Klebsiella*,

and *Citrobacter* among others [16]. The glycerol utilization pathways in *Entrerobacteriaceae* have been intensively studied with the goal of industrial production of 1,3-propanediol (1,3-PDO) [6]. These pathways may also be applied to some other bacteria that contain similar metabolic grids. Figure 2 illustrates the general metabolic pathways for glycerol utilization in *Entrerobacteriaceae*.

Figure 2. Prokaryotic pathway of glycerol utilization in *Entrerobacteriaceae* species (adapted from [4,17]). Enzymes: ACK, acetate kinase; ADH, acetaldehyde/alcohol dehydrogenase; AOR, aldehyde oxidoreductase; DHAK, dihydroxyacetone kinase; FHL, formate hydrogen lyase complex; FRD, fumarate reductase; GlyD, glycerol dehydratase; glyDH, glycerol dehydrogenase; glpF, glycerol transporter, LALDH, lactaldehyde dehydrogenase; LDH, lactate dehydrogenase; MGR, methylglyoxal reductase; MGS, methylglyoxal synthase; PFL, pyruvate formate-lyase; PEPCK, phosphoenolpyruvate carboxykinase; PTA, phosphate acetyltransferase; PYK, pyruvate kinase; 1,2-PDOR, 1,2-propanediol reductase; 1,3-PDODH, 1,3-propanediol dehydrogenase. Chemical intermediates and products: DHA, dihydroxyacetone; DHAP, dihydroxyacetone phosphate; FUM, fumarate; GAL3P, glyceraldehyde-3-phosphate; 3HPA, 3-hydroxypropionaldehyde; MAL, malate; OAA, oxaloacetate; PEP, phosphoenolpyruvate; PYR, pyruvate; 1,2-PDO, 1,2-propanediol; 1,3-PDO, 1,3-propanediol. (Dash line indicates reactions for 1,2-PDO pathway; filled box indicates potential products).

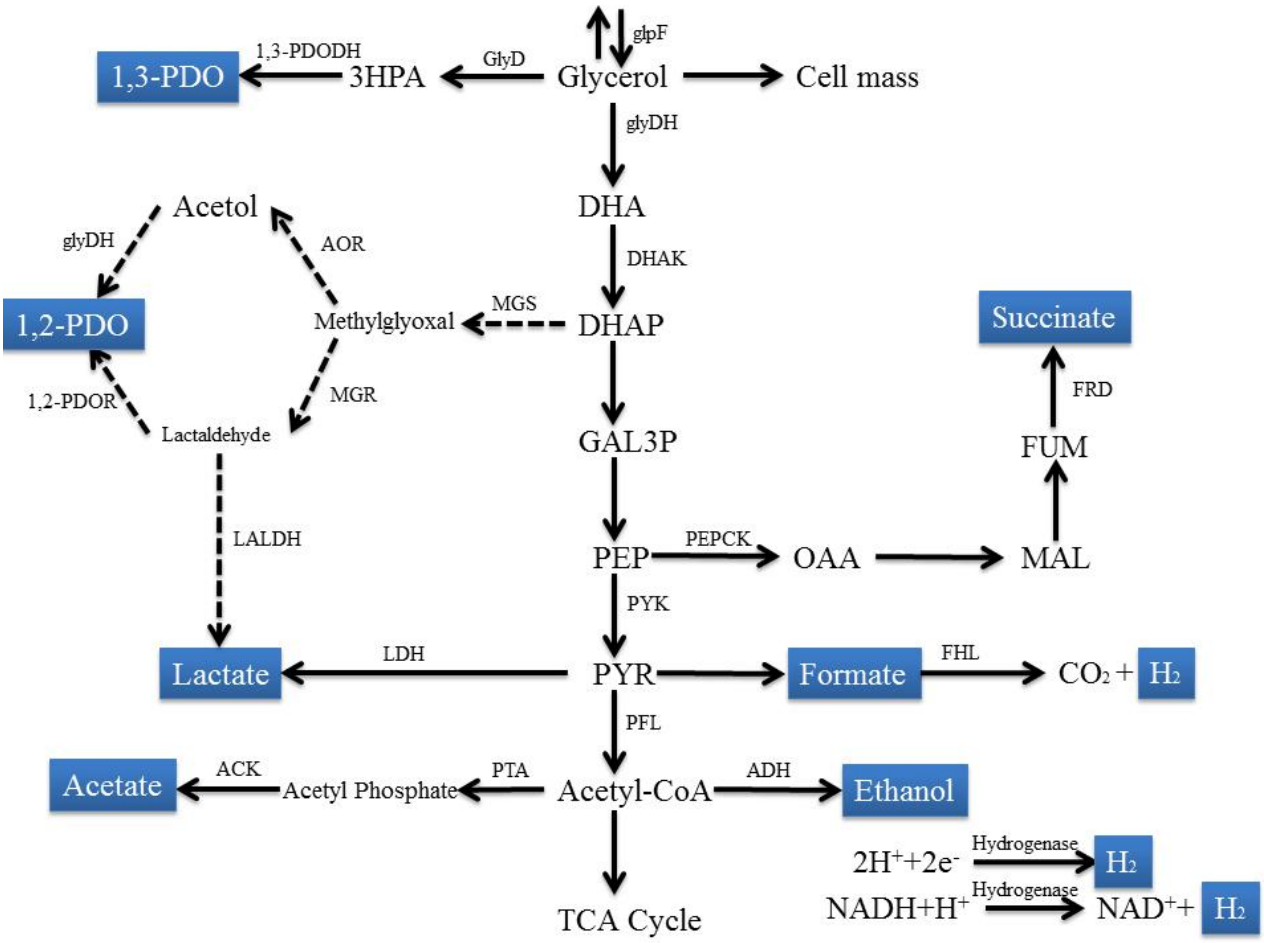

Glycerol can be actively transported inside the cytoplasm by a transporter protein (glpF) [18], known as a glycerol facilitator [19]. Intracellular glycerol is converted to dihydroxyacetone (DHA) by a NAD^+-dependent glycerol dehydrogenase (glyDH), and then phosphorylated to dihydroxyacetone phosphate (DHAP) by a phosphoenolpyruvate (PEP) dependent DHA kinase (DHAK) [6]. DHAP is further oxidized through glycolysis to form building blocks like phosphoenolpyruvate (PEP), pyruvate (PYR), and acetyl-CoA. The high-energy molecule PEP can be converted to oxaloacetate by phosphoenolpyruvate carboxykinase and then reduced stepwise to succinate in the presence of certain enzymes involved in the TCA cycle. Pyruvate can then be reduced to lactate by lactate dehydrogenase (LDH). Acetyl-CoA can be converted to acetate by both phosphate acetyltransferase (PTA) and acetate kinase (ACK), or be reduced to ethanol by acetaldehyde/alcohol dehydrogenase (ADH).

The reductive pathways act as an electron sink for oxidation, consuming reducing equivalents generated during the stepwise oxidation of glycerol to achieve redox balance. Differing from other substrates, glycerol has a high degree of reductant, therefore one particular challenge for glycerol fermenting species is the consumption of excess reducing equivalent [20]. A B_{12}-dependent glycerol dehydratase (GlyD) and a 1,3-propanediol dehydrogenase (1,3-PDODH) were identified in the reductive pathway for this purpose [21]. The 1,2-propanediol (1,2-PDO) pathway, which is present primarily in *Escherichia coli* strains, might act as an alternative mechanism for cells to regenerate NAD^+ [22]. During the reductive pathway, some of the electrons can be diverted to combine with protons and released as hydrogen gas under anaerobic conditions and low partial pressure of hydrogen [23]. It is also suggested that an acetaldehyde/alcohol dehydrogenase might carry out an important role in glycerol fermentation for regaining redox balance [18].

2.1.1. *Escherichia* Species

As the most well-studied member in *Enterobacteriaceae* family, both wild type and engineered strains of *Escherichia coli* can be considered a bacterial platform for producing value-added metabolites [24]. Glycerol fermentation performed by *Escherichia coli* can produce ethanol, lactic acid, 1,2-PDO, 1,3-PDO, and succinic acid, all of which represent value-added opportunities.

Ethanol is typically formed to fulfill the energy requirement of a bacterial cell. Ethanol can also serve as a direct fuel or as a gasoline additive for its octane booster effect [25], though ethanol conversion rates by wild type *E. coli* are often not high enough to satisfy the needs of industrial production [18,22]. To maximize ethanol production, strain SY03 was constructed by inactivating enzymes responsible for succinate and acetate synthesis (fumarate reductase and phosphate acetyltransferase). This strain was shown to be capable of producing 1 mole of ethanol and 1 mole of hydrogen gas per mole of glycerol consumed [26] (Table 1).

Table 1. Microbial conversion of glycerol to value-add products.

Bacterial species	Strain	Product	Yield (mol/mol glycerol)	Productivity (g/L/h)	Final concentration (g/L)	Ref.
Escherichia coli	Engineered *E. coli* SY03	Ethanol	1	0.051	5	[26]
	E. coli AC521	Lactic acid	0.9	0.97	85.8	[27]
	Engineered *E. coli*	D-lactic acid	0.82 (pure glycerol) 0.87 (waste glycerol)	1.5 (pure glycerol)	32 (pure glycerol) 34 (waste glycerol)	[28]
	Engineered *E. coli*	L-lactic acid	0.91	-	50	[29]
	Engineered *E. coli*	1,2-PDO	0.26	-	5.6	[30]
	Engineered *E. coli*	1,3-PDO	1.09	2.61	104.4	[31]
	Engineered *E. coli*	Succinate	0.8	-	12	[32]
Klebsiella	*K. pneumonia* (Encapsulated)	1,3-PDO	0.65 (batch) 0.43 (continuous)	4.46 (continuous)	-	[33]
	K. pneumonia (Pilot scale)	1,3-PDO	0.58	0.92	58.8	[34]
	K. oxytoca (Lactate deficient)	1,3-PDO	0.41–0.53	0.63–0.83	-	[35]
	K. pneumonia (Inactivated ADH)	1,3-PDO	0.70	1.07	-	[36]
	K. pneumonia	2,3-BD	0.36	0.18	49.2	[37]
	Engineered *K. pneumonia*	Ethanol	0.89	1.2	31.0	[38]
Citrobacter	*C. freundii* FMCC-B294	1,3-PDO	0.48	0.79	68.1	[39]
	C. werkmanii DSM 17579	1,3-PDO	0.62	2.84	-	[40]
	C. freundii H3	H_2	0.94	-	-	[41]
	Engineered *C. freundii*	Violacein	-	82.6 mg/L/h	4.13	[42]

Table 1. *Cont.*

Clostridium	*C. butyricum* VPI 3266	1,3-PDO	0.65	10.3	-	[43]
	C. butyricum AKR102a	1,3-PDO	0.63 (pure glycerol)	3.3 (pure glycerol)	93.7 (pure glycerol)	[44]
	C. butyricum VPI 1718	1,3-PDO	0.665	-	67.9	[45]
	Engineered *C. acetobutylicum*	1,3-PDO	0.66	3	-	[46]
	C. pasteurianam (immobilized)	n-butanol	0.43	0.074	8.84	[47]
	C. pasteurianam ATCC 6013	1,3-PDO and butanol	0.17 (1,3-PDO) 0.28 (butanol)	0.42 (1,3-PDO) 2.49 (butanol)	-	[48]
Propionibacterium bacteria	Engineered *P. acidipropionici* strain	Propionic acid	0.66 (pure glycerol), 0.88 (waste glycerol)	0.10 (pure glycerol), 0.085 (waste glycerol)	106 (pure glycerol)	[49]
	P. freudenreichi subsp. Shermanii NCIM 5137	Trehalose	391 mg/g biomass	-	-	[50]
Other bacteria and mixed culture	*R. palustris* CGA009	H_2	6	-	-	[51]
	P. macerans	H_2	0.801	-	-	[52]
	Thermoanaerobacterium sp.	H_2	0.30	-	-	[53]
	Mixed culture	H_2	0.96	91 mL/L/h	-	[54]
	Mixed culture	H_2/formate	0.80	-	-	[55]
	Mixed culture	H_2	0.28 (pure glycerol) 0.31 (waste glycerol)	-	-	[23]
	L. acidophilus	Probiotic cell mass	0.37 g/g	-	2.11	
	L. diolivorans	1,3-PDO	-	-	73.7	
	Anaerobic co-digestion	Biogas	-	-	1210 mL/d	[56]
	C. necator DSM 545	PHAs	-	1.1	-	[57]
	Z. denitrificans MW1	PHAs	0.31 g/g glycerol	-	-	[58]
	P. putida GO16	PHAs	-	0.11	-	[59]

Table 1. *Cont.*

Yeasts	*Y. lipolytica* NCIM 3589	Citric acid	-	-	77.4	[60]
	Y. lipolytica Wratislavia AWG7	Citric acid	0.33	1.16	139	[61]
	C. bombicola ATCC 22214	Sophorolipids	-	-	60	[62]
	P. antarctica JCM 10317	Mannosylerythritol lipid	-	-	16.3	[63]
	Cryptococcus curvatus	SCO	52% lipid content	-	17.1	[64]
	Rhodotorula glutinis	SCO	36.5% lipid content	-	5.4	[65]
	S. ruberrimus CSB 2636	Carotenoid	41.9 μg/g glycerol,	56.9μg/L/h	3425.9μg/L	[66]
	Engineered *S. cerevisiae*	Ethanol	-	-	2.4 g/L	[67]
	Engineered *S. cerevisiae*	1,2-PDO	0.258	-	2.19	[68]
Fungi	*L. edodes* strains	SCO	0.1 g/g biomass	-	0.52	[69]
	A. niger strains	SCO	0.41 to 0.57 g/g biomass	-	3.1 to 3.5	[69]
	Galactomyces geotrichum	SCO	0.44 g/g biomass	-	-	[70]
	Thamnidium elegans	SCO	-	-	11.6	[71]
	Pythium irregulare	EPA	-	14.9 mg/L/day	90 mg/L	[72]
	Blakeslea trispora	β-carotene	15 mg/g biomass	-	-	[73]
Microalgae	*S. limacinum* SR21	DHA	-	0.51	-	[74]
Microbial Electrochemical Technology	*B. subtilis* MFC	Electricity	Maximum power density 600 mW/m^2			[75]
	Single chamber MFC	Electricity	Maximum power density 2110 mW/m^2			[76]
	Single chamber MFC	Electricity	Maximum power density 4579 mW/m^3 with pure glycerol, 2324 mW/m^3 with waster glycerol			[77]
	E. aerogenes MEC	H_2	0.74	-	-	[78]
	Mixed culture MEC	H_2	3.9	-	-	[79]
	MEC with gas phase cathode	H_2	5.4	0.6 L/L/day	-	[80]

Lactic acid can be produced during glycerol fermentation by some *E. coli* strains as an alternative to NAD^+ regeneration in the absence of external electron acceptors [27]. Lactic acid has many applications as a food additive, acidulant, as well in the production of biodegradable polylactic acid [81,82]. Food-grade lactic acid has a price ranging between $1.38 per kilogram (50% purity) and $1.88 per kilogram (88% purity) [83,84]. Compared to traditional chemical synthesis methods, microbial conversion of lactic acid favors the formation of one specific configuration, either D- or L-, due to the high specificity of lactate dehydrogenase (LDH) [28,29], a property that can simplify downstream processes such as separation and purification. High chiral purity of D-lactate can be produced by fermenting glycerol using a recombinant strain that overexpresses enzymes that respond to glycolytic intermediates and inactivates fumarate reductase, phosphate acetyltransferase, alcohol/acetaldehyde dehydrogenase, and D-lactate dehydrogenase [28]. Thirty-two grams per liter of D-lactate (99.9% chiral purity) could be produced from 40 g/L of glycerol (0.82 mole lactate per mole of consumed glycerol, 1.5 g/L/h productivity). This strain was also tested for the ability to utilize waste glycerol as a substrate, and a higher yield was observed (0.87 mole lactate per mole of consumed glycerol) with the final concentration of D-lactic acid of 34 g/L [28]. Furthermore, an L-specific LDH from *Streptococcus bovis* was able to be introduced to replace the native *E. coli* D-specific LDH from the previous study. Fifty grams per liter of L-lactic acid (99.9% chiral purity) was produced from 56 g/L of waste glycerol with a yield of 0.91 mol/mol glycerol. Other than engineered strains, lactic acid production was also observed in glycerol fermentation by *E. coli* AC-521, a wild-type soil bacterium [27]. The yield reached 0.9 mole lactic acid per mole consumed glycerol with a final concentration of about 85.8 g/L (0.97 g/L/h productivity), however no data about chiral purity was presented in this study.

A 1,2-PDO-dependent glycerol fermentation capability has been discovered in some *E. coli* strains [18,22]. 1,2-PDO is a chemical that can serve as a building block for polyesters, anti-freeze agents, or solvents [85], and is currently priced around $1.08 to $1.59 per kg with an estimated global demand around 1.36 billion kilogram per year [86]. To enhance natural production of 1,2-PDO, an engineered *E. coli* was constructed by disrupting acetate and lactate synthesis and replacing the native PEP-dependent dihydroxyacetone kinase with an ATP-dependent dihydroxyacetone kinase from *Citrobacter freundii*. This causes the overexpressing enzymes responsible for the reductive 1,2-PDO pathway, and results in a strain that can produce 5.6 g/L of 1,2-PDO from the fermentation of glycerol with a yield of 0.26 mol/mol glycerol [30].

E. coli has also been genetically modified to generate desired products that are not naturally produced from glycerol by *E. coli* such as 1,3-PDO and succinate [6]. 1,3-PDO is a building block of biodegradable plastic polytrimethyleneterephthalate (PTT) and also a valuable product with various uses (resins, coolants, mortars and inks). A recombinant strain of *E. coli* was constructed by transferring the B_{12}-independent glycerol dehydratase *DhaB1* and its activating factor *DhaB2* from *Clostridium butyrium*. The final concentration, yield and overall productivity of 1,3-PDO was 104.4 g/L, 1.09 mol/mol and 2.61 g/L/h, respectively [31]. Another product capable of being produced by recombinant *E.coli.*is succinate. Succinate is one of the top twelve building block chemicals according

to the U.S. Department of Energy and is typically used for creating biodegradable plastic polybutylene succinate [87]. Current glucose to succinic acid commercial production techniques are relatively sophisticated, and are capable of producing a succinic acid yield about 1.45 mol/mol glucose [88]. However, using glycerol as a substrate has advantages such as the low cost of the feedstock and higher yield of succinic acid (on an equal 3-carbon basis) [17]. A comparable yield (0.8 mol/mol glycerol) of succinic acid production was achieved in the recombinant *E. coli*, although the final concentration was low (12 g/L) [32]. To construct this strain, phosphoenolpyruvate carboxykinase (PEPCK) was upregulated, and genes responsible for ethanol and formate formation were deleted.

2.1.2. *Klebsiella* Species

As another member in the *Enterobacteriaceae* family, *Klebsiella* is considered one of the most promising candidates for producing 1,3-PDO from glycerol [34] and over the past few years a large amount of *Klebsiella* research has been focused on enhancing the production of 1,3-PDO production during the fermentation of waste glycerol. Pilot scale studies as large as 5000 L have been launched in order to test *Klebsiella's* potential for industrial application [34]. Syntheses of other products, like 2,3-butanediol (2,3-BD) and ethanol have also been reported in considerable amounts [37,38].

To increase the production of 1,3-PDO through the fermentation of glycerol by *Klebsiella* species, genetic enhancements were employed with different strategies such as minimizing undesired byproducts or increasing the utilization of glycerol. The formation of lactate and ethanol compete with the formation of 1,3-PDO through the consumption of reducing equivalents, and often impose difficulties on the downstream processes responsible for the purification and recovery of 1,3-PDO [35,36]. By creating a lactate deficient mutant (LDH3) from *K. oxytoca* M5a1, the productivity and yield of 1,3-PDO were increased from 0.63 to 0.83 g/L/h to 0.41 to 0.53 mol/mol glycerol, respectively [35]. By inactivating aldehyde dehydrogenase (ADH), the enzyme responsible for ethanol formation in *K. pneumoniae* YMU2, less ethanol was produced in the broth (from 9.26 g/L to 1.70 g/L) with a higher productivity (from 0.81 g/L/h to 1.07 g/L/h) and yield (from 0.36 mol/mol to 0.70 mol/mol) of 1,3-PDO observed [36]. To enhance both glycerol oxidative and reductive metabolisms, formate dehydrogenase (FDH) from *Candida boidinii* was expressed in *K. oxytoca* YMU1 [89]. The subsequent yield of 1,3-PDO increased about 17.3%, from 0.39 to 0.45 mol/mol glycerol.

Other value-added chemicals can also be produced through glycerol fermentation by *Klebsiella* species. For example, 2,3-BD was found to be the major product of fermentation by *K. pneumonia* G31 under microaerobic conditions with an initial alkaline pH [37]. 2,3-BD is a high-value chemical that can serve as a precursor for chemical products like methyl ethyl ketone, γ-butyrolactone, and 1,3-butadiene [90]. The final concentration of 2,3-BD reached 49.2 g/L after 280 h of fermentation (a productivity of 0.18 g/L/h) and the overall yield was 0.36 mol/mol glycerol. An engineered strain of *K. pneumonia* can produce ethanol when the lactate dehydrogenase was inactivated and pyruvate decarboxylase along with aldehyde dehydrogenase from *Zymomonas mobilis* were introduced.

Compared to the wild type strain, final concentration, yield, and productivity were improved from 21.5 g/L to 31.0 g/L, 0.62 mol/mol glycerol to 0.89 mol/mol glycerol, and 0.93 g/L/h to 1.2 g/L/h, respectively [38].

2.1.3. *Citrobacter* Species

Citrobacter species are well-known for their ability to produce 1,3-PDO from fermenting glycerol. Studies using chemical grade glycerol in the mid-90s had revealed that the final concentration of 1,3-PDO produced by *C. freundii* to be comparable to those produced by *Klebsiella* and *Clostridium* species, although the reaction rate is much slower [91]. Recent studies have shown that both wild-type and engineered *Citrobacter* species are capable of using pretreated biodiesel waste glycerol as a substrate to produce various value-added products. For example, *C. freundii* strain (FMCC-B 294) can ferment pretreated waste glycerol to produce 1,3-PDO in fed-batch fermentation achieving final concentration of 68.1 g/L with yield of 0.48 mol/mol and volumetric productivity of 0.79 g/L/h [39]. This strain can also endure non-sterile feeding, which may reduce the energy requirement for pretreatment. Other than *C. freundii*, *C. werkmanii* DSM 17579 is another potential strain for 1,3-PDO production. The highest achieved yield per mole of glycerol consumed and productivity in fed-batch fermentation was 0.62 mol/mol and 2.84 g/L/h, respectively [40]. However, the highest yield, productivity, and final concentration of 1,3-PDO achieved by *C. freundii* was lower than those achieved by *Clostridium* species. Besides PDO, *C. freundii* H3 can ferment chemical grade glycerol to produce H_2 with a yield of 0.94 mol/mol [41]. A recombinant of *C. freundii* aimed at producing violacein was examined for its ability to ferment glycerol as substrate. Violacein is a blue-purple bacterial pigment that has antibacterial, antioxidant, antiviral, and anti-protozoal properties [92]. The maximum final concentration and productivity were 4.13 g/L and 82.6 mg/L/h, respectively [42].

2.2. Clostridium *Species*

Similar to *Klebsiella*, the glycerol fermenting ability of *Clostridium* species has been extensively studied with the goal of enhancing the production of 1,3-PDO [93]. The value-added product butanol was also discovered during fermentation.

The possible effects of dilution rate and substrate concentration on glycerol fermentation of *C. butyricum* VPI 3266 were examined [43]. The highest productivity of 1,3-PDO (10.3 g/L/h) was achieved under the dilution rate 0.30 h^{-1} and at substrate concentration of 60 g/L. The yield was around 0.65 mol/mol. Glycerol fermentation of *C. butyricum* AKR102a in an automatic fed-batch reactor can produce 93.7 g/L (3.3 g/L/h) 1,3-PDO from pure glycerol and 76.2 g/L from pretreated waste glycerol (2.3 g/L/h) [44]. *C. butyrium* VPI 1718 was tested for production of 1,3-PDO from non-

sterile waste glycerol and was found to produce 1,3-PDO with a final concentration of 67.9 g/L, and yield of 0.67 mol/mol glycerol [45]. An engineered strain was constructed by introducing the reductive pathway of *C. butyricum* to *C. acetobutylicum* [46]. This recombinant, DG1(pSPD5), was capable of fermenting glycerol with a 1,3-PDO productivity of 3 g/L/h and a yield of 0.66 mol/mol glycerol.

Other than 1,3-PDO, butanol can also be produced through the fermentation of glycerol by *Clostridium* [47]. Butanol is a chemical that can be applied as a chemical synthesis building block, solvent, or as a potential biofuel. Microbial production of butanol lost its primary advantage in the 1960s due to the increasing cost of suitable substrates [94], but with the current low price of biodiesel waste glycerol combined with advances in genetic engineering techniques this alternative pathway may now become commercially practical. The simultaneous production of 1,3-PDO and butanol was reported in *C. pasteurianam* (ATCC 6013) by feeding pretreated waste glycerol with productivities of 0.42 g/L/h (0.17 mol/mol) and 2.49 g/L/h (0.28 mol/mol), respectively [48].

2.3. Propionibacterium *Species*

Fermentative glycerol dissimilation in *Propionibacteria* strains has been investigated for the production of propionic acid and trehalose [4,17]. As an important intermediate for cellulose fibers, herbicides and perfumes, large quantities of propionic acid are produced by chemical synthesis, e.g., oxidation of propionaldehyde with air and the catalytic dehydration of glycerol [49,95,96]. One of the best natural producers of propionate from glycerol is *Propionibacterium acidipropionici*, capable of achieving a final concentration of 42 g/L propionate with an overall yield of 0.84 mol/mol of glycerol consumed and a productivity of 0.36 g/L/h using technical grade glycerol [17]. A knockout mutant strain of *P. acidipropionici* lacking acetate kinase (ACK) was studied for its ability to use glycerol as sole carbon source during fermentation [49]. The final concentration of propionate (106 g/L) from the fermentation of glycerol was much higher than wild type (42 g/L). The yield and productivity, however, were lower than wild type (0.66 mol/mol consumed glycerol and 0.10 g/L/h). When pretreated waste glycerol was used as carbon source, this mutant strain achieved a higher yield of propionate (0.88 mol/mol glycerol) and a slightly lower productivity (0.09 g/L/h).

Trehalose can also accumulate in the biomass of some *Propionibacteria* strains during glycerol fermentation. Trehalose is a non-reducing sugar that can protect bacterial cells against osmotic stress and has value in the food and cosmetic industries as well as clinical applications [97]. Although enzymatic transformations have been reported as a viable method for trehalose production [98], accumulation of trehalose in microbial biomass is considered a less expensive method when a cheap carbon source is used [93]. Wild type and osmotic sensitive mutants of *P. freudenreichi subsp. Shermanii* were analyzed for the production of trehalose from waste glycerol [50]. The final concentration of trehalose was higher in the mutant strain than in wild type (678 mg/L to 158 mg/L). The use of waste glycerol further increased the final concentration of trehalose from 678 mg/L to 1303 mg/L in the mutant strain. It was possible that impurities in waste glycerol positively influenced

trehalose accumulation by creating stressful conditions that signal the bacterial cells to accumulate trehalose [50].

2.4. Other Bacterial Species and Mixed Culture

Pure bacterial species and mixed culture communities outside of *Enterobacteriaceae*, *Clostridia*, and *Propionibacterium* species have also been investigated for their abilities to convert waste glycerol into value-added products like hydrogen, 1,3-PDO, probiotic biomass, and polyhydroxyalkanoates (PHAs). For example, *Rhodopseudomonas palustris* CGA009, a purple non-sulfur photosynthetic bacterium, has been demonstrated to have the ability to photo-ferment pretreated waste glycerol to hydrogen [51], a clean and efficient energy carrier that has received enormous attention. As previously described, glycerol fermentation theoretically produces more NADH than glucose fermentation on a 3-carbon basis, and thus has higher potential to generate hydrogen gas (one mole of H_2 per mole of excess NADH) [12,13]. Gene deletion experiments have indicated that hydrogen production in *R. palustris* is mainly due to nitrogenase, which catalyzes proton reduction in the absence of nitrogen gas. The yields of hydrogen were 6 mol/mol using pure glycerol and 4 mol/mol using waste glycerol. Some strains of *Paenibacillus macerans* were also reported to grow efficiently on glycerol as sole carbon source, but hydrogen yield (0.80 mol/mol glycerol) was much lower than that by *R. palustris* CGA009 [52]. Ethanol was the dominant liquid product while 1,2-PDO and acetone were also detected [52]. Mixed cultures have also been investigated for potential hydrogen production from waste glycerol. The estimated maximum hydrogen yields ranged from 0.8 to 0.96 mol/mol, which is comparable to the hydrogen yield with glucose as substrate on a 3-carbon basis [54,55]. Thermophilic mixed cultures were also studied for their potential ultilization of waste glycerol to produce hydrogen [53]. Although the yield (0.30 mol/mol glycerol) was not as favorable, thermophilic mixed culture fermentation might provide several advantages over mesophilic mixed culture fermentation, such as more effective pathogen control and lower risk of methanogen contamination [53,99,100].

As one of the natural producers of 1,3-PDO, *Lactobacillus diolivorans* has the potential to produce 1,3-PDO from glycerol. The highest final concentration produced was 73.7 g/L under fed-batch cultivation [101]. A recent study suggests that biodiesel waste glycerol can support cell growth of *L. acidophilus*, *L. delbrueckii*, and *L. plantarum*, with resulting probiotic cell mass obtained as a value-added product.

PHAs are typically stored by bacteria as a carbon source and energy reserve [102]. This chemical can also serve as an alternative to biodegradable polymers. Bacterial synthesis of PHAs is a cheaper way to produce this expensive compound compared to chemical synthesis techniques. *Cupriavidus necator* DSM 545 has demonstrated the capability to accumulate poly(3-hydroxybutyrate), a polyhydroxyalkanoate (PHA), in its cell mass by assimilating either pure glycerol or waste glycerol, with higher productivities able to be achieved using waste glycerol versus pure glycerol [57]. *Zobellella denitrificans* MW1 was also

reported to use glycerol as sole substrate to accumulate poly(3-hydroxybutyrate) in its cell mass [58]. The highest yield was achieved using 10 g/L of glycerol (0.31 g/g glycerol, 80.4% of the cell dry weight). A waste glycerol supplement can increase the biomass production up to 1.7 fold and PHA accumulation up to 2.2 fold in *Pseudomonas putida* GO16 (0.11 g/L/h), compared to growth on sodium terephthalate (major plastic waste from pyrolysis of Polyethylene terephthalate) alone [59].

2.5. Microbial Conversion of Glycerol by Yeast

Glycerol is one of the byproducts of sugar fermentation in yeast, acting as an osmotic regulator and a way to balance excess reducing equivalent [103]. The glycerol transportation and dissimilation pathways of yeast have been intensively studied since the 1960s (Figure 3) [104–108]. A proton symport protein encoded by the *STL1* gene in both *Saccaromyces cerevisiae* and *Candida alba* is responsible for glycerol active transportation through the cell membrane [109,110]. However, simple diffusion was also observed in *S. cerevisiae* [107]. *GUP1*, a member of membrane-bound O-acyltransferases, has been indicated to involve extracellular glycerol transportation, and thus could also be one of the membrane-bound proteins that are responsible for the active uptake of glycerol via the proton symport system. After entering the cell membrane, glycerol is then phosphorlyated by glycerol kinase (glyK) to become glycerol-3-phosphate, a glycolytic intermediate that can be dehydrogenated in the mitochondria by glycerolphosphate oxidase (gpO) to form dyhydroxyacetone phosphate (DHAP) [107]. In another species of yeast, *Schizosaccharomyces pombe*, intracellular glycerol is directly oxidized by a NAD^+-dependent dehydrogenase to DHA. DHA is subsequently phosphorylated to DHAP after which it may enter glycolysis. Glycolysis produces acetyl-CoA, one of the major building blocks to both TCA cycle and fatty acid synthesis, which is capable of subsequently generating valuable products like citric acid and glycolipids.

Figure 3. Eukaryotic pathway of glycerol utilization. Enzymes: glyK, glycerol kinase; glyP, glycerophosphatase; gpO, glycerophosphate oxidase; g3pD, glycerol-3-phosphate dehydrogenase. Chemical intermediates and products: DHA, dihydroxyacetone; DHAP, dihydroxyacetone phosphate; L-G3P, L-glycerophosphate. (Dash line indicates reactions in *Schizosaccharomyces pombe*; filled box indicates potential products).

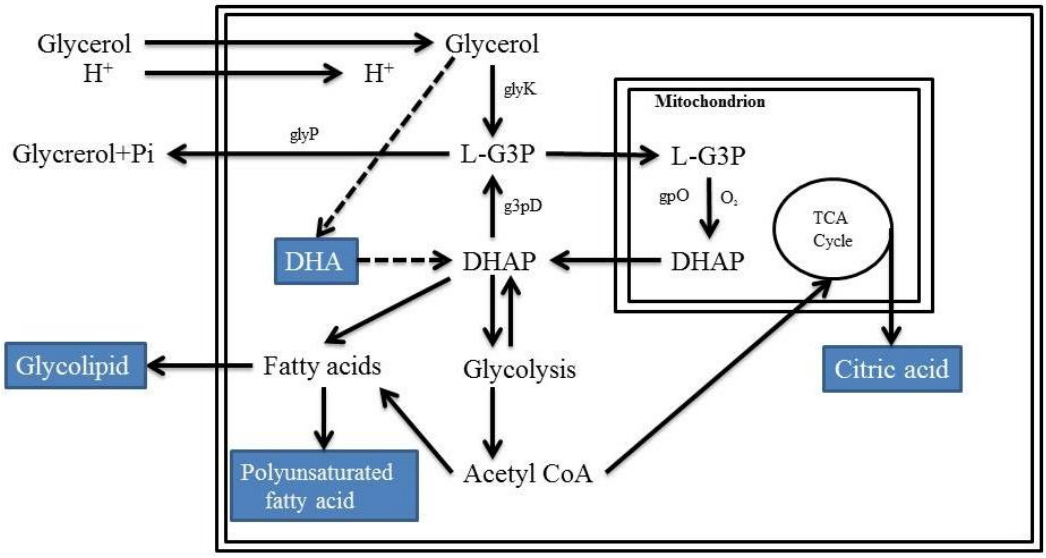

Yeast species have been screened and investigated for their potential in converting waste glycerol to various products such as citric acid, biosurfactants, single cell oil (SCO), and carotenoids [111]. Additionally, products like ethanol and 1,2-PDO can also be produced by genetically engineered *S. cerevisiae* strains.

Citric acid is a flavoring additive and preservative agent in the food industry with a current estimated annual production of more than 800,000 tons which is expected to continue to increase by 5% per year [111–113]. Citric acid production from the submerged fermentation of *Aspergillus niger* (fungus) using sugar as substrate is a well-developed technique. However, feeding glycerol to *A. niger* does not favor citric acid production [114]. As an alternative to *A. niger*, *Yarrowia lipolytica* was investigated for citric acid production using glycerol as substrate [15]. Under optimal conditions, *Y. lipolytica* NCIM 3589 has shown the ability to yield a final citric acid concentration of 77.4 g/L, which is comparable to the final concentration obtained by *A. niger* [60]. Among all the strains tested, *Y. lipolytica* Wratislavia AWG7 produced an even higher citric acid concentration of 139 g/L after 120 h with an initial glycerol concentration of 200 g/L [61].

Glycolipids like sophorolipid and mannosylerythritol can be categorized as biosurfactants, which are a series of microbial produced molecules that have similar structures and chemical properties to surfactants [115]. Compared to other surfactants, biosurfactants contain advantages such as low toxicity and biodegradability, making them environmentally friendly for remediation processes in both liquid and on solid surfaces [116,117]. The production of biosurfactants was previously believed to only be performed by bacterial species such as the rhamnolipid-producing *Pseudomonas aeruginosa*, but recent discoveries have shown similar levels of glycolipid production in *Candida* and *Pseudozyma* [115,118]. *Candida bombicola* ATCC 22214 has been proven to produce sophorolipids by fermenting biodiesel waste glycerol with a final concentration of about 60 g/L [62]. It has also been reported that *Pseudozyma antarctica* JCM 10317 was able to produce 16.3 g/L mannosylerythritol lipids from 100 g/L glycerol supplied with 2% mannose [63].

The oleaginous yeast *Cryptococcus curvatus* has the ability to grow on crude glycerol. Microbial lipophilic contents, often known as SCOs, contain multiple useful polyunsaturated fatty acids that have potential in both the medical and dietetic fields [119] in additional to potential use as a feedstock for second generation biodiesel production [69,111]. A fed-batch culture of *C. curvatus* was able to produce 32.9 g/L of biomass with a 52% lipid content within 12 days [64]. *Rhodotorula glutinis* is also oleaginous yeast that is able to grow on a mixture of crude glycerol and the thin stillage fraction from brewery waste to produce 14.8 g biomass per liter (36.50% lipid content) [65].

The value of carotenoids, a group of pigments, has increased along with the demand for use as a cosmetic additive and food colorant [14,120]. Yeast species *Sporobolomyces ruberrimus* CBS 2636 has recently been investigated for its potential to produce carotenoid using industrial glycerol from the soap manufacturing process as one of the co-substrates [14,66]. The maximum concentration that could be achieved was 3425.9 μg/L with a carotenoid productivity of 56.9 μg/L/h (41.9 μg/g glycerol).

S. cerevisiae can also be genetically engineered to produce some other products from glycerol fermentation, which are either not naturally produced or present in low concentrations, such as ethanol and 1,2-PDO. *S. cerevisiae* is an excellent ethanol producer when using sugar substrates. However, fermenting a more reduced substrate like glycerol to ethanol might require additional metabolic routes to handle the excess reducing equivalents. Simultaneous overexpression of glycerol dehydrogenase (*Gcy*) and dihydroxyacetone kinase (*Dak*) in *S. cerevisiae* was investigated for ethanol production by fermenting glycerol [67]. The final ethanol concentration was 1.66 g/L, 2.4 times greater than the wild type (0.69 g/L). The concentration was further increased to 2.4 g/L (3.4 fold improvement over the wild type) by overexpression of glycerol uptake protein GUP1. 1,2-PDO is not naturally produced by *S. cerevisiae,* yet recombinant strains of *S. cerevisiae* 499 were constructed to produce 1,2-PDO by fermenting glycerol [68]. A 1,2-PDO final concentration of 2.19 g/L with a yield of 0.258 mol/mol glycerol was achieved in strain *S. cerevisiae* 499 sJDPMG. This recombinant overexpressed glycerol dehydrogenase (*gdh*) and *GUP1* protein, along with the expressing methylglyoxal synthase (*mgs*) and glycerol dehydrogenase (*gldA*) from *E. coli*.

2.6. Microbial Conversion of Glycerol by Fungi

Microbial conversion of waste glycerol by fungi is another possible approach to generate value-added products, such as SCO, eicosapentanoic acid (EPA), and β-carotene, as studies have shown that fungi tend to accumulate lipids inside their mycelia [71]. *Lentinula edodes* strains AMRL 119 and AMRL 121 can produce a maximum of 5.2 g/L of biomass and a yield of 0.1 g/g biomass of lipid (mostly linoleic acid) under carbon limitation [69]. *A. niger* strains NRRL 364 and LFMB 1 were tested under nitrogen limiting conditions, resulting in 20.5–21.5g/L of oxalic acid production and 3.1–3.5 g/L of lipids with a yield of 0.41–0.57 g/g of biomass (composed by oleic acid and linoleic acid). *Galactomyces geotrichum* is an ascomycetous fungus that has the ability to use glycerol and FFA within waste glycerol to produce 0.44 grams of lipid per gram biomass [70]. In addition to the fungi previously mentioned *Thamnidium elegans* has been shown to be able to produce up to 11.6 g/L of oil, corresponding to 71.1% wt/wt of oil in biomass [71].

As a specific member of microbial lipohilic content, EPA is an important member in omega-3 polyunsaturated fatty acid (PUFA) family, and has medical applications for treating cardiovascular disease, cancer and Alzheimer's disease [72,121,122]. PUFA is an important part of the human diet, with most dietary PUFA extracted from fish [123]. However, fish extracted PUFAs contain undesired odors and accumulated harmful heavy pollutants. Microalgae accumulation of PUFAs was evaluated

as a commercial replacement for fish oil [123,124], but microalgae accumulation of EPA is often considered to be less efficient [72]. The fungus *Pythium irregulare* was capable of producing EPA from waste glycerol with a final concentration of 90 mg/L and a productivity of 14.9 mg/L/day [72]. Results from this study also suggest that impurities within waste glycerol like soap and methanol can inhibit cell growth, and thus should be removed by pretreatment.

A nutritional supplement, β-carotene, can be accumulated in the cell mass of *Blakeslea trispora* during grow on waste glycerol media. The highest concentration obtained was 15 mg β-carotene per gram of cell mass by using 60 g/L waste glycerol [73]. Impurities within waste glycerol did not inhibit the cell growth, but actually stimulated β-carotene synthesis.

2.7. Glycerol as Carbon Source for Microalgae Species

Being a potential biorefinery feedstock, microalgae species have raised considerable research interest [125] and accordingly waste glycerol has been studied as a possible cheap carbon source for growing microalgae biomass. Though glycerol can be metabolized by several microalgae species, even in the absence of carbon dioxide [126–128], the metabolic pathway of glycerol in microalgae has not been well developed. It is possible that in two of the *Mycobacterium* species, glycerol is first phosphorylated and then oxidized to triose phosphate [128]. Triose phosphate then goes through a stepwise oxidation and becomes pyruvate to enter TCA cycle. Therefore, triose phosphate might be one of the key intermediates for which oxygen is required. The alga species *Schizochytrium limacinum* SR21 can accumulate docosahexaenoic acid (DHA) in its cell mass, with DHA productivity of 0.51 g/L/day using waste glycerol as substrate [74]. DHA is an important omega-3 polyunsaturated fatty acid with research suggesting a role in preventing cardiovascular disease [74].

2.8. Converting Glycerol to Value-Added Products Using Fermentation, Co-Digestion, and Microbial Electrochemical Technologies

2.8.1. Fermentation

Generally speaking, fermentation processes can be operated in batch, fed-batch, and continuous modes [129]. In terms of glycerol microbial conversion, batch and fed-batch cultures were often employed because value-added metabolites and biomass can accumulate in relatively high final concentrations compared to continuous culture. For example, 67.9–104.4 g/L of 1,3-PDO can be produced by batch and fed-batch cultures [31,39,44,45], which are higher than concentrations achieved in continuous culture (35.2–48.5 g/L) [130]. However, compounds other than the desired products also accumulate during the conversion process which might lead to inefficiencies due to inhibitory effects. On the other hand, continuous cultures can regulate accumulation by adjusting dilution rate, and thus have relatively high productivities. For example, 4.9–8.8 g/L/h of 1,3-PDO can be produced under low dilution rates [130]. Although low final concentrations often accompany continuous cultures, which

might hinder downstream processes such as separation and purification [130].

Process-based enhancements like cell immobilization or co-digestion are often applied to these cultivation processes to improve glycerol utilization or metabolite production. Benefits conferred by cell immobilization might include increased stability in unfavorable environmental conditions during operation as well as avoiding washout [33,131,132]. For example, with microencapsulation, the biomass of *K. pneumoniae* was increased 2.6-fold compared to free cell cultures [33]. As the result, the final concentration of 1,3-PDO obtained in batch cultures was 63.1 g/L with a yield of 0.65 mol/mol glycerol. In continuous culture, the overall productivity of 1,3-PDO was 4.46 g/L/h with a yield of 0.43 mol/mol glycerol. By immobilizing *C. pasteurianam* cells on Amberlite, the maximum *n*-butanol yield of 0.43 mol/mol glycerol could be produced [47].

2.8.2. Anaerobic Co-Digestion

Anaerobic co-digestion of glycerol has been investigated to increase biogas productivity. Preceded by a mixed bacterial culture, this process consists of anaerobic digestion with waste glycerol as a complementary substrate to balance the C/N ratio [133]. As the result of co-digestion, useful products like biogas (consisting mainly CH_4 and CO_2) are produced. Direct utilization of waste glycerol without pretreatment could be problematic to microbes because of its alkalinity and high salt levels [134]. The application of pretreated waste glycerol has been reported as a positive supplement to increase the productivity of anaerobic digestion. For example, the methane production rate of a mixture of olive mill wastewater and slaughterhouse wastewater was increased from 479 mL/d to 1210 mL/d by volumetrically adding 1% waste glycerol as supplement [56]. Compared to mono-digestion, biogas production was also increased by about 400% under mesophilic conditions when pig manure was co-digested with 4% waste glycerol [135].

2.8.3. Microbial Electrochemical Conversion

Microbial electrochemical technologies (METs) can recover electrons from glycerol as electrical current using a microbial fuel cell (MFC) (Figure 4a) [136] or produce hydrogen using a microbial electrolysis cell (MEC) (Figure 4b) [137]. METs may contain either a mixed bacterial culture or pure culture that grows on the anode surface or in anodic chamber carrying out the oxidation of organic matter. During oxidation, electrons are released and then transferred to the anode through direct contact, electron shuttles, or conductive nanowires [136,138–141]. In an MFC, external electron acceptors (like oxygen or ferric cyanide) have to be fixed in order to create a potential difference large enough to allow current flow [142]. However, in an MEC, no external electron acceptor is added as the reduction of hydrogen ions on the cathode surface has a more negative redox potential than the anode, and thus an additional voltage must be applied to generate the current flow [143].

Figure 4. Single-Chamber microbial electrolysis cell (**a**) Single-Chamber microbial electrolysis cell (**b**) (adapted from [143]).

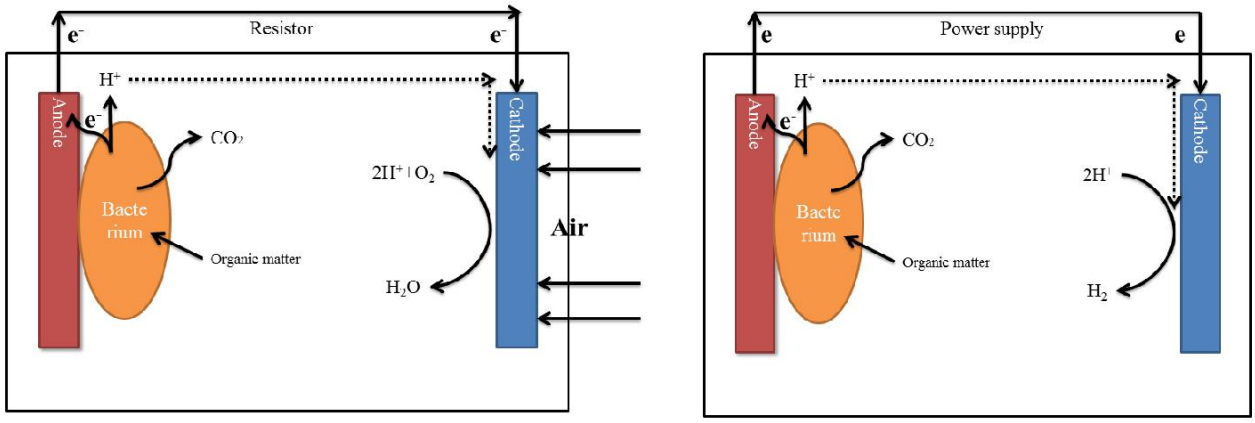

Both pure and mixed culture MFCs from which electrical power can be generated using glycerol are currently being investigated as an alternative method of biodiesel waste glycerol conversion. Enhancements have been made based on the selection of a favorable microbial consortia as well as improvements to MFC designs. Electrical power at a maximum density of 600 mW/m^2 can be generated from pure glycerol using a pure culture of *Bacillus subtilis* in a single chamber MFC with air cathode [75]. Although some pure bacterial strains, such as *Geobacter sulfurreducens*, have the ability to produce comparable power to mixed culture communities using defined substrates such as acetate [144], the use of mixed cultures in MFCs has the advantage of increased stability and a wider range of substrates capable of being utilized [145]. Electrical power can be directly generated from waste glycerol using a single chamber MFC with a mixed microbial consortium enriched from domestic wastewater [76]. The maximum power density generated from waste glycerol was 487 mW/m^2 with carbon cloth anode, but was further increased to 2110 mW/m^2 with a heat-treated carbon brush anode. An MFC with graphite fiber brush anodes can produce electrical current at power densities of 4.6 W/m^3 using pure glycerol and 2.3 W/m^3 using waste glycerol [77].

A recent study suggests that by externally applying current to a glycerol fermentation reactor inoculated with a mixed culture, metabolite formation can be significantly influenced with associated increases of highly reduced chemicals such as propanol and valerate [146]. Although the mechanism behind this metabolic shift was not clear, it is possibly related to the high hydrogen partial pressure caused by the current supplied in the vicinity of cathode. Besides producing more reduced, value-added products, attempts have also been made to achieve high levels of hydrogen production in pure and mixed culture MECs using glycerol as a substrate. Simultaneous production of hydrogen and

ethanol from pretreated waste glycerol was reported in a two compartment MEC inoculated with *Enterobacter aerogenes* NBRC 12010 [69]. The yield of hydrogen and ethanol were 0.74 and 0.92 mol/mol glycerol respectively. The consumption of glycerol can be increased from 45.7% to 84.5% through the application of a potential of 0.2 V. Mixed culture MECs with a single chamber design can produce hydrogen yields of 3.9 mol/mol and 5.4 mol/mol glycerol, higher than pure culture MECs, with applied voltages of 0.9 and 1.0 V [79,80]. The application of pretreatments like heat shock should be considered to before inoculation as a method to prevent growth of methanogens.

3. Outlook

As previously discussed, the production of biodiesel waste will continue to increase with the growth of the biofuel market. The surplus of glycerol is not only creating difficulties for the glycerol production industry but also for biodiesel plants. Microbial conversion is an efficient and sustainable method for converting waste glycerol that avoids the disadvantages of direct application and chemical transformation, such as the inability to use waste glycerol directly and low product specificity [6]. Although there are still hurdles involved in constructing a suitable industrial scale reactor to more accurately predict real production costs, encouraging results have been demonstrated (Table 1).

1,3-Propanediol is one of the various value-added products that can be generated from glycerol fermentation, and is, a chemical that is already produced nationally on a level of about 31.6 million kg per year, and appears to be an encouraging target for future waste glycerol microbial conversion efforts [147,148]. Currently, commercial synthesis of 1,3-PDO is performed either by petroleum chemicals (acrolein and ethylene) [147,148] or by glucose fermentation of engineered bacterial strains [24,149]. As natural producers of 1,3-PDO, members of the *Klebsiella*, *Citrobacter*, and *Clostridium* families have been intensively studied for potential industrial applications. Compared to these bacteria, *E. coli* has an advantage being a highly tractable, and thus easier to be manipulated for various industrial needs [31]. In fact, one of the highest 1,3-PDO concentrations achieved by glycerol fermentation was the 104.4 g/L produced using an engineered *E. coli* strain, with a yield of 1.09 mol/mol (0.9 g/g) of glycerol [31].

On the other hand, citric acid generation from waste glycerol also represents a promising conversion route that can be achieved by yeast [60,61]. Strains of *Y. lipolytica* have been investigated as an alternative to citric acid production by *A. niger*. Although concentrations achieved are still lower than the concentrations from the commercialized process using glucose as substrate [150,151], economic analysis suggests that it is more profitable to generate value-added products like 1,3-PDO ($1.8 per kg [149]) and citric acid ($1.2 to 3.2 per kg) from waste glycerol ($0.11 per kg) [60,61,152].

One of the most challenging elements of the microbial conversion of waste glycerol to water-soluble products is downstream separation and purification, but microbial electrochemical technologies like MECs and MFCs have the potential to efficiently overcome this problem. Electrical power produced from waste glycerol requires no extra cost associated with separation or purification. It was estimated that the electrical

power generated from waste glycerol by MFCs may be worth a total value of $98.4 million per year [77], a number that could be increased further by optimizing MFC designs for current generation. Similarly, as a gaseous product with low water solubility, hydrogen can be separated from reaction broth with no extensive separation cost regardless of hurdles in storage and transportation [153]. Current hydrogen production is dominated by steam reformation of natural gas, producing hydrogen at a cost ranging from $1.10 to $1.24 [154]. High hydrogen yields have been demonstrated using a photo-fermentative bacterium (6 mol/mol glycerol) [51]. However, the need for light may complicate the reactor design, increasing the difficulty in scaling-up for commercial applications. Under dark-fermentation, low hydrogen yields (0.28–0.96 mol/mol) are likely to be caused due to inefficient use of secondary metabolites such as acetate, lactate, and ethanol [23,52–55]. Through the use of an MEC design these secondary metabolites were able to be further utilized [155–157], and higher hydrogen yields (3.6–5.4 mol/mol glycerol) closer to the theoretical yields can be achieved with a relatively low investment of energy compared to dark fermentation [23,79,80,158]. Further research is needed to demonstrate the ability to efficiently scale-up promising waste glycerol to hydrogen conversion technologies, as well as life cycle analyses comparing these technologies to current stream reformation techniques.

In summary, waste glycerol represents a carbon source that is widely available at relatively low-cost and potentially suitable for many applications. Although constraints are still largely present for practical utilization of waste glycerol from biodiesel plants, advancements have been made over the past decade that warrant further research in this fascinating area. Future advancements in this field could bring great social, economic and environmental benefits to society.

Acknowledgements

The authors would like to acknowledge support from the USA National Science Foundation (CBET 0955124).

Conflicts of Interest

The authors declare no conflict of interest.

References

1. Yang, F.X.; Hanna, M.A.; Sun, R.C. Value-added uses for crude glycerol—A byproduct of biodiesel production. *Biotechnol. Biofuels* **2012**, *5*, doi:10.1186/1754-6834-5-13.
2. *Monthly Biodiesel Production Report*; U.S. Energy Information Administration: Washington, DC, USA, 2013.
3. Moser, B.R. Biodiesel Production, Properties, and Feedstocks. In *Biofuels*; Tomes, D., Lakshmanan, P., Songstad, D., Eds.; Springer: New York, NY, USA, 2011; pp. 285–347.
4. Hu, S.J.; Luo, X.L.; Wan, C.X.; Li, Y.B. Characterization of crude glycerol from biodiesel plants. *J. Agric. Food Chem.* **2012**, *60*, 5915–5921.

5. Christoph, R.; Schmidt, B.; Steinberner, U.; Dilla, W.; Karinen, R. Glycerol. In *Ullmann's Encyclopedia of Industrial Chemistry*; Morrison, L.R., Ed.;Wiley: New York, NY, USA, 2006.
6. Yazdani, S.S.; Gonzalez, R. Anaerobic fermentation of glycerol: A path to economic viability for the biofuels industry. *Curr. Opin. Biotech.* **2007**, *18*, 213–219.
7. Kerr, B.; Dozier, W.; Bregendahl, K. Nutritional Value of Crude Glycerin for Nonruminants. In Proceedings of the 23rd Annual Carolina Swine Nutrition Conference, Raleigh, NC, USA, 13 November 2007; pp. 6–18.
8. Bohon, M.D.; Metzger, B.A.; Linak, W.P.; King, C.J.; Roberts, W.L. Glycerol combustion and emissions. *Proc. Combust. Inst.* **2011**, *33*, 2717–2724.
9. Johnson, D.T.; Taconi, K.A. The glycerin glut: Options for the value-added conversion of crude glycerol resulting from biodiesel production. *Environ. Prog.* **2007**, *26*, 338–348.
10. Siles, J.A.; Martín, M.A.; Chica, A.F.; Martín, A. Anaerobic co-digestion of glycerol and wastewater derived from biodiesel manufacturing. *Bioresour. Technol.* **2010**, *101*, 6315–6321.
11. Lammers, P.J.; Kerr, B.J.; Weber, T.E.; Bregendahl, K.; Lonergan, S.M.; Prusa, K.J.; Ahn, D.U.; Stoffregen, W.C.; Dozier, W.A.; Honeyman, M.S. Growth performance, carcass characteristics, meat quality, and tissue histology of growing pigs fed crude glycerin-supplemented diets. *J. Anim. Sci.* **2008**, *86*, 2962–2970.
12. Lin, E.C.C. Glycerol dissmilation and its regulation in bacteria. *Annu. Rev. Microbiol.* **1976**, *30*, 535–578.
13. Neijssel, O.M.; Hueting, S.; Crabbendam, K.J.; Tempest, D.W. Dual pathways of glycerol assimilation in *Klebsiella aerogenes* NCIB 418. *Arch. Microbiol.* **1975**, *104*, 83–87.
14. Abad, S.; Turon, X. Valorization of biodiesel derived glycerol as a carbon source to obtain added-value metabolites: Focus on polyunsaturated fatty acids. *Biotechnol. Adv.* **2012**, *30*, 733–741.
15. Fan, X.H.; Burton, R.; Zhou, Y.C. Glycerol (byproduct of biodiesel production) as a source for fuels and chemicals. *Open Fuels Energy J.* **2010**, *3*, 17–22.
16. Imhoff, J.F. Enterobacteriales. In *Bergey's Manual® of Systematic Bacteriology*; Brenner, D.J., Krieg, N.R., Staley, J.T., Garrity, G.M., Boone, D.R., Vos, P., Goodfellow, M., Rainey, F.A., Schleifer, K.-H., Eds.; Springer: New York, NY, USA, 2005; pp. 587–850.
17. Da Silva, G.P.; Mack, M.; Contiero, J. Glycerol: A promising and abundant carbon source for industrial microbiology. *Biotechnol. Adv.* **2009**, *27*, 30–39.
18. Murarka, A.; Dharmadi, Y.; Yazdani, S.S.; Gonzalez, R. Fermentative utilization of glycerol by *Escherichia coli* and its implications for the production of fuels and chemicals. *Appl. Environ. Microbiol.* **2008**, *74*, 1124–1135.
19. Braun, T.; Philippsen, A.; Wirtz, S.; Borgnia, M.J.; Agre, P.; Kühlbrandt, W.; Engel, A.; Stahlberg, H. The 3.7 Å projection map of the glycerol facilitator glpf: A variant of the aquaporin tetramer. *EMBO Rep.* **2000**, *1*, 183–189.
20. Trinh, C.T.; Srienc, F. Metabolic engineering of *Escherichia coli* for efficient conversion of

glycerol to ethanol. *Appl. Environ. Microbiol.* **2009**, *75*, 6696–6705.

21. Bouvet, O.M.M.; Lenormand, P.; Ageron, E.; Grimont, P.A.D. Taxonomic diversity of anaerobic glycerol dissimilation in the *Enterobacteriaceae*. *Res. Microbiol.* **1995**, *146*, 279–290.
22. Gonzalez, R.; Murarka, A.; Dharmadi, Y.; Yazdani, S.S. A new model for the anaerobic fermentation of glycerol in enteric bacteria: Trunk and auxiliary pathways in *Escherichia coli*. *Metab. Eng.* **2008**, *10*, 234–245.
23. Selembo, P.A.; Perez, J.M.; Lloyd, W.A.; Logan, B.E. Enhanced hydrogen and 1,3-propanediol production from glycerol by fermentation using mixed cultures. *Biotechnol. Bioeng.* **2009**, *104*, 1098–1106.
24. Chen, X.; Zhou, L.; Tian, K.; Kumar, A.; Singh, S.; Prior, B.A.; Wang, Z. Metabolic engineering of *Escherichia coli*: A sustainable industrial platform for bio-based chemical production. *Biotechnol. Adv.* **2013**, in press.
25. Cardona, C.A.; Sánchez, Ó.J. Fuel ethanol production: Process design trends and integration opportunities. *Bioresour. Technol.* **2007**, *98*, 2415–2457.
26. Yazdani, S.S.; Gonzalez, R. Engineering *Escherichia coli* for the efficient conversion of glycerol to ethanol and co-products. *Metab. Eng.* **2008**, *10*, 340–351.
28. Hong, A.-A.; Cheng, K.-K.; Peng, F.; Zhou, S.; Sun, Y.; Liu, C.-M.; Liu, D.-H. Strain isolation and optimization of process parameters for bioconversion of glycerol to lactic acid. *J. Chem. Technol. Biotechnol.* **2009**, *84*, 1576–1581.
29. Mazumdar, S.; Clomburg, J.M.; Gonzalez, R. *Escherichia coli* strains engineered for homofermentative production of D-lactic acid from glycerol. *Appl. Environ. Microbiol.* **2010**, *76*, 4327–4336.
30. Mazumdar, S.; Blankschien, M.D.; Clomburg, J.M.; Gonzalez, R. Efficient synthesis of L-lactic acid from glycerol by metabolically engineered *Escherichia coli*. *Microb. Cell Fact.* **2013**, *12*, doi:10.1186/1475-2859-12-7.
31. Clomburg, J.M.; Gonzalez, R. Metabolic engineering of *Escherichia coli* for the production of 1,2-propanediol from glycerol. *Biotechnol. Bioeng.* **2011**, *108*, 867–879.
32. Tang, X.; Tan, Y.; Zhu, H.; Zhao, K.; Shen, W. Microbial conversion of glycerol to 1,3-propanediol by an engineered strain of *Escherichia coli*. *Appl. Environ. Microbiol.* **2009**, *75*, 1628–1634.
33. Zhang, X.; Shanmugam, K.T.; Ingram, L.O. Fermentation of glycerol to succinate by metabolically engineered strains of *Escherichia coli*. *Appl. Environ. Microbiol.* **2010**, *76*, 2397–2401.
34. Zhao, Y.-N.; Chen, G.; Yao, S.-J. Microbial production of 1,3-propanediol from glycerol by encapsulated *Klebsiella pneumoniae*. *Biochem. Eng. J.* **2006**, *32*, 93–99.
35. Cheng, K.-K.; Zhang, J.-A.; Liu, D.-H.; Sun, Y.; Liu, H.-J.; Yang, M.-D.; Xu, J.-M. Pilot-scale production of 1,3-propanediol using *Klebsiella pneumoniae*. *Process Biochem.* **2007**, *42*, 740–744.
36. Yang, G.; Tian, J.; Li, J. Fermentation of 1,3-propanediol by a lactate deficient mutant of *Klebsiella oxytoca* under microaerobic conditions. *Appl. Microbiol. Biotechnol.* **2007**, *73*, 1017–

1024.

37. Zhang, Y.; Li, Y.; Du, C.; Liu, M.; Cao, Z. Inactivation of aldehyde dehydrogenase: A key factor for engineering 1,3-propanediol production by *Klebsiella pneumoniae*. *Metab. Eng.* **2006**, *8*, 578–586.
38. Petrov, K.; Petrova, P. High production of 2,3-butanediol from glycerol by *Klebsiella pneumoniae* G31. *Appl. Microbiol. Biotechnol.* **2009**, *84*, 659–665.
39. Oh, B.-R.; Seo, J.-W.; Heo, S.-Y.; Hong, W.-K.; Luo, L.H.; Kim, S.; Kwon, O.; Sohn, J.-H.; Joe, M.-H.; Park, D.-H.; *et al*. Enhancement of ethanol production from glycerol in a *Klebsiella pneumoniae* mutant strain by the inactivation of lactate dehydrogenase. *Process Biochem.* **2012**, *47*, 156–159.
40. Metsoviti, M.; Zeng, A.-P.; Koutinas, A.A.; Papanikolaou, S. Enhanced 1,3-propanediol production by a newly isolated Citrobacter freundii strain cultivated on biodiesel-derived waste glycerol through sterile and non-sterile bioprocesses. *J. Biotechnol.* **2013**, *163*, 408–418.
41. Maervoet, V.E.T.; Beauprez, J.; de Maeseneire, S.L.; Soetaert, W.K.; de Mey, M. Citrobacter werkmanii, a new candidate for the production of 1,3-propanediol: Strain selection and carbon source optimization. *Green Chem.* **2012**, *14*, 2168–2178.
42. Maru, B.T.; Constanti, M.; Stchigel, A.M.; Medina, F.; Sueiras, J.E. Biohydrogen production by dark fermentation of glycerol using *Enterobacter* and *Citrobacter* sp. *Biotechnol. Prog.* **2013**, *29*, 31–38.
43. Yang, C.; Jiang, P.; Xiao, S.; Zhang, C.; Lou, K.; Xing, X.-H. Fed-batch fermentation of recombinant *Citrobacter freundii* with expression of a violacein-synthesizing gene cluster for efficient violacein production from glycerol. *Biochem. Eng. J.* **2011**, *57*, 55–62.
44. González-Pajuelo, M.; Andrade, J.C.; Vasconcelos, I. Production of 1,3-Propanediol by *Clostridium butyricum* VPI 3266 in continuous cultures with high yield and productivity. *J. Ind. Microbiol. Biotechnol.* **2005**, *32*, 391–396.
45. Wilkens, E.; Ringel, A.K.; Hortig, D.; Willke, T.; Vorlop, K.-D. High-level production of 1,3-propanediol from crude glycerol by *Clostridium butyricum* AKR102a. *Appl. Microbiol. Biotechnol.* **2012**, *93*, 1057–1063.
46. Chatzifragkou, A.; Papanikolaou, S.; Dietz, D.; Doulgeraki, A.I.; Nychas, G.-J.E.; Zeng, A.-P. Production of 1,3-propanediol by *Clostridium butyricu* growing on biodiesel-derived crude glycerol through a non-sterilized fermentation process. *Appl. Microbiol. Biotechnol.* **2011**, *91*, 101–112.
47. González-Pajuelo, M.; Meynial-Salles, I.; Mendes, F.; Andrade, J.C.; Vasconcelos, I.; Soucaille, P. Metabolic engineering of *Clostridium acetobutylicum* for the industrial production of 1,3-propanediol from glycerol. *Metab. Eng.* **2005**, *7*, 329–336.
48. Khanna, S.; Goyal, A.; Moholkar, V.S. Production of n-butanol from biodiesel derived crude glycerol using *Clostridium pasteurianum* immobilized on Amberlite. *Fuel* **2011**, *112*, 557–561.
49. Jensen, T.Ø.; Kvist, T.; Mikkelsen, M.J.; Christensen, P.V.; Westermann, P. Fermentation of

crude glycerol from biodiesel production by *Clostridium pasteurianum*. *J. Ind. Microbiol. Biotechnol.* **2012**, *39*, 709–717.

50. Zhang, A.; Yang, S.-T. Propionic acid production from glycerol by metabolically engineered *Propionibacterium acidipropionici*. *Process Biochem.* **2009**, *44*, 1346–1351.
51. Ruhal, R.; Choudhury, B. Improved trehalose production from biodiesel waste using parent and osmotically sensitive mutant of *Propionibacterium freudenreichii* subsp. *shermanii* under aerobic conditions. *J. Ind. Microbiol. Biotechnol.* **2012**, *39*, 1153–1160.
52. Sabourin-Provost, G.; Hallenbeck, P.C. High yield conversion of a crude glycerol fraction from biodiesel production to hydrogen by photofermentation. *Bioresour. Technol.* **2009**, *100*, 3513–3517.
53. Gupta, A.; Murarka, A.; Campbell, P.; Gonzalez, R. Anaerobic fermentation of glycerol in *Paenibacillus macerans*: Metabolic pathways and environmental determinants. *Appl. Environ. Microbiol.* **2009**, *75*, 5871–5883.
54. Sittijunda, S.; Reungsang, A. Media optimization for biohydrogen production from waste glycerol by anaerobic thermophilic mixed cultures. *Int. J. Hydrog. Energy* **2012**, *37*, 15473–15482.
55. Varrone, C.; Giussani, B.; Izzo, G.; Massini, G.; Marone, A.; Signorini, A.; Wang, A. Statistical optimization of biohydrogen and ethanol production from crude glycerol by microbial mixed culture. *Int. J. Hydrog. Energy* **2012**, *37*, 16479–16488.
56. Temudo, M.F.; Poldermans, R.; Kleerebezem, R.; van Loosdrecht, M.C.M. Glycerol fermentation by (open) mixed cultures: A chemostat study. *Biotechnol. Bioeng.* **2008**, *100*, 1088–1098.
57. Fountoulakis, M.S.; Manios, T. Enhanced methane and hydrogen production from municipal solid waste and agro-industrial by-products co-digested with crude glycerol. *Bioresour. Technol.* **2009**, *100*, 3043–3047.
58. Cavalheiro, J.M.B.T.; de Almeida, M.C.M.D.; Grandfils, C.; da Fonseca, M.M.R. Poly(3-hydroxybutyrate) production by *Cupriavidus necator* using waste glycerol. *Process Biochem.* **2009**, *44*, 509–515.
58. Ibrahim, M.H.A.; Steinbüchel, A. *Zobellella denitrificans* strain MW1, a newly isolated bacterium suitable for poly(3-hydroxybutyrate) production from glycerol. *J. Appl. Microbiol.* **2010**, *108*, 214–225.
59. Kenny, S.T.; Runic, J.N.; Kaminsky, W.; Woods, T.; Babu, R.P.; O'Connor, K.E. Development of a bioprocess to convert PET derived terephthalic acid and biodiesel derived glycerol to medium chain length polyhydroxyalkanoate. *Appl. Microbiol. Biotechnol.* **2012**, *95*, 623–633.
60. Imandi, S.B.; Bandaru, V.R.; Somalanka, S.R.; Garapati, H.R. Optimization of medium constituents for the production of citric acid from byproduct glycerol using Doehlert experimental design. *Enzym. Microb. Technol.* **2007**, *40*, 1367–1372.
61. Rywińska, A.; Rymowicz, W.; Żarowska, B.; Wojtatowicz, M. Biosynthesis of citric acid from glycerol by acetate mutants of *Yarrowia lipolytica* in fed-batch fermentation. *Food Technol. Biotechnol.* **2009**, *47*, 1–6.
62. Ashby, R.; Nuñez, A.; Solaiman, D.; Foglia, T. Sophorolipid biosynthesis from a biodiesel co-

product stream. *J. Am. Oil Chem. Soc.* **2005**, *82*, 625–630.

63. Morita, T.; Konishi, M.; Fukuoka, T.; Imura, T.; Kitamoto, D. Microbial conversion of glycerol into glycolipid biosurfactants, mannosylerythritol lipids, by a basidiomycete yeast, *Pseudozyma antarctica* JCM 10317^{T}. *J. Biosci. Bioeng.* **2007**, *104*, 78–81.
64. Liang, Y.; Cui, Y.; Trushenski, J.; Blackburn, J.W. Converting crude glycerol derived from yellow grease to lipids through yeast fermentation. *Bioresour. Technol.* **2010**, *101*, 7581–7586.
65. Yen, H.-W.; Yang, Y.-C.; Yu, Y.-H. Using crude glycerol and thin stillage for the production of microbial lipids through the cultivation of *Rhodotorula glutinis*. *J. Biosci. Bioeng.* **2012**, *114*, 453–456.
66. Valduga, E.; Tatsch, P.O.; Tiggemann, L.; Zeni, J.; Colet, R.; Cansian, J.M.; Treichel, H.; Luccio, M. Evaluation of the conditions of carotenoids production in a synthetic medium by *Sporidiobolus salmonicolor* (CBS 2636) in a bioreactor. *Int. J. Food Sci. Technol.* **2009**, *44*, 2445–2451.
67. Yu, K.O.; Kim, S.W.; Han, S.O. Engineering of glycerol utilization pathway for ethanol production by *Saccharomyces cerevisiae*. *Bioresour. Technol.* **2010**, *101*, 4157–4161.
68. Jung, J.Y.; Yun, H.S.; Lee, J.W.; Oh, M.K. Production of 1,2-propanediol from glycerol in *Saccharomyces cerevisiae*. *J. Microbiol. Biotechnol.* **2011**, *21*, 846–853.
69. André, A.; Diamantopoulou, P.; Philippoussis, A.; Sarris, D.; Komaitis, M.; Papanikolaou, S. Biotechnological conversions of bio-diesel derived waste glycerol into added-value compounds by higher fungi: Production of biomass, single cell oil and oxalic acid. *Ind. Crop. Prod.* **2010**, *31*, 407–416.
70. Marchand, K.; Lubitz, W.; Nicol, R. Utilization of biodiesel derived crude glycerol by fungal isolates for biomass and single cell oil production. *J. Biobased. Mater. Bio.* **2013**, *7*, 415–419.
71. Chatzifragkou, A.; Makri, A.; Belka, A.; Bellou, S.; Mavrou, M.; Mastoridou, M.; Mystrioti, P.; Onjaro, G.; Aggelis, G.; Papanikolaou, S. Biotechnological conversions of biodiesel derived waste glycerol by yeast and fungal species. *Energy* **2011**, *36*, 1097–1108.
72. Athalye, S.K.; Garcia, R.A.; Wen, Z. Use of biodiesel-derived crude glycerol for producing eicosapentaenoic acid (EPA) by the fungus *Pythium irregulare*. *J. Agric. Food Chem.* **2009**, *57*, 2739–2744.
73. Mantzouridou, F.; Naziri, E.; Tsimidou, M.Z. Industrial glycerol as a supplementary carbon source in the production of β-carotene by *Blakeslea trispora*. *J. Agric. Food Chem.* **2008**, *56*, 2668–2675.
74. Chi, Z.; Pyle, D.; Wen, Z.; Frear, C.; Chen, S. A laboratory study of producing docosahexaenoic acid from biodiesel-waste glycerol by microalgal fermentation. *Process Biochem.* **2007**, *42*, 1537–1545.
75. Nimje, V.R.; Chen, C.-Y.; Chen, C.-C.; Chen, H.-R.; Tseng, M.-J.; Jean, J.-S.; Chang, Y.-F. Glycerol degradation in single-chamber microbial fuel cells. *Bioresour. Technol.* **2011**, *102*, 2629–2634.

76. Feng, Y.; Yang, Q.; Wang, X.; Liu, Y.; Lee, H.; Ren, N. Treatment of biodiesel production wastes with simultaneous electricity generation using a single-chamber microbial fuel cell. *Bioresour. Technol.* **2011**, *102*, 411–415.
77. Sharma, Y.; Parnas, R.; Li, B. Bioenergy production from glycerol in hydrogen producing bioreactors (HPBs) and microbial fuel cells (MFCs). *Int. J. Hydrog. Energy* **2011**, *36*, 3853–3861.
78. Sakai, S.; Yagishita, T. Microbial production of hydrogen and ethanol from glycerol-containing wastes discharged from a biodiesel fuel production plant in a bioelectrochemical reactor with thionine. *Biotechnol. Bioeng.* **2007**, *98*, 340–348.
79. Selembo, P.A.; Perez, J.M.; Lloyd, W.A.; Logan, B.E. High hydrogen production from glycerol or glucose by electrohydrogenesis using microbial electrolysis cells. *Int. J. Hydrog. Energy* **2009**, *34*, 5373–5381.
80. Escapa, A.; Manuel, M.F.; Morán, A.; Gómez, X.; Guiot, S.R.; Tartakovsky, B. Hydrogen production from glycerol in a membraneless microbial electrolysis cell. *Energy Fuel.* **2009**, *23*, 4612–4618.
81. Hofvendahl, K.; Hahn-Hägerdal, B. Factors affecting the fermentative lactic acid production from renewable resources. *Enzym. Microb. Technol.* **2000**, *26*, 87–107.
82. Okano, K.; Tanaka, T.; Ogino, C.; Fukuda, H.; Kondo, A. Biotechnological production of enantiomeric pure lactic acid from renewable resources: Recent achievements, perspectives, and limits. *Appl. Microbiol. Biotechnol.* **2010**, *85*, 413–423.
83. John, R.P.; Anisha, G.S.; Nampoothiri, K.M.; Pandey, A. Direct lactic acid fermentation: Focus on simultaneous saccharification and lactic acid production. *Biotechnol. Adv.* **2009**, *27*, 145–152.
84. Wee, Y.J.; Yun, J.S.; Park, D.H.; Ryu, H.W. Biotechnological production of L(+)-lactic acid from wood hydrolyzate by batch fermentation of *Enterococcus faecalis*. *Biotechnol. Lett.* **2004**, *26*, 71–74.
85. Huang, L.; Zhu, Y.-L.; Zheng, H.-Y.; Li, Y.-W.; Zeng, Z.-Y. Continuous production of 1,2-propanediol by the selective hydrogenolysis of solvent-free glycerol under mild conditions. *J. Chem. Technol. Biotechnol.* **2008**, *83*, 1670–1675.
86. Shelley, S. A renewable route to propylene glycol. *Chem. Eng. Prog.* **2007**, *103*, 6–9.
87. Werpy, T.; Petersen, G. *Top Value Added Chemical from Biomass*; U.S. Department of Energy: Washington, DC, USA, 2004.
88. Chotani, G.; Dodge, T.; Hsu, A.; Kumar, M.; LaDuca, R.; Trimbur, D.; Weyler, W.; Sanford, K. The commercial production of chemicals using pathway engineering. *Biochim. Biophys. Acta* **2000**, *1543*, 434–455.
89. Zhang, Y.; Huang, Z.; Du, C.; Li, Y.; Cao, Z. Introduction of an NADH regeneration system into *Klebsiella oxytoca* leads to an enhanced oxidative and reductive metabolism of glycerol. *Metab. Eng.* **2009**, *11*, 101–106.
90. Celińska, E.; Grajek, W. Biotechnological production of 2,3-butanediol—Current state and prospects. *Biotechnol. Adv.* **2009**, *27*, 715–725.

91. Wolf-Dieter, D. Microbial conversion of glycerol to 1,3-propanediol. *FEMS Microbiol. Rev.* **1995**, *16*, 143-149.
92. Durán, N.; Menck, C.F.M. *Chromobacterium violaceum*: A review of pharmacological and industiral perspectives. *Crit. Rev. Microbiol.* **2001**, *27*, 201–222.
93. Biebl, H.; Marten, S.; Hippe, H.; Deckwer, W.-D. Glycerol conversion to 1,3-propanediol by newly isolated *Clostridia*. *Appl. Microbiol. Biotechnol.* **1992**, *36*, 592–597.
94. Lee, S.Y.; Park, J.H.; Jang, S.H.; Nielsen, L.K.; Kim, J.; Jung, K.S. Fermentative butanol production by *Clostridia*. *Biotechnol. Bioeng.* **2008**, *101*, 209–228.
95. Boyaval, P.; Corre, C. Production of propionic acid. *Lait* **1995**, *75*, 453–461.
96. Danilo, Z. Production of Propionic Acid. U.S. Patent 8,053,602 B2, 8 November 2011.
97. Cardoso, F.S.; Gaspar, P.; Hugenholtz, J.; Ramos, A.; Santos, H. Enhancement of trehalose production in dairy propionibacteria through manipulation of environmental conditions. *Int. J. Food Microbiol.* **2004**, *91*, 195–204.
98. Schiraldi, C.; di Lernia, I.; de Rosa, M. Trehalose production: Exploiting novel approaches. *Trends Biotechnol.* **2002**, *20*, 420–425.
99. Kongjan, P.; Angelidaki, I. Extreme thermophilic biohydrogen production from wheat straw hydrolysate using mixed culture fermentation: Effect of reactor configuration. *Bioresour. Technol.* **2010**, *101*, 7789–7796.
100. Kongjan, P.; Min, B.; Angelidaki, I. Biohydrogen production from xylose at extreme thermophilic temperatures (70 °C) by mixed culture fermentation. *Water Res.* **2009**, *43*, 1414–1424.
101. Pflügl, S.; Marx, H.; Mattanovich, D.; Sauer, M. 1,3-Propanediol production from glycerol with *Lactobacillus diolivorans*. *Bioresour. Technol.* **2012**, *119*, 133–140.
102. Keshavarz, T.; Roy, I. Polyhydroxyalkanoates: Bioplastics with a green agenda. *Curr. Opin. Microbiol.* **2010**, *13*, 321–326.
103. Valadi, Å.; Granath, K.; Gustafsson, L.; Adler, L. Distinct intracellular localization of Gpd1p and Gpd2p, the two yeast isoforms of NAD^+-dependent Glycerol-3-phosphate dehydrogenase, explains their different contributions to redox-driven glycerol production. *J. Biol. Chem.* **2004**, *279*, 39677–39685.
104. Adler, L.; Blomberg, A.; Nilsson, A. Glycerol metabolism and osmoregulation in the salt-tolerant yeast *Debaryomyces hansenii*. *J. Bacteriol.* **1985**, *162*, 300–306.
105. André, L.; Nilsson, A.; Adler, L. The role of glycerol in osmotolerance of the yeast *Debaryomyces hansenii*. *J. Gen. Microbiol.* **1988**, *134*, 669–677.
106. Castro, I.M.; Loureiro-Dias, M.C. Glycerol utilization in *Fusarium oxysporum* var. *lini*: Regulation of transport and metabolism. *J. Gen. Microbiol.* **1991**, *137*, 1497–1502.
108. Gancedo, C.; Gancedo, J.M.; Sols, A. Glycerol metabolism in yeasts. *Eur. J. Biochem.* **1968**, *5*, 165–172.
109. Nobre, M.F.; da Costa, M.S. The accumulation of polyols by the yeast *Debaryomyces hansenii* in response to water stress. *Can. J. Microbiol.* **1985**, *31*, 1061–1064.

110. Ferreira, C.; van Voorst, F.; Martins, A.; Neves, L.; Oliveira, R.; Kielland-Brandt, M.C.; Lucas, C.; Brandt, A. A member of the sugar transporter family, Stl1p is the glycerol/H^+ symporter in *Saccharomyces cerevisiae*. *Mol. Biol. Cell.* **2005**, *16*, 2068–2076.
111. Kayingo, G.; Martins, A.; Andrie, R.; Neves, L.; Lucas, C.; Wong, B. A permease encoded by STL1 is required for active glycerol uptake by *Candida albicans*. *Microbiology* **2009**, *155*, 1547–1557.
112. Nicol, R.W.; Marchand, K.; Lubitz, W.D. Bioconversion of crude glycerol by fungi. *Appl. Microbiol. Biotechnol.* **2012**, *93*, 1865–1875.
113. Amaral, P.F.F.; Ferreira, T.F.; Fontes, G.C.; Coelho, M.A.Z. Glycerol valorization: New biotechnological routes. *Food Bioprod. Process.* **2009**, *87*, 179–186.
114. Finogenova, T.V.; Morgunov, I.G.; Kamzolova, S.V.; Chernyavskaya, O.G. Organic acid production by the yeast *Yarrowia lipolytica*: A review of prospects. *Appl. Biochem. Microbiol.* **2005**, *41*, 418–425.
115. Xu, D.-B.; Madrid, C.P.; Röhr, M.; Kubicek, C.P. The influence of type and concentration of the carbon source on production of citric acid by *Aspergillus niger*. *Appl. Microbiol. Biotechnol.* **1989**, *30*, 553–558.
116. Amaral, P.F.F.; Coelho, M.A.Z.; Marrucho, I.M.J.; Coutinho, J.A.P. Biosurfactants from Yeasts: Characteristics, Production and Application. In *Biosurfactants*; Sen, R., Ed.; Springer: New York, NY, USA, 2010; Volume 672, pp. 236–249.
116. Banat, I.M.; Franzetti, A.; Gandolfi, I.; Bestetti, G.; Martinotti, M.G.; Fracchia, L.; Smyth, T.J.; Marchant, R. Microbial biosurfactants production, applications and future potential. *Appl. Microbiol. Biotechnol.* **2010**, *87*, 427–444.
117. Makkar, R.S.; Cameotra, S.S.; Banat, I.M. Advances in utilization of renewable substrates for biosurfactant production. *AMB Express* **2011**, *1*, doi:10.1186/2191-0855-1-5.
118. Liu, Y.; Koh, C.M.J.; Ji, L. Bioconversion of crude glycerol to glycolipids in *Ustilago maydi*. *Bioresour. Technol.* **2011**, *102*, 3927-3933.
119. Papanikolaou, S.; Komaitis, M.; Aggelis, G. Single cell oil (SCO) production by *Mortierella isabellina* grown on high-sugar content media. *Bioresour. Technol.* **2004**, *95*, 287–291.
120. Gouveia, L.; Empis, J. Relative stabilities of microalgal carotenoids in microalgal extracts, biomass and fish feed: Effect of storage conditions. *Innov. Food Sci. Emerg. Technol.* **2003**, *4*, 227–233.
121. Simopoulos, A.P. Essential fatty acids in health and chronic disease. *Am. J. Clin. Nutr.* **1999**, *70*, 560S–569S.
122. Hou, C.T. Production of arachidonic acid and dihomo-*γ*-linolenic acid from glycerol by oil-producing filamentous fungi, *Mortierella* in the ARS culture collection. *J. Ind. Microbiol. Biotechnol.* **2008**, *35*, 501–506.
123. Tonon, T.; Harvey, D.; Larson, T.R.; Graham, I.A. Long chain polyunsaturated fatty acid production and partitioning to triacylglycerols in four microalgae. *Phytochemistry* **2002**, *61*, 15–

24.
124. Grima, E.M.; Pérez, J.A.S.; Camacho, F.G.; Medina, A.R.; Giménez, A.G.; López Alonso, D. The production of polyunsaturated fatty acids by microalgae: From strain selection to product purification. *Process Biochem.* **1995**, *30*, 711–719.
125. Chisti, Y. Biodiesel from microalgae. *Biotechnol. Adv.* **2007**, *25*, 294–306.
126. Ingram, L.O.; Calder, J.A.; van Baalen, C.; Plucker, F.E.; Parker, P.L. Role of reduced exogenous organic compounds in the physiology of the blue-green bacteria (algae): Photoheterotrophic growth of a "heterotrophic" blue-green bacterium. *J. Bacteriol.* **1973**, *114*, 695–700.
127. Ingram, L.O.; Van Baalen, C.; Calder, J.A. Role of reduced exogenous organic compounds in the physiology of the blue-green bacteria (algae): Photoheterotrophic growth of an "autotrophic" blue-green bacterium. *J. Bacteriol.* **1973**, *114*, 701–705.
128. Neilson, A.H.; Lewin, R.A. The uptake and utilization of organic carbon by algae: An essay in comparative biochemistry. *Phycologia* **1974**, *13*, 227–264.
129. Villadsen, J.; Nielsen, J.; Lidén, G. *Bioreaction Engineering Principles*; Springer: New York, NY, USA, 2011.
130. Menzel, K.; Zeng, A.-P.; Deckwer, W.-D. High concentration and productivity of 1,3-propanediol from continuous fermentation of glycerol by *Klebsiella pneumoniae*. *Enzym. Microb. Technol.* **1997**, *20*, 82–86.
131. Gungormusler, M.; Gonen, C.; Azbar, N. Continuous production of 1,3-propanediol using raw glycerol with immobilized *Clostridium beijerinckii* NRRL B-593 in comparison to suspended culture. *Bioprocess Biosyst. Eng.* **2011**, *34*, 727–733.
132. Gungormusler, M.; Gonen, C.; Azbar, N. Use of ceramic-based cell immobilization to produce 1,3-propanediol from biodiesel-derived waste glycerol with *Klebsiella pneumoniae*. *J. Appl. Microbiol.* **2011**, *111*, 1138–1147.
133. Yen, H.-W.; Brune, D.E. Anaerobic co-digestion of algal sludge and waste paper to produce methane. *Bioresour. Technol.* **2007**, *98*, 130–134.
134. Yazdani, S.; Mattam, S.; Gonzalez, R. Fuel and Chemical Production from Glycerol, a Biodiesel Waste Product. In *Biofuels from Agricultural Wastes and Byproducts*; Blaschek, H.P., Ezeji, T.C., Scheffran, J., Eds; Wiley-Blackwell: Oxford, UK, 2010; doi:10.1002/9780813822716.ch6.
135. Astals, S.; Nolla-Ardèvol, V.; Mata-Alvarez, J. Anaerobic co-digestion of pig manure and crude glycerol at mesophilic conditions: Biogas and digestate. *Bioresour. Technol.* **2012**, *110*, 63–70.
136. Harnisch, F.; Schröder, U. From MFC to MXC: Chemical and biological cathodes and their potential for microbial bioelectrochemical systems. *Chem. Soc. Rev.* **2010**, *39*, 4433–4448.
137. Nevin, K.P.; Hensley, S.A.; Franks, A.E.; Summers, Z.M.; Ou, J.; Woodard, T.L.; Snoeyenbos-West, O.L.; Lovley, D.R. Electrosynthesis of organic compounds from carbon dioxide is catalyzed by a diversity of acetogenic microorganisms. *Appl. Environ. Microbiol.* **2011**, *77*, 2882–2886.
138. Logan, B.E. Exoelectrogenic bacteria that power microbial fuel cells. *Nat. Rev. Microbiol.* **2009**,

7, 375–381.

139. Malvankar, N.S.; Lovley, D.R. Microbial nanowires: A new paradigm for biological electron transfer and bioelectronics. *ChemSusChem* **2012**, *5*, 1039–1046.
140. Roden, E.E.; Kappler, A.; Bauer, I.; Jiang, J.; Paul, A.; Stoesser, R.; Konishi, H.; Xu, H. Extracellular electron transfer through microbial reduction of solid-phase humic substances. *Nat. Geosci.* **2010**, *3*, 417–421.
141. Lovley, D.R. Powering microbes with electricity: Direct electron transfer from electrodes to microbes. *Environ. Microbiol. Rep.* **2011**, *3*, 27–35.
142. Liu, H.; Cheng, S.; Logan, B.E. Production of electricity from acetate or butyrate using a single-chamber microbial fuel cell. *Environ. Sci. Technol.* **2005**, *39*, 658–662.
143. Liu, H.; Hu, H.; Chignell, J.; Fan, Y. Microbial electrolysis: Novel technology for hydrogen production from biomass. *Biofuels* **2010**, *1*, 129–142.
144. Nevin, K.P.; Richter, H.; Covalla, S.F.; Johnson, J.P.; Woodard, T.L.; Orloff, A.L.; Jia, H.; Zhang, M.; Lovley, D.R. Power output and columbic efficiencies from biofilms of Geobacter sulfurreducens comparable to mixed community microbial fuel cells. *Environ. Microbiol.* **2008**, *10*, 2505–2514.
145. Du, Z.; Li, H.; Gu, T. A state of the art review on microbial fuel cells: A promising technology for wastewater treatment and bioenergy. *Biotechnol. Adv.* **2007**, *25*, 464–482.
146. Dennis, P.G.; Harnisch, F.; Yeoh, Y.K.; Tyson, G.W.; Rabaey, K. Dynamics of cathode-associated microbial communities and metabolite profiles in a glycerol-fed bioelectrochemical system. *Appl. Environ. Microbiol.* **2013**, *79*, 4008–4014.
147. Kraus, G.A. Synthetic methods for the preparation of 1,3-propanediol. *CLEAN—Soil Air Water* **2008**, *36*, 648–651.
148. Saxena, R.K.; Anand, P.; Saran, S.; Isar, J. Microbial production of 1,3-propanediol: Recent developments and emerging opportunities. *Biotechnol. Adv.* **2009**, *27*, 895–913.
149. Emptage, M.; Haynie, S.L.; Laffend, L.A.; Pucci, J.P.; Whited, G. Process for the Biological Production of 1,3-Propanediol with High Titer. U.S. Patent 7,504,250 B2, 17 March 2009.
150. Nakamura, C.E.; Whited, G.M. Metabolic engineering for the microbial production of 1,3-propanediol. *Curr. Opin. Biotechnol.* **2003**, *14*, 454–459.
151. Zeng, A.-P.; Biebl, H. Bulk Chemicals from Biotechnology: The Case of 1,3-Propanediol Production and the New Trends. In *Tools and Applications of Biochem. Engineering Science*; Schügerl, K., Zeng, A.-P., Aunins, J.G., Bader, A., Bell, W., Biebl, H., Biselli, M., Carrondo, M.J.T., Castilho, L.R., Chang, H.N., *et al.*, Eds.; Springer: Berlin, Germany, 2002; Volume 74, pp. 239–259.
152. Sánchez, Ó.J.; Cardona, C.A. Trends in biotechnological production of fuel ethanol from different feedstocks. *Bioresour. Technol.* **2008**, *99*, 5270–5295.
153. Holladay, J.D.; Hu, J.; King, D.L.; Wang, Y. An overview of hydrogen production technologies. *Catal. Today* **2009**, *139*, 244–260.

154. Dillich, S.; Ramsden, T.; Melaina, M. *Hydrogen Production Cost Using Low-Cost Natural Gas*; U.S. Department of Energy: Washington, DC, USA, 2012.
155. Hu, H.; Fan, Y.; Liu, H. Hydrogen production using single-chamber membrane-free microbial electrolysis cells. *Water Res.* **2008**, *42*, 4172–4178.
156. Logan, B.E.; Call, D.; Cheng, S.; Hamelers, H.V.M.; Sleutels, T.H.J.A.; Jeremiasse, A.W.; Rozendal, R.A. Microbial electrolysis cells for high yield hydrogen gas production from organic matter. *Environ. Sci. Technol.* **2008**, *42*, 8630–8640.
157. Lu, L.; Ren, N.; Xing, D.; Logan, B.E. Hydrogen production with effluent from an ethanol—H_2-coproducing fermentation reactor using a single-chamber microbial electrolysis cell. *Biosens. Bioelectron.* **2009**, *24*, 3055–3060.
158. Liu, H.; Grot, S.; Logan, B.E. Electrochemically assisted microbial production of hydrogen from acetate. *Environ. Sci. Technol.* **2005**, *39*, 4317–4320.